Svoluji k zapůjčení své diplomové práce ke studijním účelům a prosím, aby byla vedena přesná evidence vypůjčovatelů. Převzaté údaje je vypůjčovatel povinen řádně odcitovat.

Univerzita Karlova v Praze

Přírodovědecká fakulta

Studijní program: Biologie

Studijní obor: Genetika, molekulární biologie a virologie

Bc. Markéta Polidarová

Využití částic myšího polyomaviru pro dopravu látek do buněk

Utilization of mouse polyomavirus derived virus-like particles for cargo delivery into cells

Diplomová práce

Školitel: RNDr. Hana Španielová, Ph.D.

Praha, 2016

Prohlášení:

Prohlašuji, že jsem závěrečnou práci zpracovala samostatně a že jsem uvedla všechny použité informační zdroje a literaturu. Tato práce ani její podstatná část nebyla předložena k získání jiného nebo stejného akademického titulu.

V Praze, 4. 8. 2016

Podpis

Poděkování:

Děkuji své školitelce, RNDr. Haně Španielové, Ph.D. za vedení této diplomové práce, neocenitelnou pomoc, rady a připomínky a za její motivující přístup.

Děkuji doc. RNDr. Jitce Forstové, CSc. za cenné rady.

Děkuji Mgr. Jiřině Žáčkové Suchanové za neocenitelnou pomoc, trpělivost a cenné rady, a také za zhotovení elektronmikroskopických snímků.

Děkuji Mgr. Martinu Fraiberkovi za zhotovení ultratenkých řezů a elektronmikroskopických snímků.

Děkuji Mgr. Ondřeji Šebestovi a Dr. Jozefu Jandovi za zhotovení snímků z konfokální mikroskopie.

Děkuji RNDr. Tomáši Maškovi, Ph.D. za zapůjčení přístroje na přípravu sachrázového gradientu.

Děkuji laborantkám Vlastě Sakařové a Ivaně Polívkové za péči o buněčné linie a přípravu laboratorního materiálu.

Děkuji všem spolupracovníkům z Laboratoře Virologie za vytvoření příjemného pracovního prostředí.

Dále děkuji svým rodičům za umožnění studia. Své rodině, kamarádům a příteli děkuji za morální i duševní podporu během celého mého studia.

Abstract and key words

Mouse polyomavirus-derived virus-like particles composed from major capsid protein VP1 (MPyV VP1-VLPs) are interesting structures for use as a delivery system of various cargos into cells. VP1 protein self-assembles into icosahedral particles of 45 nm in diameter that are hollow highly regular nanoparticles.

In this work, model small molecule cargo, Cyclodextrin-Based Bimodal Fluorescence/MRI Contrast Agent, was encapsidated into MPyV VP1-VLPs. The cargo was stably associated with VLPs and was delivered into mammalian cells using these VLPs.

To prevent VLPs entrapment in endolysosomal compartments and increase the potential of VLPs applications, MPyV VP1 protein was modified by insertion of histidine-tag (6 histidine long sequence surrounded by glycine and serine) sequences into VP1 surface loop DE, because histidine modification of synthetic systems had enhancing effect on endosome escape and cargo delivery. With the use of in Bac-to-Bac® baculovirus expression system His-VP1 protein was expressed in insect cells and a variety of VP1-assemblies was obtained: long tubules and small 20nm VLPs formed from VP1 with 4 histidine-tags in DE loop, and novel VP1 nanostructure, which we named nano-jumpers, formed from VP1 with 2 histidine-tags. Nonetheless the endosome escape properties of His-VLPs and nanostructures were analysed and it was proved that histidine modification enhanced endosome escape of these structures.

Moreover, the effects of histidine-rich peptide ($KH_{27}K$) and known endosome disrupting agent polyethylenimine (PEI) were tested. $KH_{27}K$ had similar effect on endosome disruption as PEI, which was detected using endocyted fluorescent antibody. The effect of $KH_{27}K$ and PEI on MPyV infectivity was also investigated. It was shown for the first time that endosome membrane disruption enhances MPyV infectivity.

Key words:

mouse polyomavirus, VLPs, endosome escape, cargo, delivery, histidine

Abstrakt a klíčová slova

Virům podobné částice odvozené od myšího polyomaviru tvořené hlavním kapsidovým proteinem VP1 (MPyV VP1-VLPs) mohou být využity jako systém pro dopravu různých látek do buněk. Protein VP1 je schopný se samouspořádat do ikosahedrálních částic o průměru 45 nm, tedy vysoce pravidelných dutých nanočástic.

V této práci byl do MPyV VP1-VLPs zabalen modelový náklad, bimodální malá molekula založená na cyklodextrinu umožňující detekci pomocí fluorescence a zároveň kontrastní látka pro zobrazování pomocí magnetické rezonance. Tento náklad stabilně asocioval s VLPs a byl pomocí těchto částic doručen do savčích buněk.

Aby se zabránilo uvíznutí VLPs v endolysozomálních kompartmentech a zvýšilo se tak potenciální využití VLPs, MPyV VP1 protein byl modifikován vložením sekvencí bohatých na histidin (histidinový tag dlouhý 6 histidinů ohraničený glycinem a serinem) do povrchové smyčky DE. Tento přístup byl zvolen, protože modifikace umělých částic histidinem zvýšila jejich únik z endozomů a dopravu látek do buněk. Produkce His-VP1 proteinu v bakulovirovém expresním systému Bac-to-Bac® vedla ke vzniku různých struktur tvořených proteinem VP1: dlouhých tubulárních útvarů a malých 20nm VLPs při produkci VP1 se 4x vloženými histidinovým tagem ve smyčce DE, a nové nanostruktury, které jsme pojmenovali nano-jumpers, při produkci VP1 s 2x vloženým histidinovým tagem. Nicméně analýza His-VLPs a nanostruktur prokázala, že modifikace histidinem zvýšila jejich únik z endozomů.

Kromě toho byl také testován účinek peptidu bohatého na histidin ($KH_{27}K$) a polyethyleniminu (PEI), který umí narušit membránu endozomů a zvyšuje únik z těchto organel. $KH_{27}K$ měl podobný efekt na narušení endozomální membrány jako PEI za použití endocytované fluorescenční protilátky pro vizualizaci úniku z endozomů. Efekt $KH_{27}K$ a PEI na infektivitu MPyV byl také prozkoumán a poprvé bylo ukázáno, že narušení endozomální membrány zvyšuje infektivitu MPyV.

Klíčová slova:

myší polyomavirus, VLPs, únik z endozomů, náklad, doprava, histidin

Obsah

List of abbreviations

AB	antibody
AB-VLPs	MPyV VP1-VLPs reassembled in presence of fluorescently labeled antibody GαM Atto594
APS	ammonium persulfate
ATB	antibiotics
α	anti
BG	O^6-benzylguanine
BG-GLA-NHS	O^6-benzylguanine – γ-linolenic acid – N-hydroxysuccinimide, substrate for BG modification of proteins
BG-His-VLPs	BG modified His-VLPs
BG-VP1-VLPs	BG modified VP1-VLPs
BKV	BK virus
bp	base pairs
BSA	bovine serum albumin
CD	β-cyclodextrin modified by two fluorescein isothiocyanate moieties and five gadolinium complexes
CD-VLPs	MPyV VP1-VLPs reassembled in presence of CD
CD+DNA-VLPs	MPyV VP1-VLPs reassembled in presence of CD and DNA
CTB	cholera toxin
D	donkey
DMEM	Dulbecco's Modified Eagle Medium
DOX	doxorubicin
d. p. i.	days post infection
DTT	dithiotreitol
Dx	fluorescently labeled dextran
ECL	enhanced chemiluminescence
EDTA	ethylenediaminetetraacetic acid
EGTA	ethylene glycol-bis(β-aminoethyl ether)-N,N,N',N'-tetraacetic acid
EM	electron microscopy
FBS	foetal bovine serum
FITC	flurescein isothiocyanate
FITC-AB	FITC-conjugated swine anti mouse antibody
FU	fluorescence units (infectivity measurement)

G	goat
GAPDH	glyceraldehyde 3-phosphate dehydrogenase
Gd	gadolinium
GST-tag	glutathion S-transferase tag
hAGT	human O^6-alkylguanine-DNA alkyltransferase
HaPyV	Hamster polyomavirus
HEPES	4-(2-hydroxyethyl)-1-piperazineethanesulfonic acid
His_6	six histidine long sequence inserted into MPyV VP1 DE loop
His-VLPs	MPyV VP1-VLPs modified by His_6 insertion into VP1 DE loop
His-VP1	MPyV VP1 modified by His_6 insertion into DE loop
hr(s)	hour(s)
IPTG	isopropyl-β-D-thiogalactosid
ITC	isothiocyanate
JCV	JC virus
$KH_{27}K$	histidine-rich peptide, lysine-27 histidine moieties-lysine
LT	MPyV large T antigen
M	mouse
MPyV	Mouse (or murine) polyomavirus
MRI	magnetic resonance imaging
NC	negative control
NC-VLPs	VP1-VLPs reassembled without cargo
NTA	nitrilotriacetic acid
PBS	phosphate buffered saline
PC	positive control
PCR	polymerase chain reaction
PEG	polyethylenglycol
PEI	polyethylenimine
PFU	plaque forming units (infectivity measurement)
p. i.	post infection
PTA	phosphotungstic acid
R	rat
Rb	rabbit
rpm	rounds per minute
SDS	sodium dodecyl sulfate
SDS-PAGE	SDS polyacrylamide gel electrophoresis
SNAP-tag	protein tag derived from hAGT

SV40	Simian vacuolating virus 40
Sw	swine
TAE	tris-acetate-EDTA
TBE	tris-borate-EDTA
TC	tissue culture
TEMED	tetramethylethylenediamine
UCF	ultracentrifuge/ultracentrifugation
VLP(s)	virus-like particle(s)
VP1-BCmut	*VP1* construct with modified BC loop with inserted restriction sites
VP1-BCmut+DE7less	*VP1* construct with modified BC and DE loops with inserted restriction sites
wtVP1	wild type *VP1* sequence
X-gal	5-bromo-4-chloro-3-indolyl-β-D-galactopyranoside

1. Introduction

Treatment of human diseases is often accompanied by unwanted side effects damaging healthy tissues. Encapsidation of drug or diagnostic molecule into nanoparticles can protect cargo from degradation, allow targeting the specific cell type and therefore help reduce side effects. This leads to better therapeutic index of drugs and increases sensitivity of diagnostic methods. Small molecules, proteins and nucleic acid can be delivered using various nanoparticles into cells. Although more extensive research has been done on synthetic nanoparticles, viruses are natural targeted carriers of nucleic acids and were first used for gene therapy.

Virus-like particles (VLPs) can be derived from various human and non-human viruses, including Mouse polyomavirus. VLPs have similar structure to infectious virions, but they do not contain virus genome, thus cannot replicate in cells. However, they can still enter cells in similar manner as virions, thus deliver encapsidated cargo into cells. When compared to synthetic nanoparticles, VLPs share many similarities, such as size in nanometers, regular shape and cargo delivery abilities. Some of the benefits of MPyV VLPs are easy and cheap production in expression systems, biocompatibility and biodegradability.

One of the biggest obstacles in cargo delivery into cells is the endosomal systems. The majority of synthetic and virus-derived delivery systems enter cells in endocytic vesicles. Delivery systems must be able to escape endosomes to prevent cargo degradation in lysosomes. Many viruses have mechanisms allowing them to escape endosomal compartments, whereas synthetic nanoparticles usually have to be modified to gain the endosomal escape properties.

In this work the potential use of MPyV-derived VP1-VLPs as a delivery system was investigated. We aimed for small molecule and protein encapsidation into VLPs and its delivery into cells. Moreover, because we used VLPs composed only from major protein VP1 that may be less efficient in endosomal escape, we were interested in enhancing MPyV VP1-VLPs delivery potential using approaches successful in synthetic delivery systems.

2. Literature review

2.1 Polyomaviruses

The viruses from the *Polyomaviridae* family can be described as small non-enveloped viruses with circular double stranded approx. 5.3 kbp long DNA as their genome. Polyomaviruses are also tumorigenic as some polyomavirus infections can lead to carcinogenesis.

The first discovered was mouse polyomavirus (or murine polyomavirus, MPyV) followed by simian vacuolating virus 40 (SV40), both becoming models for polyomaviruses and cancer biology. There are also many human polyomaviruses of known or unknown pathologies. The best described are JC virus (JCV) and BK virus (BKV) causing neurodegenerative disorder and kidney failure respectively in immunocompromised patients, and Merkel cell polyomavirus (MCPyV) which is a causative agent of a subtype of aggressive skin cancer.

Polyomavirus symmetrical icosahedral protein capsid of approx. 45 nm in diameter that is able to self-assemble, bind and enter specific cell type is a promising starting point for biocompatible nanoparticles development.

2.1.1 Biology of mouse polyomavirus

Mouse polyomavirus was the first discovered member of *Polyomaviridae* family (Gross, 1953; Stewart et al., 1958). This virus was found to cause diverse tumors in mice. Together with SV40 it is the best described polyomavirus but a lot still remains to be uncovered.

MPyV virions are composed of structural proteins VP1, VP2 and VP3, which form the icosahedral capsid, and the viral genome DNA with bound cellular histone core proteins (histones H2A, H2B, H3 and H4). The MPyV capsid is approx. 45 nm in diameter. It has icosahedral symmetry with the triangulation number T=7. The capsid is composed of 72 VP1 pentamers (that is 360 VP1 proteins). Each VP1 pentamer contains one of the minor proteins VP2 or VP3 but these are not exposed on the capsid surface. From the 72 pentamers there are 60 hexavalent (they are surrounded with 6 other pentamers) and 12 pentavalent (figure 2.1) (DeCaprio et al., 2013; Rayment et al., 1982).

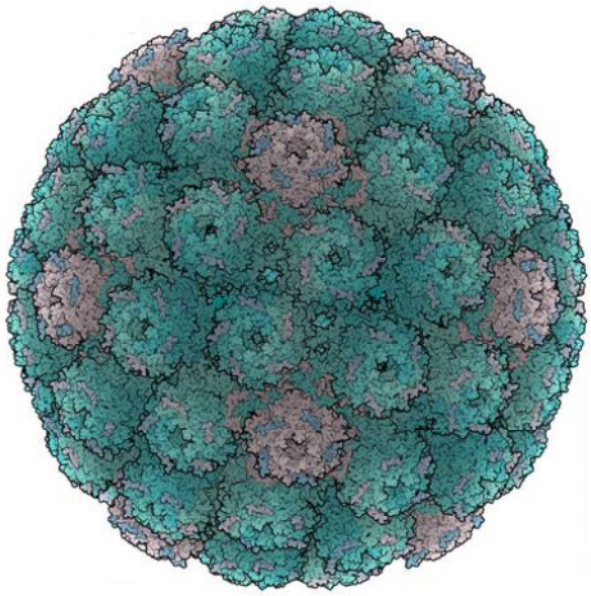

Figure 2.1: Polyomavirus capsid structure
Polyomavirus icosahedral capsid is composed of 72 pentamers, 60 hexavalent (turquoise) and 12 pentavalent (pink). (Adapted from Stehle and Harrison, 1996)

MPyV double stranded circular genomic DNA is 5297 base pairs long. It contains the regulatory region with the origin of replication, promoters and enhancers; the early region that is transcribed in the early phase of infection and continues during the life cycle; and the late region transcribed in the late phase of infection. The early region encodes for large, middle and small T-antigen, all involved in the regulation of virus life cycle and cell transformation. The late region encodes for the structural proteins VP1, VP2 and VP3 (DeCaprio et al., 2013).

The first step of the MPyV infection is the attachment to the cell surface. Gangliosides GD1a and GT1b act as the viral receptors (Tsai et al., 2003). The gangliosides contain sialic acid which is recognized by surface loops of VP1 protein. α4β1 integrin was identified to be a MPyV co-receptor acting after the attachment (Caruso et al., 2003). The virus is then internalized in clathrin independent manner and is delivered into early endosomes (Gilbert et al., 2003; Liebl et al., 2006; Mannová and Forstová, 2003; Richterová et al., 2001). It requires low pH of the endosomes for productive infection (Liebl et al., 2006). After, the virus is transported to the endoplasmic reticulum in not yet clear manner. The gangliosides are proposed to be important in the mechanism as they are transported together with the virus (Gilbert and Benjamin, 2004; Qian and Tsai, 2010; Qian et al., 2009). Interestingly MPyV was never observed in Golgi apparatus and the pathway to the endoplasmic reticulum bypassing Golgi remains to be uncovered (Gilbert and Benjamin, 2004; Liebl et al., 2006; Mannová and Forstová, 2003; Qian et al., 2009). The virus then exits the endoplasmic reticulum, enters cytoplasm and finally the nucleus. However the mechanisms are still not clear.

Once MPyV genome enters the nucleus, early transcription using cellular RNA polymerase II starts. Large T-antigen then promotes viral genome replication and the transcription of late gene

starts as well. The capsid proteins are translated in the cytoplasm and have to be transported into the nucleus for assembly (DeCaprio et al., 2013). The minor proteins VP2 and VP3 must bind to VP1 in order to be transported into the nucleus (Forstová et al., 1993). Once there is enough of new genomes and capsid proteins, the components assemble into new viral particles inside the nucleus (DeCaprio et al., 2013). DNA binds to VP1 protein N-terminus and is encapsidated in sequence independent manner (Španielová et al., 2014). Finally new virions exit the cells by cell lysis (DeCaprio et al., 2013).

2.1.2 VP1 protein

The major structural protein of the polyomavirus capsid, VP1 protein, is expressed in the late phase of infection. It is 384 amino acids long and has molecular weight 45 kDa. The crystallographic studies revealed its structure which is mostly β-strands organized into "jelly-roll" fold (figure 2.2). Individual β-strands are connected with loops that are exposed on the surface of MPyV capsid. These surface loops create a pocket, the binding site for MPyV receptor. There are four surface loops, BC, DE, EF and HI, and only the BC and HI loop bind directly to the sialic acid (Stehle and Harrison, 1996; Stehle and Harrison, 1997; Stehle et al., 1994). DE and EF loops were described to be interacting with the co-receptor α4β1 integrin (Caruso et al., 2003).

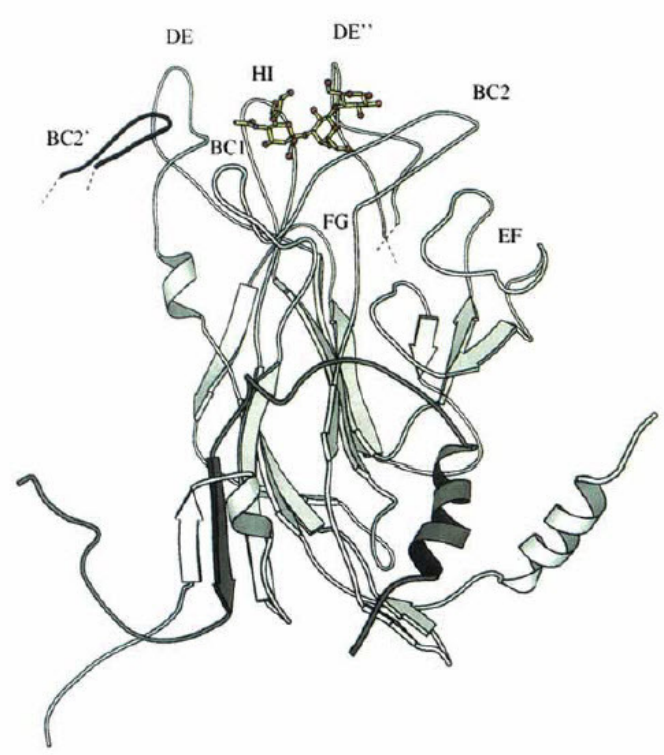

Figure 2.2: VP1 protein structure
Structure of MPyV VP1 protein with marked surface loops binding to the ligand. BC and HI loops are the ones directly interacting with the receptor. BC loop has two parts (BC1 and BC2). Loops of other pentamers are also shown in the structure – BC2' and DE''.
(Adapted from Stehle et al., 1994)

Five VP1 proteins assemble into a pentamer and these assemble into an icosahedral capsid. The VP1 flexible C-terminus was found to be necessary for the capsid assembly as it connects together different pentamers (Garcea et al., 1987). The C-terminus also binds calcium ions that help stabilize the capsid together with disulfide linkages between pentamers (Brady et al., 1977; DeCaprio et al., 2013; Ludlow and Consigli, 1987).

The VP1 protein is also responsible for DNA packaging into the capsid (Carbone et al., 2004; Gillock et al., 1997). DNA binding site and nuclear localization signal are localized on the N-terminus which is oriented inside the capsid (Gillock et al., 1998; Chang et al., 1992; Chang et al., 1993; Moreland et al., 1991).

In addition, the VP1 protein has 6 different forms varying in the post-translational modifications. The modifications affect DNA binding, receptor interaction or even the assembly (Bolen et al., 1981; Li and Garcea, 1994).

Finally VP1 pentamer interacts with one of the minor capsid proteins VP2 or VP3. The C-terminus of a minor protein is localized inside the central cavity of a pentamer (Barouch and Harrison, 1994).

2.1.3 Minor proteins VP2 and VP3

The capsid of MPyV also contains minor proteins VP2 and VP3. One of the minor proteins is associated with VP1 pentamer via its C-terminus. VP2 and VP3 have identical C-terminal sequence. VP2 has extended N-terminus where it is posttranslationally modified by myristylation (DeCaprio et al., 2013).

The minor proteins are not necessary for capsid formation as the VP1 protein alone can assemble into virus-like particles when produced in cells (Montross et al., 1991) but they are important for the virus infectivity (Mannová et al., 2002). The function of minor proteins in polyomavirus infection is still unclear. When the minor proteins are expressed alone in baculovirus expression system they are associated with cellular membranes (Forstová et al., 1993; Mannová et al., 2002). In mammalian cells, expression of minor proteins alone causes cell death by apoptosis, but this effect is much smaller in polyomavirus infection suggesting their role is not cellular destruction (Huerfano et al., 2010). VP2 and VP3 caused hemolysis *in vitro* suggesting their possible role as viroporins (Burkert et al., 2014).

2.2 Virus-like particles derived from polyomaviruses

As mentioned in chapter 2.1, the polyomavirus capsids are suitable for nanoparticles development. They are approximately 45 nm in diameter and have icosahedral symmetry. In addition, only the major VP1 protein is responsible for capsid assembly and it has self-assembly

properties. When VP1 is expressed alone, it spontaneously assembles into icosahedral particles called virus-like particles, VLPs, which have similar morphology as the capsids but lack the viral DNA (Salunke et al., 1986). When VP1 is expressed with minor proteins VP2 and VP3, the VLPs also assemble and the minor proteins are inserted into the VP1 pentamers as in virions (An et al., 1999).

VLPs do not contain polyomavirus genome DNA, thus are not infectious, but they can incorporate fragments of cellular or other DNA because of VP1 protein's DNA binding properties (An et al., 1999; Gillock et al., 1997). Because polyomaviruses-derived VLPs are composed of the VP1 protein, which is responsible for binding to cell receptors and mediating entry into the cytoplasm (Tsai et al., 2003), VP1-VLPs are still able to enter cells in vesicles. However, the minor proteins may be important in further steps, because complete absence of minor proteins is lethal for MPyV (Mannová et al., 2002) and VP1-VLPs are less efficient in cell transduction than wt virus or VLPs assembled with minor proteins, as investigated on SV40 polyomavirus (Enomoto et al., 2011; Mukherjee et al., 2007). On the other hand, VP1-VLPs derived from JCV are efficient in nucleic acid delivery (Fang et al., 2015; Chou et al., 2010).

2.2.1 Production of polyomavirus-derived VLPs

There are several approaches to prepare polyomavirus-derived VLPs. A variety of expression systems can be used for polyomavirus capsid proteins production ranging from prokaryotic systems using *Escherichia coli* strains, eukaryotic systems with yeast, insect, mammalian or even plant cells, to cell-free systems. The most commonly used systems are described in following chapters.

2.2.1.1 Prokaryotic expression system and *in vitro* assembly

The prokaryotic expression system was the first used for MPyV VP1-VLPs production (Salunke et al., 1986). Prokaryotic expression system allows production of the recombinant polyomavirus VP1 protein in large quantities (Teunissen et al., 2013). VP1 protein organizes into pentamers in bacterial cells but VLPs are usually produced during purification process and *in vitro* assembly in low ionic strength (Salunke et al., 1986). Because the expression of proteins in bacteria is usually fast, the proteins may end up in insoluble inclusion bodies from which the purification yield can be quite low and requires optimization (Leavitt et al., 1985). VP1 protein can be N-terminally fused with glutathione S-transferase tag (GST-tag) for easier purification. GST-tag must be removed for *in vitro* VLPs assembly (Lipin et al., 2006). With this approach the scientists were able to scale-up the production of wild type or modified MPyV VP1 protein (Liew et al., 2010; Middelberg et al., 2011). Despite all the advantages of prokaryotic expression system, such as low cost and high yield, the proteins produced in this system lack the posttranslational

modifications. Another complication may be the necessity of complete removal of expression tags, bacterial toxins and nucleic acids for applications in human medicine (Teunissen et al., 2013).

2.2.1.2 Eukaryotic expression systems

On the contrary to the prokaryotic expression system, polyomavirus-derived VLPs assemble inside the eukaryotic cells and the posttranslational modifications are present although they can differ among the systems (Teunissen et al., 2013).

Yeast expressions systems were used with success for VLPs derived from various polyomaviruses. The first produced VLPs in *Saccharomyces cerevisiae* were derived from hamster polyomavirus (HaPyV) (Sasnauskas et al., 1999). Shortly after, VLPs derived from JCV and BKV human polyomaviruses were produced in the same system (Hale et al., 2002) and followed by many others both non human and human polyomavirus-derived VLPs (Norkiene et al., 2015; Sasnauskas et al., 2002). Yeast expression systems are the cheapest of the eukaryotic expression systems and also have the highest yield. In addition produced VLPs are free from any toxins and there is only small contamination with host nucleic acids that is easy to remove, which makes the yeast expression system suitable for vaccine production (Gedvilaite et al., 2000; Palková et al., 2000; Teunissen et al., 2013). MPyV VP1-VLPs accumulate in yeast nuclei and interact with microtubules of the mitotic spindle (Palková et al., 2000). Moreover, it was found that the VLPs produced in yeast expression system are more stable than the ones produced in prokaryotic system, which suggests that cellular components aid the proper assembly of VLPs (Simon et al., 2014).

Baculovirus expression system using insect cell lines for recombinant protein production is another safe commonly used system for polyomavirus-derived VLPs production. Recombinant baculovirus carrying the gene for polyomavirus major capsid protein VP1 is used cells infection. They then produce VP1 in cytoplasm which is transported into the nuclei thanks to its nuclear localization signal and assembles into VLPs inside the nuclei (Chang et al., 1997). Even though the yield is much lower than the one of yeast expression system, produced VLPs are closely similar to VLPs from mammalian cells and virions because insect cells produce posttranslational modifications similar to the mammalians' (Teunissen et al., 2013). The biggest advantage of baculoviru expression system is the possibility to express more than one viral protein at the same time, thus not only VP1-VLPs but also VLPs with one or both minor proteins can be produced (An et al., 1999). The VLPs produced in baculovirus expression system contain cellular or baculovirus DNA packed with cellular histones (Gillock et al., 1997; Pawlita et al., 1996). The contaminating DNA can be removed during disassembly and DNase treatment followed by reassembly of the VLPs (Teunissen et al., 2013). VLPs derived from various polyomaviruses with

or without minor proteins were prepared using this expression system (An et al., 1999; Gillock et al., 1997; Chang et al., 1997; Li et al., 2003; Touzé et al., 2010).

Other eukaryotic expression systems were also used with success such as vector based insect cell expression (Montross et al., 1991; Ng et al., 2007), mammalian expression systems, although these are quite expensive and are not commonly used (Shishido et al., 1997; Teunissen et al., 2013), or even expression in plants (Catrice and Sainsbury, 2015).

2.2.2 Assembly mechanisms of polyomavirus-derived VLPs

Major protein VP1 is sufficient and necessary for VLPs assembly (Chang et al., 1997; Salunke et al., 1986). In eukaryotic systems, VP1 protein is expressed in the cytoplasm and is transported to the nucleus where the VLPs assembly occurs (Chang et al., 1997; Montross et al., 1991). When the minor proteins were expressed alone, they could not reach the nuclei, VP2 was localized outside of the nuclei and VP3 was dispersed throughout the cytoplasm. Expression of the minor proteins together with VP1 leads to nuclear transport of minor proteins in association with VP1 (Forstová et al., 1993).

The structure of VLPs is stabilized by disulfide bonds and calcium ions as addition of chelating agents (ethylenediaminetetraacetic acid, EDTA) and reducing agents (dithiotreitol, DTT) leads to disassembly of the VLPs to pentamers (Chang et al., 1997; Ishizu et al., 2001; Kosukegawa et al., 1996; Sandalon and Oppenheim, 1997). Disulfide bonds are formed between VP1 proteins of a pentamer (Schmidt et al., 2000) whereas the calcium ions strengthen the binding between different pentamers mediated by the VP1 C-terminus (Chuan et al., 2010; Liddington et al., 1991). It was proposed that the disulfide bonds are not necessary for VLPs formation but they help to complete the assembly and stabilize the VLPs. When formation of disulfide bonds is unabled, VLPs of SV40 virus do not assemble (Jao et al., 1999) whereas the MPyV VLPs are still able to assemble with lesser efficiency (Schmidt et al., 2000). The disulfide bonds may stabilize the particle by protecting the calcium ions from chelation (Chen et al., 2001; Ishizu et al., 2001).

The *in vitro* assembly of polyomavirus-derived VLPs is dependent on pH, ionic strength and calcium ions concentration and changes in the conditions can give rise to VLPs of various sizes, tubular and irregular structures (Kanesashi et al., 2003; Salunke et al., 1989). Based on this knowledge and research done on other polyomaviruses, a protocol for disassembly and reassembly of MPyV VP1-VLPs was developed and optimized in the Laboratory of Virology. The VLPs are disassembled in low ionic strength in the presence of chelating agent and reducing agent, the pentamers are separated from not disassembled and aggregated material and the VLPs are then reassembled in high concentration of ammonium sulfate in presence of Ca^{2+} ions (chapter 4.2.4.11, modified according to Mukherjee et al., 2010 and Suchanová, 2012).

2.2.3 Polyomavirus-derived VLPs as vaccine platforms

The polyomavirus capsids can be used as carriers for immunogenic epitopes or whole proteins for recombinant vaccine production or other immunizing agents. Use of the VLPs is safe because they can be produced without nucleic acids. In addition, the VLPs are immunogenic so no adjuvant may be needed (Kawano et al., 2013).

Short immunogenic epitope can be inserted into some of the VP1 surface loops, mainly DE or HI. Various immunogenic epitopes, for example from hepatitis B virus or influenza virus, have been successfully tested in MPyV, HaPyV or recently in SV40 and Trichodysplasia Spinulosa-Associated polyomavirus-derived VLPs (Gedvilaite et al., 2000; Gedvilaite et al., 2015; Kawano et al., 2014; Skrastina et al., 2008).

The other approach is fusion of whole protein with polyomvirus minor protein (Bouřa et al., 2005; Eriksson et al., 2011; Pleckaityte et al., 2015; Tegerstedt et al., 2005). Such constructs are attractive for immunization against cancer cells and can lead to specific anti-tumor T-cell mediated immunity activation (Eriksson et al., 2011; Tegerstedt et al., 2005).

2.2.4 Polyomavirus-derived VLPs as drug and gene delivery system

Polyomavirus-derived VLPs are hollow, thus they can be also used as nanoparticles for delivery of various molecules encapsidated into the particle in a process of disassembly and reassembly as described in chapters 2.2.2 and 4.2.4.11. The benefits of nanoparticles for cargo delivery, when compared with uncoated cargo, can be higher stability of cargo in extracellular environment, lower toxicity or immunogenicity of cargo, possible cell type targeting, better cellular uptake and cellular compartment targeting.

The natural cargo for VLPs is DNA. Gene delivery was tested with success using VLPs derived from various polyomaviruses (Forstová et al., 1995; Kimchi-Sarfaty et al., 2002; Krauzewicz et al., 2000; Touzé et al., 2001; Voronkova et al., 2007). Recently, suicide genes were delivered using JCV VLPs into human tumors and leukemia studied in a mouse model. Such gene delivery led to growth inhibition of a tumor or leukemic cells (Fang et al., 2015; Chao et al., 2015; Chen et al., 2010)

RNA (Chou et al., 2010) or peptide nucleic acid (PNA, Macadangdang et al., 2011) were also encapsidated into the VLPs and their cellular delivery led to gene silencing *in vitro* (Macadangdang et al., 2011) or also *in vivo* (Hoffmann et al., 2016; Chou et al., 2010).

Proteins and peptides can also be encapsidated into VLPs and delivered into cells either as fusion proteins with minor polyomavirus proteins (Abbing et al., 2004; Inoue et al., 2008) or by modification of VP1 protein by adding a domain noncovalently binding specific protein sequences (Günther et al., 2001).

Finally small molecules can be a cargo for VLPs, both drugs and diagnostic molecules. For example fluorescent agent propidium iodide was successfully internalized into SV40 VLPs using disassembly and reassembly of VLPs (Goldmann et al., 2000). Also quantum dots were encapsidated into SV40 VLPs (Li et al., 2009). The delivery of therapeutic agents was successful as well. Methotrexate was bound to VP2 protein of MPyV VLPs and delivered into the cytoplasm of leukemia cells where the cytostatic effect was observed (Abbing et al., 2004). Encapsulation of hydrophobic drugs into VLPs strongly enhances their therapeutic potential and a system of their controlled release is being developed (Niikura et al., 2013b).

One of the challenging tasks of drug or gene delivery by any nanoparticle is the specific cell type targeting. Targeting epitope must be present on the surface of the. It can be achieved by chemical modifications of the particle surface or, in the case of protein nanoparticles such as VLPs, by modification of protein sequence using gene engineering techniques. As targeting was not part of my project it is not further described here. Another challenging task is the importance of endosome escape for cargo delivery into the cytoplasm or nucleus which will be described in the next chapters.

2.3 Endosome escape enhancement in nanoparticles

Most of the drug or gene carriers enter the cell by endocytosis. In order to successfully deliver the drug, protein or nucleic acid into the cell they have to prevent lysosomal sequestration and degradation, thus escape from the endolysosomal pathway. Viruses use various mechanisms for endosome escape, for example RNA injection through endosomal membrane, a mechanism used by Picornaviruses, or a rupture of endosomal membrane so the whole virions can reach cytoplasm, observed in Adenovirus infection (Bílkova et al., 2014). The enveloped viruses can escape the endosomes via membrane fusion.

As synthetic nanoparticle delivery systems lack such mechanisms, they must be modified in order to achieve higher efficiency of cargo delivery. Several mechanisms were described for nucleic acid delivery systems. Lipid nanoparticles can interact with endosomal membrane which can lead to nucleic acid release into the cytoplasm. Another approach is the use of cell-penetrating peptides which can disrupt endosomal membrane. Endosomal rupture can also be regulated by use of photosensitizers that are activated by visible light. Finally cationic peptides with buffering capacity may use the “proton sponge effect” which will be described in the next chapter (Liang and W. Lam, 2012).

2.3.1 Cationic polymers and their mechanism of endosome escape

Cationic polymers are one of the synthetic nanoparticle systems used mainly for DNA delivery into cells. The positive charge allows them to make complexes with DNA (polyplexes) that

protect DNA from the environment and allows the cellular entry by endocytosis. There are two types of cationic polymers, those without buffering capacity, such as polylysine, and those with pKa close to physiological pH, such as polyethylenimine (PEI), polyamidoamine and others, which have buffering properties in slightly acidic environment. Such cationic polymers were found to be more efficient in DNA delivery than the ones without buffering capacity. The difference was in the efficiency of endosome escape which was first described to be based on a "proton sponge effect" (Liang and W. Lam, 2012).

The mechanism of "proton sponge effect" is described as follows (figure 2.3): The endosomes are acidified by active pumping of protons into the lumen. The cationic molecules with pKa close to the endosomal pH are able to bind and accumulate protons on their surface, thus buffer and prevent the endosome acidification. However, proton influx is followed by chloride ions and these are in turn followed by water. Thus, the water accumulation leads to endosome disruption, endosome escape of a carrier and cargo release (Behr, 1997).

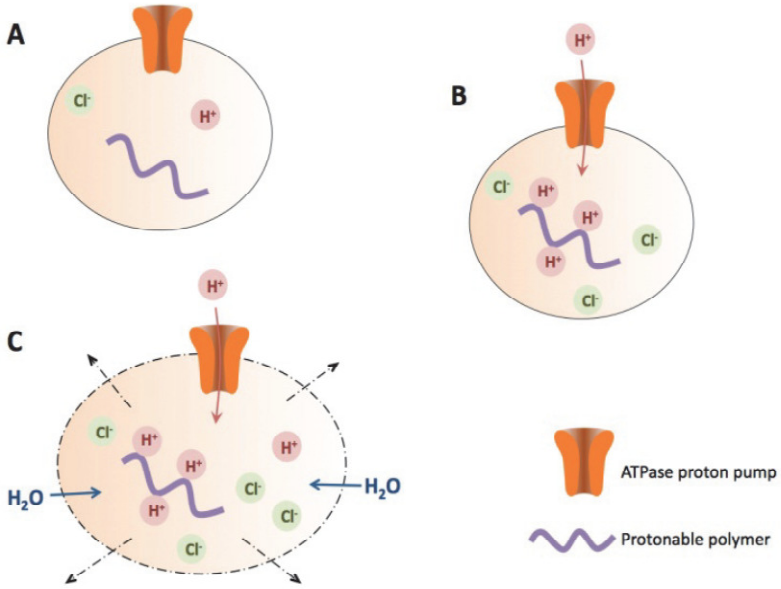

Figure 2.3: The "proton sponge effect"
A. Vesicle formed after endocytosis of proton sponge molecule (protonable polymer). B. Endosome starts to acidify, that is pumps protons inside the lumen. The protons are followed by chloride anions. The protonable polymer binds protons on its surface, thus buffers and prevents endosome from acidification. C. Accumulating chloride anions are followed by water into the lumen of endosome leading to endosome membrane disruption and content release.
(Adapted from Liang and Lam, 2012)

Several studies using the most efficient cationic polymer polyethylenimine supported this model. Sonawane and colleagues (2003) showed increase of volume of endosomes, slowed acidification and Cl^- ions accumulation in endosomes in cells treated with PEI. Another study showed that PEI effect was pH dependent because inhibition of endosomal proton pump

reduced the PEI mediated transfection. In addition, PEI prevented endosomal acidification below pH 6.1 (Akinc et al., 2005).

However, the "proton sponge effect" model was questioned because not all cationic polymers with buffering capacity had the desired effect on DNA delivery (Funhoff et al., 2004). Moreover, no changes in pH of endosomes and lysosomes in cells treated with PEI polyplex were observed in a recent study with more sensitive pH detection (Benjaminsen et al., 2013). In the study they postulated another possible mechanism of PEI mediated endosome escape. Protonated PEI may induce pores formation in the endosomal membrane due to combination of buffering capacity and interaction with membranes. Computer modeling supported this theory when it showed that protonated PEI interacted with lipidic membrane and induced water or ion channels formation (Choudhury et al., 2013). Further modeling showed difference of PEI interaction with zwitterionic and anionic membranes. Protonated PEI interacted more extensively with anionic membranes and led to their reorganization, however no fragmentation was observed (Kwolek et al., 2016).

The endosome escape due to membrane interaction in low pH is supported also by the notice that excess of free polymer has positive effect on endosome escape (Boeckle et al., 2004; Yue et al., 2011). Moreover, PEI treatment of cells before or after incubation with polyplex of less potent cationic polymer led to increase of gene delivery. This resulted into the theory that polymers in complex with DNA only carry it into the cells whereas unbound polymer interacts with endosomal membrane and enables the endosome escape (Vaidyanathan et al., 2016).

2.3.2 Histidine modifications of drug and gene delivery systems

Cationic polymers without buffering capacity as well as other delivery systems can be modified by various short peptides with buffering capacity. Also peptides with positive charge and buffering capacity can be used as a delivery system. Some of the most commonly used are modifications with L-histidine moieties or histidine-rich amphipatic peptides (Liang and W. Lam, 2012). Histidine is an amino acid with imidazol ring protonable in slightly acidic environment such as the one in endosomes.

It was observed in early study by Midoux and Monsigny (1999) that modification of peptide DNA carrier by histidine moieties increases the transfection efficiency and that it depends on acidic environment. A mechanism similar to "proton sponge effect" was suggested to be responsible for transfection enhancement of histidine-rich peptide delivery system (Kichler et al., 2003). However, histidine-rich peptide antibiotics were also found to interact with negatively charged lipid membranes (Kichler et al., 2006). As "proton sponge effect" was questioned extensively for PEI (chapter 2.3.1) it is possible that histidine mediated endosome escape can be based on the interaction with endosomal negatively charged membrane as well. A computer modeling study

using dendrimer delivery system modified by three histidine and one arginine moieties was observed to interact with negatively charged asymmetric membranes in acidic pH and led to thinning and increased permeability of such membranes (Tu et al., 2013).

L-histidine modification of various DNA delivery systems increased transfection efficiency when compared to unmodified system. This effect was based on enhanced endosome escape of histidine-modified carriers (Hwang et al., 2014; Chang et al., 2010; Nam et al., 2015; Thomas et al., 2012; Wen et al., 2012; Zhao et al., 2014). In addition, histidine modification led to lower cytotoxicity (Hwang et al., 2014; Nam et al., 2015; Wen et al., 2012; Zhao et al., 2014), higher *in vitro* hemolytic activity (Hwang et al., 2014) and better serum tolerance of a carrier system, that is the serum components had milder inhibiting effect on cellular uptake of histidine-modified polymer (Wen et al., 2012).

Histidine-modified polymers and direct RNA modifications with histidine-rich peptide were also used for RNA delivery. Similarly to DNA transfection experiments, RNA was delivered more efficiently when histidine moieties were present (Asseline et al., 2008; Langlet-Bertin et al., 2010; Nakagawa et al., 2014).

Delivery of small molecules was investigated as well. The studies focus mostly on doxorubicin (DOX) delivery. Histidine-modified delivery systems allowed low pH triggered release of DOX into cytoplasm from endosomes or lysosomes without significant disruption of endosomal membrane (Johnson et al., 2014; Li et al., 2015; Zhang et al., 2014).

2.3.3 Endsome escape detection methods

The endosome escape based on membrane pores formation or rupture can be detected with various methods. Probably the most commonly used are tracer molecules that are endocyted and do not diffuse across lipidic membranes. They can reach cytoplasm only when the endosomal membrane is permeabilized or ruptured. Most commonly used tracers are fluorescent molecules that can be observed with fluorescent microscopy. Another option is an indirect detection of endosomal escape. Biologically active cargos (proteins, gene carrying DNA) are delivered into the cells and their effect is observed only when they reach cytoplasm or nucleus (Martens et al., 2014).

2.3.3.1 Dextran assay

Fluorescently labeled dextrans (Dx) of various sizes are one of the possible tracer molecules. They are endocyted and label the endosomes creating a spot pattern. When the endosomal membrane is disrupted, Dx molecules diffuse in cytoplasm resulting in less intense diffused labeling of a whole cell (figure 2.4).

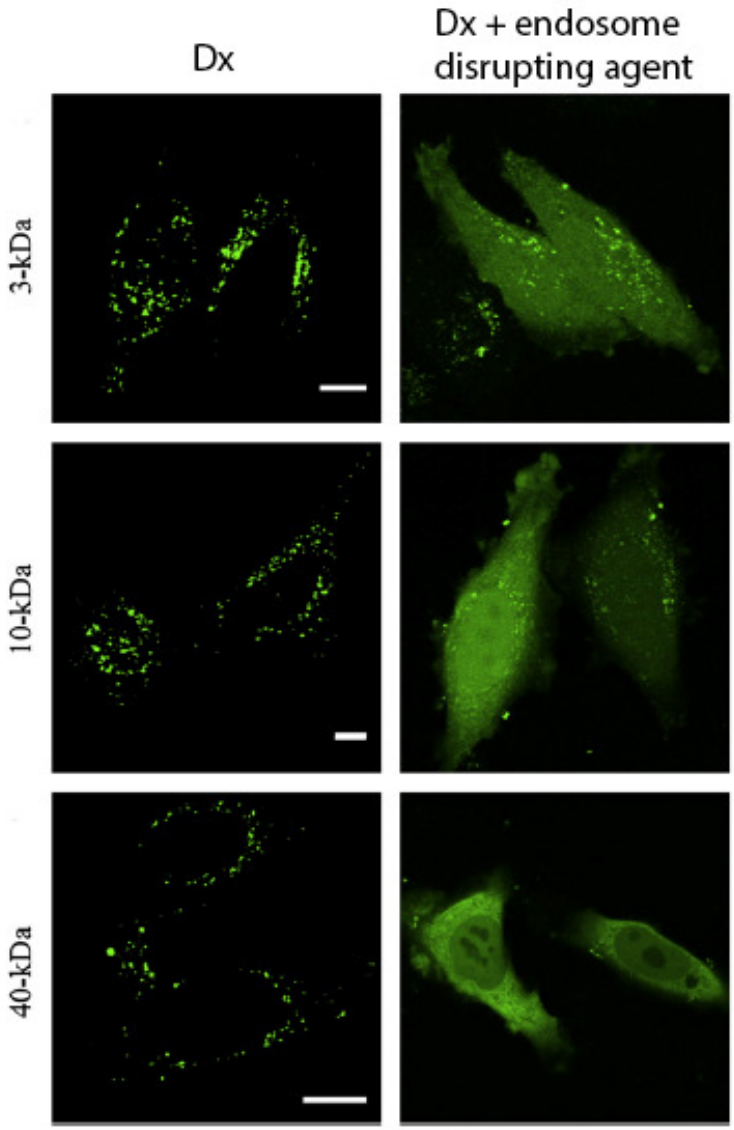

Figure 2.4: Dextran assay
Fluorescently labeled dextrans (Dx) of various sizes are endocyted and label endosomes as bright spots. When endosome disrupting agent is present Dx diffuses from the spots into the cytoplasm and stains the whole cell. (Adapted from Salomone et al., 2012)

Dextran assay was used to study endosome escape of viruses. Fluorescein isothiocyanate (FITC) conjugated dextran and Cy5 conjugated dextran of 70kDa and 10kDa molecular weights were used for virus endosome escape study using life cell imaging. Both 10 kDa and 70 kDa Dxs escaped the endosomes in adenovirus infection whereas only 10 kDa Dx was able to escape in picornavirus infection (Brabec et al., 2005). That is in agreement with the fact that adenoviruses escape through endosome rupture, whereas picornaviruses create pores in endosomal membrane (Bílkova et al., 2014). Picornavirus endosomal escape was also investigated with rhodamine conjugated Dx in fixed cells (Suikkanen et al., 2003). Dextran assay is also suitable tool for studies of endosome escape mediated by membrane penetrating peptides used in synthetic delivery systems (Salomone et al., 2012).

2.3.3.2 SNAP-Trap assay

SNAP-tag is a 20kDa protein tag developed by modification of human O^6-alkylguanine-DNA alkyltransferase (hAGT), which is a DNA repair protein. It binds covalently and irreversibly to its substrate O^6-alkylguanine-DNA via its cystein residue and is also able to bind O^6-benzylguanine (BG). The genetic modifications strengthened hAGT binding to BG (Gronemeyer et al., 2006; Heinis et al., 2006; Juillerat et al., 2003; Keppler et al., 2003; Keppler et al., 2004). This tag was originally developed to serve *in vivo* protein labeling with small fluorescent molecules but it was also used for investigation of protein-protein interactions (Maurel et al., 2008). In addition the covalent binding can be used for modification of nanoparticles for cell targeting and drug delivery (Hussain et al., 2011; Hussain et al., 2013).

Recently, a novel tool for localization of exogenous protein within cell, called SNAP-Trap assay, was developed (Geiger et al., 2013). SNAP-tag can be used as a reporter gene of selected cellular compartment. Expressed alone, SNAP-tag localizes to cytoplasm, or it can be expressed as a fusion protein for targeting to various organelles. If the protein of interest is modified with BG it only interacts with SNAP-tag when it is present in the same cellular compartment. Such interaction is studied using SDS-PAGE and western blot analysis, as the SNAP signal after interaction with BG-modified protien appears in molecular weight of studied protein plus 20kDa (figure 2.5). This assay was used to study viruses (SV40 and adenovirus) and cholera toxin (Geiger et al., 2011; Geiger et al., 2013).

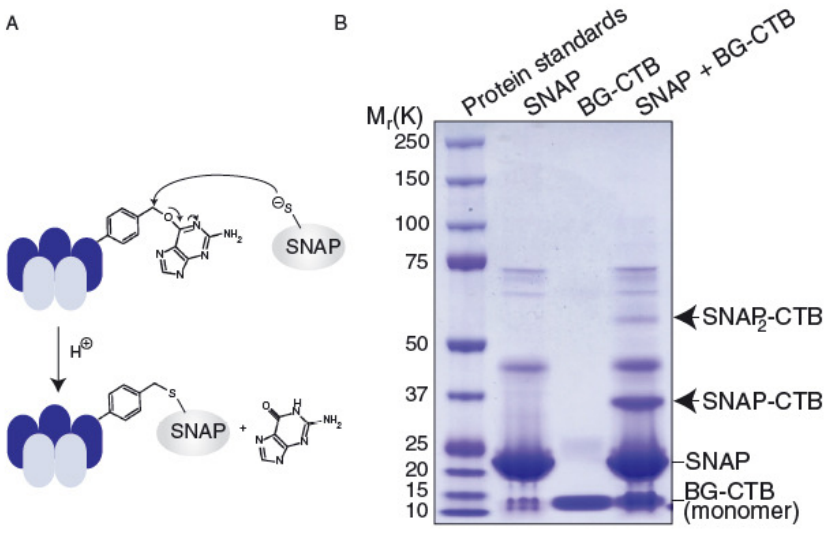

Figure 2.5: SNAP-Trap assay principle
A: BG-modified cholera toxin (CTB) reacts with SNAP creating a covalent bond through cystein residue of SNAP. **B:** Example of *in vitro* interaction of BG-CTB and SNAP. The proteins were separated using SDS-PAGE and Coomassie Blue staining. SNAP alone had 20 kDa, BG-CTB monomer had 13 kDa. When SNAP and BG-CTB interacted they created two products SNAP-CTB and $SNAP_2$-CTB of larger size. (Modified according to Geiger et al., 2013)

3. Aims of the thesis

The aim of this work was to investigate a possible use of MPyV-derived VP1-VLPs as a delivery system of a cargo. Such delivery system has to be able to encapsidate the selected cargo and deliver it into cell cytoplasm or nuclei. For the latter efficient endosome escape is necessary. Thus the general goal of this work was to investigate one possible way of how to prepare MPyV VP1-VLPs with enhanced endosome escape properties that are able to encapsidate cargo and efficiently deliver it into the cytoplasm. The project consisted of three specific aims performed in steps described below:

Aim 1: To prepare a universal VP1 construct for various surface loops modification.

- In a donor plasmid of baculovirus expression system prepare modified MPyV VP1 sequence with restriction sites in BC loop.
- In a donor plasmid of baculovirus expression system prepare modified MPyV VP1 sequence with restriction sites in both BC and DE loop.

Aim 2: To demonstrate that MPyV VP1-VLPs can be used as a delivery system into mammalian cells.

- Disassemble and reassemble the VLPs in the presence of model cargo cyclodextrin (CD) with bound gadolinium (Gd) and fluorescein isothiocyanate (FITC) of fluorescently labeled antibody.
- Verify cargo and VLPs association
- Confirm that CD is delivered by VLPs with into the eukaryotic cell line

Aim 3: In attempt to increase drug and gene delivery by enhanced endosome escape prepare histidine (His) modified MPyV VP1-VLPs and determine their endosome escape properties.

- In a donor plasmid of baculovirus expression system modify the DNA sequence of MPyV VP1 gene in the DE loop with His_6 coding oligonucleotide.
- Produce modified His-VLPs in baculovirus expression system.
- Optimize the isolation of His-VLPs for the best yield
- Determine the endosome escape properties of His-VLPs

4. Material and methods

4.1 Material

4.1.1 Frequently used solutions

1M Tris-HCl:	Tris-(hydroxymethyl)-aminomethane (Serva) in dH_2O, required pH adjusted using HCl (Lachner)
Buffer B:	10 mM Tris-HCl, pH 7.4 (Serva) 150 mM NaCl (Lachner) 0.01 mM $CaCl_2$ (Sigma-Aldrich)
Phosphate buffered saline (PBS):	137 mM NaCl (Lachner) 2.7 mM KCl (Lachema) 10 mM Na_2HPO_4 (Penta) 1.8 mM KH_2PO_4 (Lachner) pH 7.4
0.1M EGTA, pH 8.0	EGTA (Serva) in demiH_2O, pH adjusted with NaOH (Sigma-Aldrich)
0.5M EDTA, pH 8.0	$Na_2EDTA.2H_2O$ (EDTA, disodium salt, dihydrate, Serva) in dH_2O, pH adjusted with NaOH (Sigma-Aldrich)
Insect medium with serum:	TNM-FH insect medium (Sigma-Aldrich) 10% Foetal Bovine Serum (FBS; Gibco) 1/100 volume of antibiotic mixture for tissue cultures (TC)
Serum-free insect medium:	TNM-FH insect medium (Sigma-Aldrich)
DMEM with serum:	Dulbecco's Modified Eagle's Medium (Sigma-Aldrich) 10% FBS (Gibco) 2mM L-glutamine (GlutaMAX by Gibco) 1/100 volume of antibiotic mixture for TC

Serum-free DMEM:	Dulbecco's Modified Eagle's Medium (Sigma-Aldrich) 2mM L-glutamine (GlutaMAX by Gibco)
Antibiotic mixture for TC (KRD):	100x concentrated solution, 1 ml contains: 10000 units of penicillin 10 mg streptomycin 25 mg amphotericine B

4.1.2 Kits and other tools

Nucleospin® Gel and PCR Clean-up Kit (Machinery-Nagel)

- for PCR product purification
- for DNA fragment gel extraction
- manual: http://www.mn-net.com/Portals/8/attachments/Redakteure_Bio/Protocols/DNA%20clean-up/UM_PCRcleanup_Gelex_NSGelPCR.pdf

High Pure Plasmid Isolation Kit (Roche)

- for isolation of purified plasmid DNA by alkaline method
- manual: https://pim-eservices.roche.com/LifeScience/Document/2db950a5-9e27-e411-ed82-00215a9b0ba8

GenElute™ Plasmid Miniprep Kit (Sigma-Aldirch)

- for minipreparation of plasmid DNA from *E. coli* cultures
- manual: https://www.sigmaaldrich.com/content/dam/sigma-aldrich/docs/Sigma/Bulletin/pln70bul.pdf

GenElute™ RNA/DNA/protein purification Kit (Sigma-Aldrich)

- for isolation of genomic DNA, bacmids
- manual: http://www.sigmaaldrich.com/content/dam/sigma-aldrich/docs/Sigma/Bulletin/1/e5163bul.pdf

Dynabeads® His-tag isolation and pulldown (Invitrogen)

- magnetic beads for His-tag protein isolation
- cobalt-based immobilized metal affinity chromatography (IMAC) chemistry
- manual:

https://tools.thermofisher.com/content/sfs/manuals/DynabeadsHisTagIsolationPulldown_man.pdf

HisTrap FF Crude columns (GE Healthcare Life Sciences)

- Ni Sepharose prepacked columns for His-tag protein isolation
- immobilized metal affinity chromatography (IMAC)
- manual: http://wolfson.huji.ac.il/purification/PDF/Tag_Protein_Purification/Ni-NTA/AMERSHAM_HisTrapFFcrude.pdf

His-select® Nickel Affinity Gel (Sigma-Aldrich)

- Ni Sepharose beads for His-tag protein isolation
- immobilized metal affinity chromatography (IMAC)
- manual: http://www.sigmaaldrich.com/content/dam/sigma-aldrich/docs/Sigma/Bulletin/p6611bul.pdf

Slide-A-Lyzer® MINI Dialysis Devices (Thermo Scientific)

- mini dialysis devices
- manual: https://tools.thermofisher.com/content/sfs/manuals/MAN0011740_SlideALyzer_MINI_Dialy_Device_UG.pdf

4.1.3 Equipment

Centrifuge 3K30 (Sigma-Aldrich), rotors 12171 and 19776-H

Centrifuge GS-15R (Beckman)

Centrifuge Megafuge 1.0R (Heraeus Sepatech)

Centrifuge Microfuge (Beckman)

CO_2 thermostat (Forma Scientific)

Confocal microscope ZMS 880 (Zeiss)

Cultivation shaker Orbi-Safe TS (Gallenkamp)

Cultivation shaker Orbital Shaker (Forma Scientific)

Electroporator Gene Pulser Apparatus (Bio-Rad)

Fluorescence microscope BX-60 (Olympus)

Fluorometer Molecular Imager FX (Bio-Rad)

Horizontal agarose electrophoresis apparatus multiSub Mini (Cleaver)

Laminar flow box (Forma Scientific)

Magnetic mixer B212 (Bibby)

Magnetic mixer Big Squid (Ika)

Microcentrifuge Microfuge (Beckman), rotor F241.5

Nanodrop – Spectrofotometr ND-1000 (NanoDrop Technologies)

PCR cycler Mastercycler EPgradient S (Eppendorf)

pH meter PH 114 (Snail Instruments)

pH meter S20 SevenEasy (Mettler Toledo)

Protein electrophoresis apparatus (Bio-Rad)

Quibit Fluorometer (Invitrogen)

Refractometer ABBE (Carl Zeiss Jena)

Shaker Duomax 1030 (Heidoph)

Shaker 30 (Labnet)

Side light magnifier (Olympus)

Sonicator Bransonic 5 (Cole-Parmer Instrument Company)

Sonicator Soniprep 150 (Schoeller Pharmacia Praha)

Sonicator UP50H (Schoeller Pharmacia Praha)

Spectrophotometer Spekol 11 (Carl Zeiss-Jena)

Sucrose gradient maker Gradient Master (BioComp)

Thermoblock CH-100 (Biosan)

Thermostat TCH 100 and Labtech LIB-080M

Transmission electron microscope JEOL JEM 1200EX

Ultracentrifuge Optima TM L-90K, rotor SW41 (Beckman)

UV transluminator (BioLum)

Voltage source Consort EV265 (Isogen)

Voltage source E-C Apparatus EC3000P (Lehman)

Voltage source Gene Line Power Supply (Beckman)

Voltage source OSP-250L Power Supply (Lightning Volt)

Vortex-Genie (Scientific Industries)

Western blot apparatus (Bio-Rad)

4.1.4 Molecular weight markers

DNA length marker

GeneRuler 1kb Plus DNA Ladder (Fermentas) – fragment sizes (bp): 20000; 10000; 7000; 5000; 4000; 3000; 2000; 1500; 1000; 700; 500; 400; 300; 200; 75

SDS-PAGE molecule weight marker (Sigma-Aldrich):

α2-macroglobulin (173 kDa)

β-galactosidase (114 kDa)

Phosphofructokinase (96 kDa)

Pyruvate kinase (66 kDa)

Fumarase (58 kDa)

Lactate dehydrogenase (38 kDa)

Triosephosphate isomerase (32 kDa)

4.1.5 Antibodies

Primary antibodies:

- MαVP1-D4: mouse monoclonal IgG antibody anti DE loop of MPyV VP1; dilution 1:5 – 1:20 (Morávková 2001)
- MαVP1-A: mouse monoclonal IgG antibody anti C-terminal sequence epitope of MPyV VP1; dilution 1:100 (Forstová et al., 1993)
- RbαVP1: rabbit polyclonal IgG antibody anti MPyV VP1; dilution 1:5000 (laboratory production by Exbio)
- GαFITC: goat polyclonal IgG antibody anti fluorescein isothiocyanate; dilution 1:500 (Abcam)
- MαHis: mouse monoclonal IgG antibody anti histidine tag; dilution 1:500 (Invitrogen)
- RαLT-1: rat monoclonal IgG antibody anti MPyV large T antigen 1:50 (Dilworth and Griffin, 1982)
- RbαSNAP: rabbit polyclonal IgG antibody anti SNAP-tag; dilution 1:300 (New England BioLabs)
- RbαGAPDH: rabbit polyclonal IgG antibody anti glyceraldehyde 3-phosphate dehydrogenase (GAPDH); dilution 1:500 (Santa Cruz Biotechnology)

Secondary antibodies:

Peroxidase:

- GαM Px: Goat antibodies anti mouse antibodies conjugated with horseradish peroxidase; dilution 1:1000 (BioRad)
- DαG Px: Donkey antibodies anti goat antibodies conjugated with horseradish peroxidase; dilution 1:500 (Santa Cruz Biotechnology)
- GαRb Px: Goat antibodies anti rabbit antibodies conjugated with horseradish peroxidase; dilution 1:1000 (Biorad)

Fluorescent:

- GαRb AF488: Goat antibodies anti rabbit antibodies conjugated with Alexa Fluor 488; dilution 1:1000 (Molecular Probes)
- GαRb AF546: Goat antibodies anti rabbit antibodies conjugated with Alexa Fluor 546; dilution 1:1000 (Molecular Probes)
- GαR AF488: Goat antibodies anti rat antibodies conjugated with Alexa Fluor 488; dilution 1:1000 (Molecular Probes)
- DαG AF488: Donkey antibodies anti goat antibodies conjugated with Alexa Fluor 488; dilution 1:1000 (Molecular Probes)
- DαRb AF546: Donkey antibodies anti rabbit antibodies conjugated with Alexa Fluor 546; dilution 1:1000 (Molecular Probes)
- DαM AF488: Donkey antibodies anti mouse antibodies conjugated with Alexa Fluor 488; dilution 1:1000 (Molecular Probes)
- DαR AF488: Donkey antibodies anti rat antibodies conjugated with Alexa Fluor 488; dilution 1:1000 (Molecular Probes)
- SwαM FITC: Swine antibodies anti mouse antibodies conjugated with fluorescein isothiocanate (ServaPharma)
- GαM Atto594: Goat anti mouse antibodies conjugated with Atto 594 (Sigma Aldrich)

4.1.6 Primers for PCR and oligonucleotides

The synthesis of primers and oligonucleotides was made by Integrated DNA Technologies (IDT)

Primers:

MK(BG)3 (forward primer for DE loop insertion control):
5'-GAT GAT GGA TCC GGG TCT GGC TCT GGA ATT TCC ACT CCA GTG-3'

MK(BG)2 (reverse primer for DE loop insertion control):
5'-GAT GAT GGA TCC TGA GCC GCT ACC GGG TTT GTT GAA CCC ATG-3'

pUC/M13 -F (primer for bacmid control):
5´- CCC AGT CAC GAC GTT GTA AAA CG – 3´

pUC/M13 -R (primer for bacmid control):
5´- AGC GGA TAA CAA TTT CAC ACA GG – 3´

MK1: MPyV VP1-1F:

5‘-GAT GAT GAA TCC **ATG** GCC CCC AAA AGA AAA AGC GGC-3‘

EcoRI **start** complementary to VP1

MK4: MPyV VP-4R:

5‘- GCT GCT GGT ACC **TTA** ATT TCC AGG AAA TAC AGT CTT TG-3‘

KpnI **stop** complementary to VP1

BC-RSins-Fw:

5‘-GCT AGC ACC GGT GGC GCC GGG GGA TCA GGA GGG CAA TAC TAT GGT TGG AGC-3‘

NheI AgeI EheI gly-ser linker complementary to VP1

BC-RSins-Rw:

5‘-GCC GCC ACC GGT GCT AGC GCC GCC ACT ACC TCC CTC TGT TAG GCT TTC AGG-3‘

EheI AgeI NheI gly-ser linker complementary to VP1

MPyV VP1_Sal-RW:

5‘-GCT GCT GTC GAC **TTA** ATT TCC AGG AAA TAC AGT CTT TG-3‘

SalI **stop** complementary to VP1

Phosphorylated oligonucleotides:

Old HIS-oligo 1:

5´-(Phos) GAT CCC ACC ACC ACC ACC ACC ACG-3´

Old HIS-oligo 2:

5´-(Phos) CGT GGT GGT GGT GGT GGT GGG ATC-3´

New HIS-oligo 1:

5´-(Phos) GAT CCG GTC ACC ATC ACC ATC ACC ACG-3´

New HIS-oligo 2:

5´-(Phos) GAT CCG TGG TGA TGG TGA TGG TGA CCG-3´

4.1.7 Vectors

pFastBac1_VP1_7less

- Baculovirus donor vector pFastBac™1 vector with deleted BamHI restriction site and inserted MPyV VP1 sequence with modified DE loop. The DE loop has deleted 7 amino acids replaced with DNA sequence coding for glycine-serine polylinker and BamHI restriction site. (Kojzarová, 2011)

pFastBac1_noBamHI

- Baculovirus donor vector pFastBac™1 vector with deleted BamHI restriction site. (Kojzarová, 2011)

pFastBacDUAL VP1/VP3

- Baculovirus donor vector with full unchanged MPyV VP1 sequence used as a PCR template (Bouřa et al., 2005)

pmaxGFP

- control plasmid carrying a *GFP* gene for expression an mammalian cells (Amaxa® kit, Lonza)

$pSNAP_f$ vector

- plasmid for mammalian cells transfection and SNAP-tag protein expression in the cytoplasm (New England BioLabs)

4.1.8 Viruses

MPyV (Mouse Polyomavirus)

- BG strain (GenBank, accession number: AF442959)
- The DNA sequence of its capsid proteins is used in the expression system for preparation of VLPs (*VP1* genome sequence 2932 – 4086, *VP2* genome sequence 4055-5014, *VP3* genome sequence 4055 – 4669).
- A stock of virus with protein concentration 1mg/ml and infectivity $3x10^8$ PFU/ml (plaque forming units) and $3x10^7$ FU/ml (fluorescence units) was used for infectivity experiments.

AcVP1

- recombinant baculovirus derived from *Autographa californica* Multiple Nuclear Polyhedrosis Virus
- produces MPyV VP1 protein
- (Forstová et al., 1993)

4.1.9 Bacterial strains

***Escherichia coli* Stellar™ Competent cells (Clonetech)**

- a chemically competent strain for a donor plasmid production
- high transformation efficiency
- manual: http://www.clontech.com/CZ/Products/Cloning_and_Competent_Cells/Competent_Cells/ibcGetAttachment.jsp?cItemId=17313&fileId=5877577&sitex=10023:22372:US

***Escherichia coli* DH10Bac**

- a component of the baculovirus Bac-to-Bac® expression system
- a strain containing a bacmid able to recombine with a donor plasmid pFastBac
- recombination can be detected thanks to lacZ gene
- (collection of Department of Genetics and Microbiology)

4.1.10 Eukaryotic cell lines

Sf9

- insect cell line derived from ovaries of *Spodoptera frugiperda* butterfly suitable for baculovirus infection (ATCC No. CRL—1711)

NIH 3T6

- stable mouse fibroblast cell line suitable for MPyV infection (prof. Griffin, Royal Postgraduate School, London)

293TT

- modified human embryonal kidney cells (HEK-293) by integration of SV40 polyomavirus genome
- suitable for recombinant protein expression

4.1.11 Baculovirus expression system (Invitrogen)

The recombinant baculovirus expression system Bac-to-Bac® was used for the construction of modified MPyV VP1-VLPs. The baculovirus expression system is based on preparation of recombinant baculovirus that encodes for the gene of interest under strong polyhedrin promoter. Polyhedrin is a baculovirus protein expressed in late phase of infection in large quantities thus the same can be achieved with the protein of interest. Bac-to-Bac® is a method based on site-specific transposition for preparation of a recombinant baculovirus. This method is much faster than the original method using homologous recombination where the recombinant baculovirus must be selected, isolated and purified in the plaque assay.

In principle, the gene encoding for the protein of interest is cloned into a donor plasmid. pFastBac™1 was used in this work. The donor plasmid is then isolated used for transformation of DH10Bac *E. coli* electrocompetent cells. DH10Bac strain contains 136kb bacmid which is a plasmid containing kanamcin resistance and a baculovirus genome with a gene for LacZα. DH10Bac strain also carries a helper plasmid encoding for a transposase. The transposase allows site-specific transposition between mini-Tn7 elements on pFastBac1 donor plasmid and mini-attTn7 target sites on bacmid. If the transposition is successful and correct, the LacZα gene is disrupted and the positive bacterial colonies on media with inducing agent IPTG and the chromogenic substrate X-gal are white whereas the ones with incorrect transposition are white. The white colonies contain recombinant bacmid which is isolated, tested and used for Sf9 cells transfection using the Cellfectin II reagent (Invitrogen). Such transfection leads to production of a recombinant baculovirus into the medium and the protein of interest production in the cells.
The "Bac-to-bac® instruction manual" (Invitrogen) was used for the recombinant baculovirus preparation: http://tools.thermofisher.com/content/sfs/manuals/bactobac_man.pdf
Cellfectin® II reagent manual was used for transfection:
https://tools.thermofisher.com/content/sfs/manuals/CellfectinIIReagent_protocol.pdf

4.1.12 SNAP-Trap assay

(modified according to Geiger et al., 2013)
SNAP-Trap assay is suitable fool for studies of protein cellular localization. It is based on protein tag SNAP (SNAP-tag, 20 kDa) covalent binding to its substrate benzyl guanine (BG-GLA-NHS, New England BioLabs, chapter 2.3.3.2). SNAP-tag can be used as a reporter gene of selected cellular compartment. Expressed alone localizes to cytoplasm or it can be expressed as a fusion protein for targeting to mitochondria, endoplasmic reticulum and other organelles. If the protein of interest is modified with BG-GLA-NHS it only interacts with SNAP-tag when in the same cellular compartment. Such interaction is studied using SDS-PAGE and western blot analysis. We used this assay to study endosome escape properties of histidine modified VLPs.
First, selected cell line (293TT) was transfected with plasmid encoding SNAP-tag ($pSNAP_f$) using TurboFect™ reagent (chapter 4.2.6.5) and after 24 - 48 hrs a cell lysate was prepared according to Geiger et al., 2013. This was a control lysate. Then, VLPs or MPyV were dialyzed over night at 4 °C from buffer B to carbonate buffer (150mM $NaHCO_3$, pH 8.3, 0.01mM $CaCl_2$) because Tris in buffer B blocks the SNAP substrate benzyl guanine (BG-GLA-NHS) binding to lysine residues of the protein via NHS ester (chapter 5.2.4.4). 6 µl of 20mM BG-GLA-NHS (New England BioLabs) in DMSO was used per 100 µg of protein and rotated over night at 4 °C. The solution was then transferred into SW41 ultracentrifugation test tube and diluted in buffer B which blocked all of the unbound BG-GLA-NHS. The sample was centrifuged for 3 hrs, 35 000 rpm (rotor SW41) at 4 °C

through high 10% sucrose cushion to remove unbound substrate from VLPs (chapter 4.2.4.3). After the supernatant was removed and the pellet was dissolved in 100 µl of buffer B and washed with short sonication with additional 50 µl of buffer B. The protein concentration was measured using Quibit Fluorometer.

BG-GLA-NHS modification was then tested. 20 µl of cell lysate from SNAP-tag transfected 293TT cells was mixed with 300 ng of BG-modified VLPs and incubated for 30 min at 37°C. After, 5x sample buffer for SDS PAGE was added, the samples were boiled for 5 minutes and SDS PAGE followed by western blot and VP1 and SNAP immunodetection with chemiluminescence (chapters 4.2.3.3, 4.2.3.5 and 4.2.3.6). If the modification was successful the SNAP signal would appear in molecular weight of VP1 (45 kDa) or higher.

With BG-modified VLPs (BG-VLPs) or virus (BG-virus) the endosome escape experiment was performed. 293TT cells were seeded on 12-well dish. Confluent cells on 10cm dish were washed with 5 ml of Versen and resuspended using 1 ml of Trypsin, incubated few minutes at 37°C. 9 ml of 293TT medium were added and the cells were well resuspended. 175 µl per well of the cell suspension were diluted in 25 ml media and 2 ml of 293TT suspension were seeded per well and incubated 24 hrs. 293TT cells in 12-well dish were transfected with $pSNAP_f$ plasmid using TurboFect™ transfection reagent (chapter 4.2.6.5) and incubated for 24 hrs. After, the sample BG-VLPs were added in 1 mg per well in serum-free DMEM and the pseudoinfection lasted 6 hrs (chapter 4.2.6.6). The cells were then collected into the media, transferred into the micro test tubes and centrifuged for 5 min at 300 g. The supernatant was removed and the cells were resuspended in 1 ml of PBS and centrifuged again. This step was repeated once. Finally the cell pellet (approx. 10 µl) was mixed with 20 µl of 1.5x concentrated sample buffer for SDS PAGE, boiled for 5 minutes and sonicated 4 times with hand sonicator. The samples were then used in SDS PAGE and western blot and VP1 and SNAP-tag were detected using immunodetection with chemiluminescence.

4.2 Methods

4.2.1 Sterilization

Laboratory glass was closed using an aluminium foil and sterilized with hot air at 160 °C for 3 hrs. Small tools such as tweezers or microbiological hockey sticks were immersed in ethanol and sterilized in flame. Micro test tubes, micropipette tips and solutions were sterilized in an autoclave at 127 °C, 120 kPa for 30 min. Some solutions cannot be sterilized in an autoclave, thus they were filtered through 0.2 µm filters.

4.2.2 Work with DNA

4.2.2.1 Horizontal agarose electrophoresis

(Green and Sambrook, 2012)

Horizontal agarose electrophoresis allows separation of DNA molecules based on their size. This method was used frequently to detect isolation of plasmids, PCR products and fragments of DNA after restriction endonuclease digestion.

The agarose gel was prepared by boiling the required amount of agarose in 30 ml 0.5x concentrated TBE buffer (Tris-borate-EDTA) using microwave until completely dissolved. Usually 1% agarose gel was prepared which required 0.3 g of agarose. When the gel cooled to approx. 50°C, 15 µl of 1000x concentrated ethidium bromide were added. Then the gel was poured into a gel tray with rubber on two sides and a gel comb placed 1 cm below the upper edge of the gel. The gel was left to solidify for approx. 30 min at room temperature. After, the gel comb was removed as well as the rubber sides. The gel in a tray was placed into an electrophoretic apparatus and covered with 0.5x concentrated TBE buffer. The samples were mixed with 6x DNA Loading Dye to achieve 1x DNA Loading Dye concentration and loaded into the wells in the gel. The electrophoresis ran in 70 V (5 V/cm) for 50-60 min. The DNA was visualized using an UV transluminator and photographed.

Material:

Agarose (Sigma-Aldrich)

0.5x TBE buffer: 20mM Tris-HCl (pH 8.0) (Serva)
45mM boric acid (Serva)
1mM EDTA-NaOH (pH 8.0) (Serva)

Ethidium bromide (Serva) 10mg/ml of H_2O

6x concentrated DNA Loading Dye (Fermentas)

4.2.2.2 Horizontal agarose electrophoresis for DNA isolation

The protocol described in 4.2.2.1 was used. Instead of 1% Sigma agarose only a 1:1 ratio of Sigma agarose and NuSieve low melting agarose in 1x TAE (Tris-acetate-EDTA) was used. After electrophoresis, the selected DNA fragments were cut out of the gel under an UV transluminator and transferred into pre-weighed micro test tubes for further work.

Material:

Agarose (Sigma-Aldrich)

NuSieve low melting agarose (Lonza)

1x TAE: 40mM Tris-HCl (pH 8.0) (Serva)
20mM acetic acid (Penta)

1mM EDTA-NaOH (pH 8.0) (Serva)

Ethidium bromide (Serva) 10mg/ml of H_2O

6x concentrated DNA Loading Dye (Fermentas)

4.2.2.3 Oligonucleotides annealing

Oligonucleotides were diluted in PCR H_2O to reach 100mM concentration. 300 pmol (3µl) of each oligonucleotide were added into 30 µl HD buffer. The mixture was denatured for 5 minutes at 99 °C and then it was cooled down continuously to 25°C for 5 hours in PCR cycler to achieve annealing.

Material:

HD buffer: 70mM Tris-HCl (pH 7.6) (Serva)
10mM $MgCl_2$ (Sigma-Aldrich)
5mM Dithiotreitol (DTT; Sigma-Aldrich)
50mM NaCl (Lachema)
in ddH_2O

4.2.2.4 Polymerase chain reaction (PCR) for DNA amplification

PCR was used for multiplication of DNA fragments used for further work and as a method to verify presence of a sequence in given DNA molecule.

The PCR mixture was prepared on ice. The DNA polymerase was added last just before the beginning of PCR. Samples in 0.2ml thin-walled micro test tubes were placed in PCR cycler with required program (see below). PCR results were confirmed using horizontal agarose electrophoresis and immediately used or stored at -20°C.

Colony PCR

Colony PCR was used to detect presence of insert after ligation directly in a bacterial culture. Sample of chosen bacterial colony on agar plate was transferred with sterile toothpick into 50 µl of PCR H_2O and well resuspended. The cell suspension was incubated for 5 min at 96 °C, left to cool down and used as a template in the PCR reaction.

PCR mixture (20 µl):

2.5 µl template (bacteria in water)

0.6 µl forward primer

0.6 µl reverse primer

0.4 µl 40mM dNTPs (each dNTP 10mM; New England BioLabs)

0.2 µl Vent polymerase (New England BioLabs)

2 µl ThermoBuffer (New England BioLabs)

2 µl Triton 1% (Serva)

11.7 µl PCR H_2O

PCR program:

3 min	95 °C (initial denaturation)	
30 s	95 °C	
30 s	temperature based on the primers	30x
60 s	72 °C	
10 min	72°C	

PCR detection of inserted sequence in recombinant bacmid

PCR mixture (50 µl):

3 µl template

1.5 µl forward primer

1.5 µl reverse primer

1 µl 40 mM dNTPs (each dNTP 10mM; New England BioLabs)

5 µl Thermobuffer (2mM Mg^{2+}) (New England BioLabs)

36.5 µl PCR H_2O

1 µl 100mM $MgSO_4$ (New England BioLabs)

0.5 µl Vent polymerase (New England BioLabs)

PCR program:

3 min	94 °C	
30 s	94 °C	
30 s	53 °C	30x
5 min	72 °C	
10 min	72°C	

PCR for multiplication of DNA fragments

PCR mixture (50 µl):

2 µl template DNA (5 ng DNA)

1.5 µl forward primer

1.5 µl reverse primer

1 µl 40mM dNTPs (each dNTP 10mM; New England BioLabs)

0.5µl Vent polymerase (New England BioLabs)

5 µl Thermobuffer (New England BioLabs)

38.5 µl ddH_2O

PCR program:

3 min	94 °C	
40 s	94 °C	
50 s	61 °C	30x
60 s	72 °C	
10 min	72°C	

4.2.2.5 Restriction endonuclease digestion of DNA

Recommended protocol from the manufacturer (Fermentas or Takara) for restriction endonuclease digestion of DNA was used. The mixture was incubated in optimal conditions for 2 – 4 hrs after deactivated as recommended.

Reaction mixture:

Sample DNA

Recommended buffer

Restriction endonuclease

ddH_2O

4.2.2.6 5'-end dephosphorylation of a vector

After restriction endonuclease digestion, the ends of vector were dephosphorylated using FastAP™ alkalic phosphatase (1unit/µl, Fermentas), 1unit for 1 µg of DNA and incubated 20 min at 37°C and after inactivated 5 min at 75°C.

4.2.2.7 Ligation

Fragments of DNA were ligated into selected vector after restriction endonuclease digestion. Classical ligation ratio was 3:1 (insert to vector) but also 10:1 and 50:1 ratios were used in some cases.

Reaction mixture:

50 ng vector

required amount of insert

2 µl T4 DNA ligase buffer (Fermentas)

0.2 µl T4 DNA ligase (Fermentas)

ddH_2O to final volume 20µl

4.2.2.8 Sequencing

Sequencing reaction and analysis was performed by Laboratory of DNA sequencing (Faculty of Science, Charles Univerzity in Prague). The laboratory uses 2 analyzers from Applied Biosystems: 3130 Genetic Analyzer with 4 capillaries and 3130XL Genetic Analyzer with 16 capillaries.

Sequencing reaction samples were prepared into 0,2ml thin-walled micro test tubes based on Laboratory of DNA sequencing recommendation. That was mixing the template (3-5ng/100bp for plasmid, 5-10ng/100bp for PCR products) with sequencing primer (5 pmol) and ddH_2O to final volume 8 µl.

4.2.3 Work with proteins

4.2.3.1 Preparation of a cell lysate

Infected Sf9 cells from a dish (diameter 6 cm) were collected into the medium and transferred to 15ml Falcon tube. They were centrifuged 7 min at 2000 rpm, the medium was stored as an inoculum and the pellet was resuspended in 1 ml PBS and transferred into a micro test tube. It was centrifuged 20s at 10000 rpm (Centrifuge Microfuge, Beckman) and then the supernatant was removed. The pellet was resuspended in 80 µl of SDS-free RIPA buffer and incubated 20 min on ice. After it was mixed thoroughly and centrifuged 5 min at 4°C at maximum speed. 1 µl of the supernatant was used on dot blot.

Material:

SDS-free RIPA buffer: 150mM NaCl (Lachner)
5mM EDTA (Sigma-Aldrich)
50mM Tris – HCl (pH = 7,4) (Serva)
0,05% Nonidet P-40 (Sigma-Aldrich)
1% deoxycholic acid (Sigma-Aldrich)
1% Triton X-100 (Serva)

4.2.3.2 Dot blot

(Green and Sambrook, 2012)

1-2 µl of protein samples were applied on a nitrocellulose membrane. After the samples dried, the membrane was used for detection on fluorometer Molecular Imager FX (Bio-Rad) (if fluorescent agent was present) or for immunological detection (immuno-dot blot).

Material:

Nitrocellulose membrane NC45 (Serva)

4.2.3.3 SDS-PAGE

(Green and Sambrook, 2012)

Sample preparation:

Samples were mixed in 4:1 ratio with 5x concentrated Laemli buffer (sample buffer) and incubated 5 minutes at 100 °C.

Gel preparation:

The BioRad apparatus was used. The electrophoretic glasses were cleaned thoroughly with cleaning powder, distilled water and denatured ethanol. Dried glasses were placed to the gel preparation apparatus and the end of the gel comb was marked. The separation gel was loaded approximately 0.5 cm below the gel comb end, overlayered with demineralized water and polymerized for approx. 30 min.

After, the water was removed and dried and the stacking gel was loaded to the top of the apparatus and the gel comb was placed on top. The gel polymerized for approx. 20 min. The comb was removed and the gel was transferred into the electrophoretic apparatus. The electrophoretic apparatus was filled with 1x electrophoretic buffer.

Protein separation:

The marker of molecular weight and the samples were loaded into the wells. The apparatus was closed and connected to the source of voltage. The electrophoresis was running at 80 V for the first 30 min and after at 120 V in Biorad apparatus until the samples reached the bottom of the gel (approx. 1.5 hrs).

Material

5x Laemli buffer:	1.25% SDS (sodium dodecyl sulfate; Sigma-Aldrich)
	50mM Tris – HCl (pH = 6,8) (Serva)
	25% ß-mercaptoethanol (Serva)
	50% (v/v) glycerol (Lachema)
	0,005% bromphenol blue (Lachema)
Separating gel:	4 ml 30% acrylamide (Serva)
	4.5 ml Tris-HCl (pH = 8,8) (Serva)
	120 µl 10% SDS (Sigma)
	3.25 ml ddH2O
	40 µl 10% APS (ammonium persulfate; Serva)
	8.5 µl TEMED (tetramethylethylenediamine; Sigma)
Stacking gel:	0.5 ml 30% acrylamide (Serva)
	0.375 ml Tris – HCl (pH = 6,8) (Sigma)

30 µl 10% SDS (Sigma)

2.11 ml ddH2O

20 µl 10% APS (Serva)

5µl TEMED (Sigma)

APS and TEMED were added just before loading of the gel into the apparatus.

Electrophoretic buffer: 25mM Tris (Serva)

192mM glycine (Sigma)

0.1 % SDS (Sigma)

pH = 8.3

4.2.3.4 Gel staining after SDS-PAGE

The gels were washed 3x 5 min in demineralized water before incubating in the GelCode™ Blue Stain for at least 60 min up to overnight. The gel was then washed in distilled water several times and scanned.

Material:

GelCode™ Blue Stain Reagent (ThermoFisher)

4.2.3.5 Western blot

(Green and Sambrook, 2012)

Filter papers, Whatman papers and the nitrocellulose membrane of the gel size were prepared. The blotting buffer was cooled to 4°C. The polyacrylamide gel after SDS-PAGE was incubated for 10 min in the blotting buffer. The filter papers, Whatman papers and the nitrocellulose membrane were soaked in the blotting buffer before adding to the blotting apparatus. The order was 4 filter papers, 1 Whatman, polyacrylamide gel, nitrocellulose membrane, 1 Whatman, 4 filter papers. All layers were smoothened out to remove any bubbles. Prepared blotting sandwich was inserted into the blotting apparatus. The blotting took 1.5 – 3 hrs at 250 mA. After, the nitrocellulose membrane was washed in demineralized water and used for immunodetection (chapter 4.2.3.6).

Material:

Nitrocellulose membrane NC 45 (Serva)

Whatman and filter papers

Blotting buffer: 25mM Tris (Serva)

195 mM glycine (Sigma-Aldrich)

20% methanol (Lachema)

pH 8.3

4.2.3.6 Immunodetection of proteins immobilized on nitrocellulose membrane

A nitrocellulose membrane with immobilized proteins was incubated for 30 min in 5% fat-free milk in PBS. After, it was incubated 1.5 hrs with primary antibody diluted as recommended in 5% fat-free milk in PBS. It was then washed 3 times for 10 min in PBS before incubated 30 min with secondary antibody conjugated with horse radish peroxidase diluted as recommended in 5% fat-free milk in PBS. Finally it was wash 3 times for 10 min in PBS.

The detection was performed in a dark room using enhanced chemiluminescence (ECL). The membrane was immersed into mixture of chemiluminescence solutions ECL 1 and 2 for 20s, dried, placed into a foil and an rtg film was placed on top. The exposition was set based on the signal. The film was evoked regularly with developer and stabilizer baths.

Material:

PBS

Dried fat-free milk

Luminol (3-aminophthalygrazide; Sigma-Aldrich A8511): 250mM solution in DMSO, 200µl aliquots stored at -70°C in the dark

Coumaric acid (Sigma-Aldrich C9008): 90mM solution in DMSO, 80µl aliquots stored at -70°C in the dark

ECL chemiluminescence solution 1:	80 µl Coumaric acid
	200 µl Luminol
	2 ml 1M Tris-HCl (pH 8.5) (Sigma-Aldrich)
	18 ml dH_2O
ECL chemiluminescence solution 2:	12 µl H_2O_2 (30% Sigma-Aldrich)
	2 ml 1M Tris-HCl (pH 8.5) (Sigma-Aldrich)
	18 ml dH_2O

Both ECL solutions were mixed just before use in 1:1 ratio.

RTG film (Foma)

Developer (Foma)

Stabilizer (Foma)

4.2.3.7 Protein concentration measurement

The protein concentration was measured using Quibit Fluorometer (Invitrogen) and the procedure described in the manual:

http://fg.cns.utexas.edu/fg/research_archive_of_manuals_files/qubit.pdfhttp://fg.cns.utexas.edu/fg/research_archive_of_manuals_files/qubit.pdf

4.2.4 Work with VLPs

4.2.4.1 Isopycnic centrifugation in a CsCl gradient

(Türler and Beard, 1985)

Isopycnic centrifugation in the CsCl gradient is a method that separates large biomolecules based on their buoyant density. This way the virus like particles can be isolated from a cell lysate.

The cell lysate was transferred into the ultracentrifuge (UCF) test tube, the Buffer B was added up to the final weight of 8 g and 3.7 g of CsCl was added and dissolved. Refractive index was measured to be between 1.363 – 1.364. The sample was overlayered with paraffin oil and the weight was balanced. After the UCF test tubes were transferred into the UCF cuvettes and centrifuged 20-22 hrs at 18°C and 35000 rpm (rotor SW41). The fractions were then separated with gradient separator into micro test tubes. The refractive index of each fraction was measures and 1 µl of each fraction was used for immuno-dot blot (chapter 4.2.3.6). The fractions were connected based on the refractive index and dot blot results for dialysis.

Material:

CsCl (Serva)

Buffer B

Paraffin oil (Rieder de Häen)

4.2.4.2 Isokinetic centrifugation in a sucrose gradient

Isokinetic centrifugation allows separation of particles based on their size. This way the VLPs can be separated from debris, unfolded particles and also allows separation of VLPs of different sizes.

The 10-40% sucrose gradient was prepared using a gradient maker. 10% and 40% sucrose in Buffer B were filter-sterilized and loaded into an UCF test tube according to the gradient maker manual. First 10% sucrose was loaded and then underlayred with 40% sucrose so there was 400 µl left for a sample. Then it was placed on a gradient maker which made the linear gradient. 400 µl of the sample was loaded on top of the gradient. The weight of the UCF test tubes was balanced and corrected with Buffer B. The samples were centrifuged 2 hrs at 4 °C and 35000 rpm (rotor SW41) with slow acceleration and deceleration. The fractions were then separated with gradient separator into micro test tubes. The refractive index of each fraction was measure and 1 µl was used for immuno-dot blot (chapter 4.2.3.6). The fractions were connected based on the refractive index and dot blot results for dialysis.

Material:

Sucrose (Serva)

Buffer B

4.2.4.3 Centrifugation through 10% sucrose cushion

Centrifugation through a sucrose cushion allows crude purification as well as sample concentration.

The sample was transferred into UCF test tube and the Buffer B was added approx 1.2 cm below the top. 10% sucrose solution in Buffer B was filtered through 45 μm filter. The sample in a test tube was underlayered with approx. 1 cm thick layer of 10% sucrose in Buffer B and centrifuged for 3 hr at 4°C and 35000 rpm (rotor SW41). After, the supernatant was transferred to 15 ml test tubes and the sediment was dried from sucrose and then resuspended in 100 – 200 μl of Buffer B and let dissolve on ice overnight. It was then transferred into silicon-coated test tube and the UCF test tube was washed with 50 μl of B buffer and short sonication.

Material:

Sucrose (Serva)

Buffer B

4.2.4.4 Dialysis

Dialysis membrane was cut to suitable size and boiled for 10 minutes in distilled water. The sample was transferred into the membrane and closed with clamps on both sides. The dialysis was against 100 – 200x sample volume of selected buffer overnight at 4°C while mixing, the fresh buffer was replaced at least once. The samples were concentrated by centrifugation through sucrose cushion or using PEG 20000.

The dialysis was also performed in a small scale using minidialysis devices Slide-A-Lyzer® 3.5K MWCO (Thermo Scientific) against 500x sample volume of selected buffer.

4.2.4.5 Isolation of VLPs using sonication

Pellet from recombinant baculovirus (coding for MPyV VP1 protein or VP1-His) infected Sf9 cells (chapter 4.2.6.2) was thawed and resuspended in Buffer B (1.3 ml/10cm dish). The suspension was sonicated 3x 45 s with amplitude 10 μ in an ice bath. The breaking of the cells was verified with light microscopy. If the cells weren't disrupted completely, 1 or 2 sonication rounds followed. After sonication, the suspension was centrifuged for 15 min at 4°C and 2000x g.. The supernatant was transferred into UCF test tube. DNase treatment followed if required ($MgCl_2$ was added to final concentration of 0.5 mmol/l and then 0.1 mg/ml of DNase I was added and incubated in room temperature for 2 hrs). Finally the sample was used for CsCl centrifugation followed by dialysis against Buffer B and the sucrose cushion centrifugation (as described above).

Material:

Buffer B

4.2.4.6 Isolation of VLPs using cell lysis

Pellet from recombinant baculovirus (coding for MPyV VP1 protein or His-VP1) infected Sf9 cells (chapter 4.2.6.2) was thawed and resuspended in the same volume of DPBS + Mg (9.5 mM). After, Triton X-100 (10%) was added to final concentration 0.25% and Benzonase® to final concentration 0.1 %. The suspension was incubated 2h at 37 °C and then at 0°C overnight. 5M NaCl was then added up to the final concentration 850mM and the sample was incubated 10 min on ice. The mixture was centrifuged 10 min at 10 000 rpm (rotor 19776-H, Centrifuge 3K30, Sigma-Aldrich) and the supernatant was transferred into an UCF test tube. The pellet was resuspended in Buffer B and 5M NaCl was added to final concenration 850 mM. The sample was incubated 10 min on ice, centrifuged 10 min at 10 000 rpm (rotor 19776-H, Centrifuge 3K30, Sigma-Aldrich) and the supernatant added to the UCF test tube. The isolation followed with CsCl gradient centrifugation, dialysis against buffer B and the sucrose cushion centrifugation.

Material:

Buffer B

Dulbecco's PBS with 9.5 mM Mg^{2+} (Lonza)

Benzonase® nuclease (Sigma-Aldrich)

Triton X-100 (Serva)

5M NaCl (Lachner)

4.2.4.7 Acidic Isolation of His-VLPs

Frozen pellets from VP1-His recombinant baculovirus infected Sf9 cells (from 10 dishes of 10 cm diameter) were resuspended in 2 ml of 50mM acetate buffer, pH 5.0. The suspension was sonicated on ice 5x 45 s with amplitude 10 μ in an ice bath. Tx-100 was added into final concentration 0.5% and mixed thoroughly. The suspension was centrifuged 10 min 3328x g 4°C. The supernatant was transferred into SF41 UCF tube. The pellet was resuspended in 1 ml of Acetate buffer and Tx-100 was added in concentration 0.5% and transferred into Eppendorf tube. It was centrifuged for 3 min at 4°C and 12500x g. The supernatant was added into UCF tube and the pellet was kept in 4°C. The CsCl gradient centrifugation followed in 50mM acetate buffer with 0.5% Tx-100.

Material:

100 mM acetate buffer pH 5.0 (from this 50 mM Acetate Buffer as working buffer)

10% Triton X-100 (added to final concentration 0.5%)

4.2.4.8 Isolation of His-VLPs using magnetic Dynabeads® for His-Tag isolation

Approximately ¼ of frozen pellet of Sf9 cells infected with recombinant baculovirus encoding for His-VP1 (from 9 dishes of 10 cm diameter) was transferred into fresh 50ml Falcon tube and resuspended in 700 µl 1x Binding/Wash Buffer (from the kit). The suspension was sonicated 3x 30 s with amplitude 10 µ in an ice bath. After DNaseI was added into final concentration of 0.1 mg/ml and incubated 20 min on ice. Then the manual Dynabeads® His-Tag Isolation and Pulldown was followed (chapter 4.1.2).

Material:

DNaseI

4.2.4.9 HisTrap FF crude 1ml column isolation of His-VLPs

Frozen pellets of Sf9 cells infected with recombinant baculovirus encoding for His-VP1 (from 8 dishes of 10 cm diameter) were used. The pellets were thawed on ice and resuspended in 4.75 ml 2x binding buffer and ½ of proteases inhibitor tablet. 250 µl of 10% Triton X-100 was added into the suspension so the final concentration was 0.5 %. 25 µl of 1M $MgCl_2$ was added so the final concentration was 5 mmol/l and finally DNase I was added so the final concentration was 0.05 mg/ml. The suspension was vortexed and incubated 30 min at 37 °C. ddH_2O was added to the suspension so the concentration of binding buffer was 1x and the lysate was stored at -20 °C. Just before the isolation the lysate was thawed on ice again, sonicated 5x30s, amplitude 8 µ in an ice bath. After it was centrifuged at 4°C and 4800x g for 20 min and the supernatant was filtrated through a 45 µm filter. pH of the filtrate was measured and adjusted to be approx. 7.4. The columns were prepared and the samples were run through the column as described in the manual (chapter 4.1.2).

Material:

Proteases inhibitor tablets (cOmplete™ ULTRA Tablets, Mini, EASY pack; Roche)
Triton X-100 (Serva)
1M $MgCl_2$ (Sigma-Aldrich)
DNaseI

2x Binding buffer:	100mM HEPES (Sigma-Aldrich)
	1000mM NaCl (Lachner)
	40mM imidazol (Serva)
	pH 7.4 (adjusted with NaOH; Sigma-Aldrich)
1x Elution buffer:	50mM HEPES (Sigma-Aldrich)
	500mM NaCl (Lachner)
	500mM imidazol (Serva)
	pH 7.4 (adjusted with HCl; Lachner)

4.2.4.10 His-select® Nickel Affinity Gel His-VLPs isolation

Flow through from 4.2.4.10 was transferred into dialysis membrane and dialyzed overnight in Wash-equilibrium buffer. The buffer was changed once after 1 hr.

The sample was then divided into 3 parts. One was left unmodified, to second imidazol was added to final concentration 20 mmol/l and to the third imidazol was added to final concentration 20 mmol/l and NaCl to 1 mol/l. The manual was followed (chapter 4.1.2) and the samples were analyzed using SDS-PAGE and western blot.

Material:

Wash-equilibrium buffer:	50mM HEPES
	0.3M NaCl
	pH 8.0
Elution buffer:	50mM HEPES
	0.3M NaCl
	250 mM imidazol
	pH 8.0
2M imidazol	

4.2.4.11 Disassembly and reassembly

(modified according to Suchanová 2011 and Mukherjee et al., 2010))

The VLPs of known protein concentration were disassembled in 14ml or 50ml mini dialysis devices Slide-A-Lyzer® 3.5K MWCO (GeneTICA). They were incubated 90 minutes in Disassembly buffer 1 (on ice, shaking) and after in Disassembly buffer 2 for 90 minutes, in fresh disassembly buffer 2 over night and again in fresh buffer 90 minutes, all shaking in 4 °C.

The dialyzed sample was transferred into 1.5ml test tubes and centrifuged for 30 min at 4°C, 20 000x g. The supernatant was transferred into a fresh test tube and its protein concentration was measured using Quibit fluorometer (Invitrogen). Also the negative staining samples for electron microscopy (EM) were prepared from the supernatant (pentamers) and pellet (aggregates). 1.5 µmol of the pentamers were used into reassembly reactions.

The reassembly reactions composed of pentamers and cargos for encapsulation were mixed and incubated in 1.5ml test tubes on ice. The samples were then transferred into 14 ml mini dialysis devices Slide-A-Lyzer® 3.5K MWCO (GeneTICA) with Assembly buffer. The samples were incubated twice in fresh Assembly buffer for 60 min in 4°C, shaking and finally transferred to fresh Assembly buffer and incubated overnight. Negative staining sample for EM was taken from negative control.

Finally, the assembled samples were dialyzed against Buffer B (4 °C, shaking) that was changed 3 times before incubating in fresh Buffer B over night. The samples were transferred into silicone 1.5ml test tubes and negative staining samples for EM were prepared. Further purification using sucrose gradient centrifugation and concentration using sucrose cushion centrifugation followed.

Material:

Buffer B

Disassembly buffer 1:	20mM Tris-HCl pH 8.8 (Serva)
	50mM NaCl (Lachner)
	2 mM DTT (Sigma-Aldrich)
	5 mM EGTA (Sigma-Aldrich)
Disassembly buffer 2:	20mM Tris-HCl pH 8.8 (Serva)
	50mM NaCl (Lachner)
	2 mM DTT (Sigma-Aldrich)
	2 mM EGTA (Sigma-Aldrich)
Assembly buffer:	2M $(NH_4)_2SO_4$ (Serva)
	2mM $CaCl_2$ (Sigma-Aldrich)
	pH 7.2

4.2.5 Work with bacteria

4.2.5.1 Cultivation of bacteria

The bacteria were cultivated overnight either on solid medium with agar at 37°C in thermostat or in liquid medium in a shaker at 37°C. The bacteria with plasmid encoding for antibiotic resistance were cultivated on/in a medium with selective antibiotic in recommended concentration.

Material:

Nutrient agar no. 2 (Imuna)

Miller LB medium:	1% Pepton (Imuna)
	0,5% Yeast autolysate (Imuna)
	1% NaCl (Lachner)
Miller LB agar:	1% Pepton (Imuna)
	0,5% Yeast autolysate (Imuna)
	1% NaCl (Lachner)
	1.5% Agar (Imuna)

4.2.5.2 Preparation of electrocompetent DH10Bac *E. coli* strain

DH10Bac bacteria from a frozen stock were streaked with sterile toothpick on LB agar plate containing tetracycline (10 μg/ml) and kanamycin (50 μg/ml). The bacteria were streaked so they grew in monocolonies after overnight cultivation at 37°C. One monocolony was inoculated into 20 ml of LB medium containing tetracycline (10 μg/ml) and kanamycin (50 μg/ml) and incubated overnight in a shaker (200 rpm, 37°C). The suspension was diluted with LB medium so the final optic density OD_{560} in 500 ml was 0.1. The suspension was cultivated aerobically and the OD_{560} was measured until it reached 0.5 – 0.7. The suspension was centrifuged 10 min at 4°C and 2000x g. The supernatant was discarded and the pellet was resuspended in 500 ml of demineralized water cooled to 4°C. The suspension was centrifuged 10 min at 4°C and 2000x g. The supernatant was discarded and the pellet resuspended in 250 ml of demineralised water cooled to 4°C. The pellet was resuspended in 20 ml of 10% glycerol cooled to 4 °C. The suspension was centrifuged 10 min at 4°C and 2000x g. The supernatant was discarded and the pellet was resuspended in 10 ml of 10% cooled glycerol. The suspension was centrifuged at 4°C and 2000x g. The supernatant was discarded and the pellet was resuspended in 1 ml of 10% cooled glycerol and the suspension was divided into micro test tubes by 50 μl (1 dose) or 100 μl (2doses). Bacterial suspension in micro test tubes was frozen in liquid nitrogen and stored at -80 °C.

Material:

Miller LB agar
Miller LB medium
Glycerol (Lachema)
Tetracycline (Sigma-Aldrich) 10 mg/ml
Kanamycin (Sigma-Aldrich) 50 mg/ml

4.2.5.3 Transformation of chemically competent Stellar™ competent cells using a heat shock

Stellar™ competent cells were transformed with 5 ng of DNA, usually the ligation mixtures (see 4.2.2.8) as described in the manual (see chapter 4.1.2).

4.2.5.4 Transformation of electro-competent DH10Bac bacteria using electroporation

(modified according to Dower et al., 1988 and Bac-to-Bac® instruction manual by Invitrogen)
The DH10Bac bacteria in the Bac-to-Bac® baculovirus expression system are usually chemically competent but we used electro-competent strain, thus the protocol was modified.

The competent cells were thawed on ice. 1 - 2µl (100 – 300 ng DNA) of pFastBac1 plasmid was added to 45 µl of cell suspension, mixed and incubated 1 minute on ice. After, the suspension was transferred into cooled electroporation cuvette so there were no air bubbles. The electroporator was set to 25 µF, 2.5 kV and 200Ω. An electric pulse was applied on the suspension and its optimal length was 4-5 ms. 1 ml of SOC medium was added to the suspension immediately after the pulse. The suspension was transferred into sterile Erlenmeyer flask and shaked for 3 hrs at 37°C and 200 rpm.

The cell suspension was seeded on a Miller LB agar with tetracycline (10µg/ml), kanamycin (50 µg/ml), gentamycin (7 µg/ml), IPTG (20 µg/ml) and X-gal (20 µg/ml). Typically 10 µl, 100 µl and 890 µl were seeded. The bacteria were cultivated 36 – 40 hrs at 37°C which allowed the blue-white selection.

Material:

Miller LB agar

SOC medium: 2% Peptone (Imuna)
0.5% Yeast autolysate (Imuna)
10mM NaCl (Sigma)
2.5mM KCl (Lachema)
20mM Glucose (Serva)
10mM $MgCl_2$ (Sigma-Aldrich)
10mM $MgSO_4$ (Sigma-Aldrich)

$MgCl_2$ and $MgSO_4$ solutions were sterilized separately and added into medium just before use.

Tetracycline (Sigma) 10 mg/ml

Kanamycin (Sigma) 50 mg/ml

Gentamycin (Gibco) 10 mg/ml

X-gal (Fermentas) 20 mg/ml

IPTG (Fermentas) 20 mg/ml

4.2.5.5 Stock preparation of *E. coli* bacteria

The bacteria were cultivated aerobically in liquid medium overnight at 37 °C. The cell suspension was divided into micro test tubes and 50% sterile glycerol was added so its final concentration was 15 – 20%. Such stocks were stored at -80 °C.

Material:

Glycerol (Lachema)

4.2.6 Work with eukaryotic cell lines

4.2.6.1 Insect cells passaging

(Summers and Smith, 1988)

Confluent insect Sf9 cells on a Petri dish were collected using rubber scratching tool. The cells were resuspended and divided on fresh Petri dishes with required amount of TNM-FH insect medium with 10% FBS so the final ration of cell suspension and fresh medium was 1:4. The cells were well resuspended to cover equally the whole Petri dish and cultivated at 28°C for 2 to 3 days before the next passage.

Material:

TNM-FH insect medium with 10% FBS

4.2.6.2 Baculovirus infection of insect cells

(Summers and Smith, 1988)

Confluent Sf9 cells were passaged into serum-free TNM-FH insect medium in 1:3 ratio and cultivated at 28°C until they attached to Petri dish surface (approx. 30 min). The medium was removed and the baculovirus inoculum was added (10 PFU per cell). The cells were incubated for 60 min in room temperature while rocking. After, the TNM-FH insect medium with 10% FBS was added and the cells were incubated for 3 – 4 days at 28 °C.

The infected cells were collected into 50 ml test tube and centrifuged for 7 min in room temperature and 2000x g. The supernatant was collected and stored at 4 °C as an inoculum. The pellet was washed with PBS and centrifuged for 7 min in room temperature. The supernatant was discarded and the pellet stored at -20°C.

Material:

TNM-FH insect medium with 10% FBS

Serum-free TNM-FH insect medium

Baculovirus inoculum

PBS for tissue cultures (Lonza)

4.2.6.3 Plaque assay and recombinant baculovirus isolation

(Summers and Smith, 1988)

Confluent Sf9 cells were collected into Serum-free TNM-FH insect medium, counted on cell counting Bürker chamber and plated on 6-well dish so there was $1x10^6$ cells per well. After the cells attached to the surface of the well (approx. 30 min) the medium was removed and the cells were infected with 0.5 ml of baculovirus inoculum in dilutions 10^{-3} – 10^{-7}. The cells were incubated for 60 min in room temperature while rocking. After the cells were overlayered with 4 ml of sterile 1.5% SeaPlaque agarose mixed with 10% FBS and 1x TNM-FH insect medium with

antibiotics for tissue cultures (ATB for TC) and the agarose was left to solidify. The cells were incubated 6 – 8 days at 28°C until the viral plaques were visible.

The plaques were counted (when the plaque forming units, PFU were determined) and marked under magnifier with the 30x magnification. The plaque with the agarose was picked and resuspended in 0.5 ml of serum-free TNM-FH insect medium. Such a plaque was immediately used for further infection of Sf9 insect cells. The supernatant was stored as a new inoculum and the cell pellet was used as a lysate for dot blot.

Material:

10% FBS

Antibiotics for tissue cultures

Serum-free TNM-FH insect medium

Baculovirus inoculum

Sea Plaque agarose (Lonza)

4.2.6.4 Mammalian cells passaging

The medium was removed from confluent mammalian cells on a Petri dish (diameter 6 cm). The cell culture was washed with 2.5 ml Versen. After removal of Versen, 300 μl of 0.25% trypsin in PBS were added and incubated 2-5 min at 37°C until the cells were freed from the dish. 5.5 ml of DMEM with 10% FBS were added. The cells were resuspended and the suspension was divided between 6 Petri dishes with 5 ml of DMEM with 10% FBS and resuspended to cover equally the whole Petri dish. The cells were incubated at 37°C in 5% CO_2 for 4 or 5 days.

When the cells were passaged on 24-well dish with cover slips (12-well dish), the cells in the initial cell suspension were counted in cell counter Bürker chamber and required amount was added into 1 ml (2ml) of DMEM with 10% FBS in the wells. Usually 40 – 60 μl were used (150-200 μl). The cells were incubated at 37°C in 5% CO_2 for 24 hrs.

Material:

DMEM with 10% FBS (and Gibco® MEM Non-Essential Amino Acids, ThermoFisher Scientific, for 293TT cells)

Versen in PBS (Sevac)

0.25% trypsin (Sigma-Aldrich) in PBS (Lonza)

4.2.6.5 Mammalian cells transfection for recombinant protein expression

The mammalian cells were transfected using TurboFect™ reagent (Thermo Scientific) as described in the manual (https://tools.thermofisher.com/content/sfs/manuals/MAN0013148_TurboFect_invivo_Transfection_Reagent_UG.pdf).

4.2.6.6 Mammalian cells infection

Cells grown on microscopic cover slips 24-well dish were used for immunofluorescence experiment (cells grown in 12-well dish were used for SNAP-Trap) (chapter 4.2.6.4). The medium was removed and the cells were washed with 1 ml (2ml) of serum-free DMEM. The serum-free medium was removed and 200 μl (300 μl) of sample diluted in serum-free DMEM was added. The cells were incubated 30 – 90 min (depending on an experiment) at 37°C rocked every 10 min. 0.3 to 1 ml (2 ml) of DMEM with 10% FBS and ATB was then added and the cells were incubated 2-6 hrs (entry experiments) or 24-30 hrs (infectivity experiments) at 37°C in 5% CO_2. In some experiments the inoculum was removed, the cells were washed with serum-free DMEM and 1 ml of fresh DMEM with 10% FBS and ATB was added before incubation. Finally, the cells were fixed (see below).

Material:

DMEM medium with 10% FBS and ATB (and Gibco® MEM Non-Essential Amino Acids, ThermoFisher Scientific, for 293TT cells)

Serum-free DMEM medium

4.2.6.7 Mammalian cells fixation with paraformaldehyde

The medium was removed from the infected cells. The cells were washed with 1 ml of PBS which was removed immediately and 500 μl of 4% paraformaldehyde in PBS were added to each well. The cells were fixed for 20 min in room temperature. After, the paraformaldehyde was removed and the cells were washed with 1 ml of PBS which was removed immediately. The cells were then permeabilized for 5 min in 0.5% Triton X-100 in PBS and washed 3x for 10 min in 1 ml of PBS. If DAPI staining only followed, the cells were washed in PBS and demineralised water, slightly dried and placed on 3μl drop of DAPI in 70% glycerol. If indirect immunofluorescence followed the wells were saturated with 500 μl of 0.25% gelatin and 0.25% bovine serum albumin (BSA) solution in PBS (saturating solution).

Material:

4% paraformaldehyde (Sigma-Aldrich) in PBS

0.5% Triton X-100 (Sigma-Aldrich) in PBS

Saturating solution: 0.25% gelatin (Sigma-Aldrich) and 0.25% BSA (Sigma-Aldrich) in PBS

PBS for tissue cultures (Lonza)

4.2.6.8 Indirect immunofluorescence

Saturating solution was removed from the fixed cells and 200 μl of the primary antibody diluted in saturating solution was added. The cells were incubated for 60 min in room temperature while gently rocking. The antibody was removed and the cells were washed 3x for 10 min in PBS. 200 μl of the secondary antibody diluted in saturating solution was added and the cells were incubated for 30 min in room temperature while gently rocking. The antibody was washed 3x for 10 min in PBS and once in demineralised water. The cover slips were slightly dried and placed into 3μl drop of DAPI in 70% glycerol. The samples were observed under fluorescence microscope.

Material:

Saturating solution

PBS for tissue cultures (Lonza)

DAPI in 70% glycerol (Lachema)

4.2.6.9 Electron microscopy

The electron microscopy experiments in this diploma thesis were photographed by Mgr. Jiřina Suchanová and ultrathin sections were prepared and photographed by Mgr. Martin Fraiberk.

Negative staining

Whole process was done on parafilm. 5-10 μl of the sample were placed in drops on the parafilm, next to it two 100 μl drops of demineralized water and two 50 μl drops of 2% phosphotungstic acid (PTA). Copper or cobalt electron microscopy grids with parlodion membrane covered in carbon were placed on the sample drops and incubated for 5 min. If the sample was low in protein concentration the drop was placed on top of the grid and let to dry. After, the grid was washed on the demineralised water drops (each 30 – 60 s) and stained on the 2% PTA drops (each 1 min).

Then the grid was carefully dried and placed on filter paper before observed.

Material:

2% phosphotungstic acid (PTA)

5. Results

5.1. Preparation of universal *VP1* construct for surface loops modification

There are several projects using MPyV VP1 protein in the Laboratory of Virology. Many of them require VP1 surface loop modification with different peptide, for example for vaccine preparation. We decided to make a universal *VP1* constructs for various insertion using restriction enzymes; one with restriction sites in BC loop which is one of the loops that directly bind virus receptor (Stehle and Harrison, 1997; Stehle et al., 1994) and one construct with restriction sites in BC and DE loops that offers more possibilities and combinations of modifications.

5.1.1 Preparation of MPyV *VP1* modified DNA sequence with restriction sites in BC loop (*VP1-BC-mut*)

This construct was prepared in pFastBac1 plasmid which is a donor plasmid for Bac-to-Bac® baculovirus expression system (see chapter 4.1.11), thus it can be directly used for VLPs production.

5.1.1.1 Construction design

Plasmid pFastBac1 with deleted BamHI restriction site (pFastBac1 noBamHI) prepared by Martina Kojzarová (2011) was used as a vector, because it was further combined with Kojzarová's construct to prepare MPyV *VP1* with restriction sites in BC loop and BamHI site in DE loop, so modification of both surface loops would be possible (chapter 5.1.2).

PCR primers in the BC loop with non-complementary overhangs that encode for flexible glycine-serine linkers and three restriction sites for NheI, AgeI and EheI were designed (the primers are called BC-RSins-Fw and BC-RSins-Rw, chapter 4.1.6). Two other primers complementary to the ends of the *VP1* sequence and non-complementary overhangs with restriction sites were used for cloning into the vector (for 5' end MPyV VP1_1F with EcoRI site and for 3' end MPyV VP1_Sal-Rw with SalI site, chapter 4.1.6). The designed change with primers is shown in figure 5.1.1.

Two sets of primers: MPyV VP1_1F + BC-RSins-Rw and BC-RSins-Fw + MPyV VP1_Sal-Rw were designed to get *VP1* fragments (*VP1 short* with 5' end, approx. 200 bp, and *VP1 long* with 3' end, approx. 1000 bp). After restriction endonuclease digestion of both fragments and the vector, the *VP1* fragments could be inserted into the pFastBac1 noBamHI vector under the strong polyhedrin promoter that would result into *VP1* sequence with the designed BC loop change (figure 5.1.2).

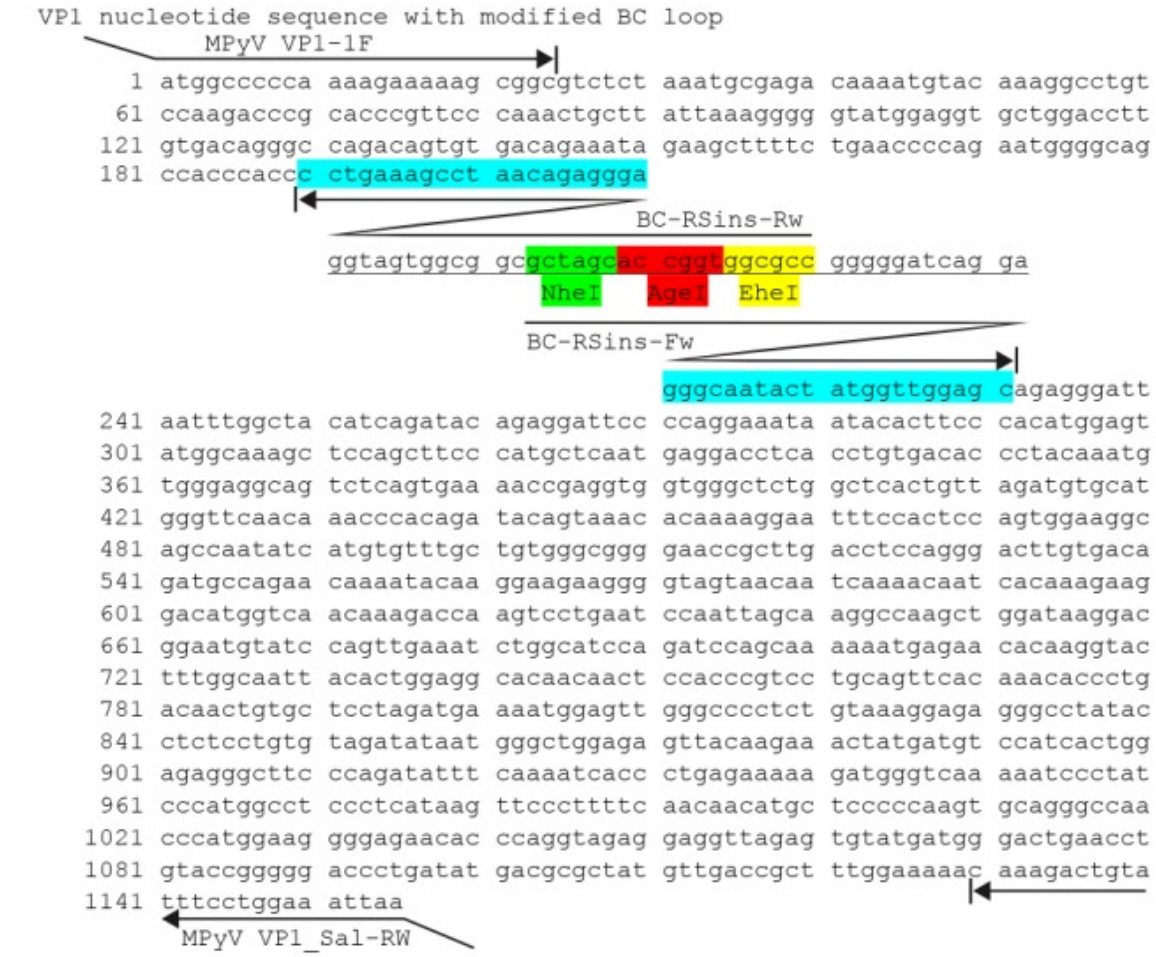

VP1 amino acid sequence with modified BC loop

Figure 5.1.1: *VP1_BCmut* design
Nucleotide (upper part) and amino acid (lower part) sequence of VP1 protein with designed changes in BC loop (turquoise). Flexible glycine-serine linker (underlined) and three different restriction sites NheI, AgeI and EheI (green, red and yellow respectively) were designed to be inserted into the BC-loop of *VP1* using primers with non-complementary ends (arrows in nucleotide sequence, BC-RSins-Fw, BC-RSins-Rw). The primers at the ends of *VP1* sequence were designed to be used for cloning into the vector (MPyV VP1-F, MPyV VP1_Sal-RW).

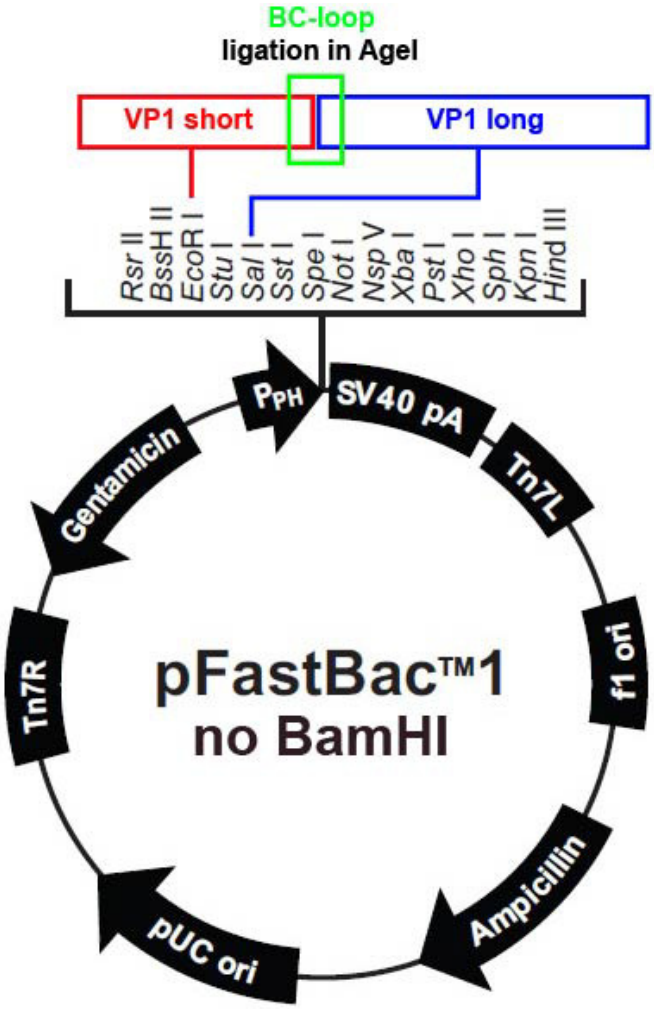

Figure 5.1.2: Cloning design
Two fragments of *VP1* (*VP1 short* and *VP1 long*) are the products of two PCR with two sets of primers: MPyV VP1_1F + BC-RSins-Rw and BC-RSins-Fw + MPyV VP1_Sal-Rw (figure 5.1). These fragments overlap in the designed insertion in BC loop and after restriction digestion in AgeI site can be ligated together. And after digestion with EcoRI and SalI can be inserted into the vector resulting in *VP1-BCmut* construct in pFastBac1 vector.

5.1.1.2 Molecular cloning

VP1 fragments were prepared using PCR. Primers MPyV VP1_1F and BC-RSins-RW were used for the 200 bp long *VP1 short*, BC-RSins-FW and MPyV VP1_Sal-Rw for the 1000 bp long *VP1 long* fragment and MPyV VP1_1F and MPyV VP1_Sal-Rw for the control full length VP1 (*wtVP1*). The construct called pFastBacDual VP1/tVP3 (Bouřa et al., 2005) was used as a template. The PCR was analyzed using agarose electrophoresis. All three fragments of expected size were obtained (figure 5.1.3). They were then purified with GenElute™ RNA/DNA/protein purification Kit (Sigma-Aldrich).

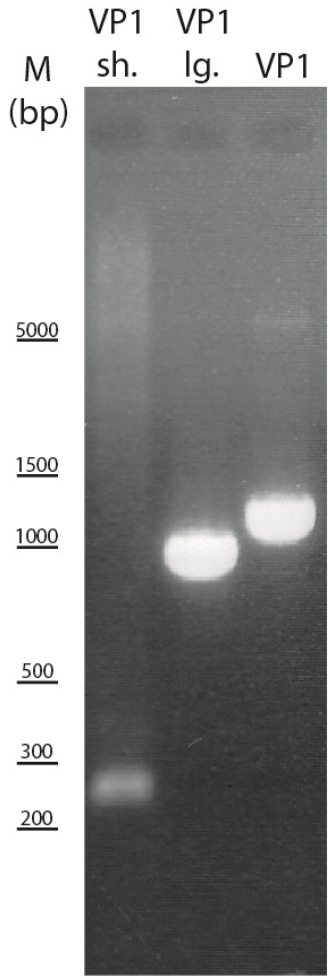

Figure 5.1.3: Preparation of *VP1 short* and *VP1 long*, an electrophoretic control of PCR products
VP1 short and *VP1 long* fragments were prepared using designed primers to insert restriction sites into the BC loop of *VP1* DNA sequence. Unchanged *wtVP1* was prepared as a control. The PCR products were separated and visualized on agarose electrophoresis. *VP1 short* (VP1 sh. approx. 200 bp), *VP1 long* (VP1 lg. approx. 1000 bp) and *wild type VP1* (*wtVP1,* approx 1200 bp) were successfully produced.

The first approach was to insert both *VP1 short* and *VP1 long* into the vector in one ligation step. However, possibly due to lower probability of correct ligation of three fragments in combination with some transformation problems of the competent cells, we were not able to obtain any colonies. Thus we decided to first ligate *VP1 short* and *VP1 long* together and after ligate this new *VP1* fragment into the vector. The process is described below.

The fragments *VP1 short* and *VP1 long* were digested with restriction endonuclease AgeI (which we then inactivated) and ligated in 1:1 molar ratio of ends. After ligase inactivation, the ligation mixture was digested with EcoRI and SalI restriction endonucleases. Purified *wtVP1* and pFastBac1 noBamHI vector were digested with EcoRI and SalI as well. The enzymes were inactivated and the fragments were separated using agarose electrophoresis (figure 5.1.4). The fragments of expected sizes were then purified from the gel using Nucleospin® kit.

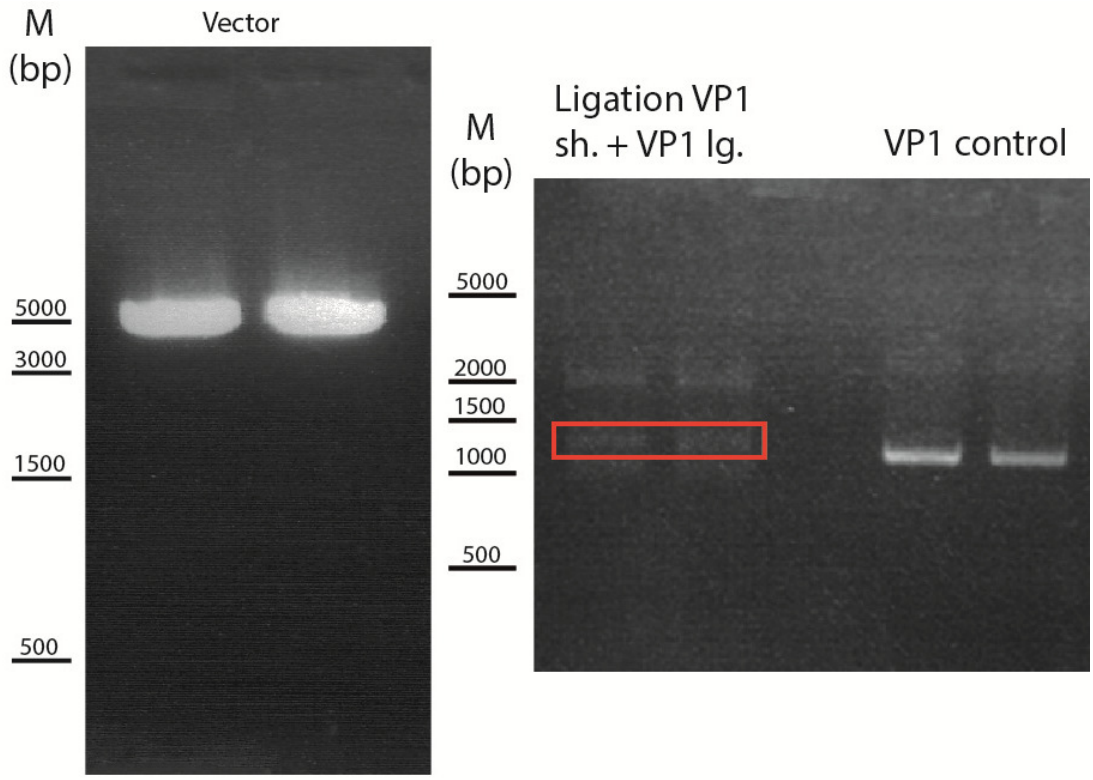

Figure 5.1.4: Purification of fragments from agarose electrophoresis
The vector, ligation mixture of *VP1 short* and *VP1 long* and control *wtVP1* PCR product digested using EcoRI and SalI were separated using agarose electrophoresis. The products of expected sizes were cut out of the gel and purified. The size of linearized vector was approx. 4.8 kbp, control *wtVP1* approx. 1200 bp. Several products were in the ligation mixture as expected. The product of approx. 1200 bp of ligation mixture was selected (although it moved slightly slower than the unmodified VP1). The selected product called *VP1-BCmut* is highlighted in red rectangle.

After, the purified fragments were used in ligation. The *VP1* product of *VP1 short* and *VP1 long* ligation (which we call *VP1-BCmut*) or control wtVP1 were ligated into the vector in 3:1 molar ends ratio. We obtained 7 colonies in *VP1-BCmut* transformation, 9 colonies in *wtVP1* transformation and 1 colony in negative control, all incubated on ampicillin plates. All colonies were restriped on a fresh ampicillin plate and analyzed using colony PCR to detect presence of the insert using primers MPyV VP1_1F and MPyV VP1_Sal-Rw. The results in figure 5.1.5 show the positive colonies that have a DNA product of approx. 1200 bp. There were 6 out of 9 positive colonies in *wtVP1* transformation and 5 out of 7 positive colonies in *VP1-BCmut*, namely colony 2, 3, 6, 7 and a very weak signal was in colony 4.

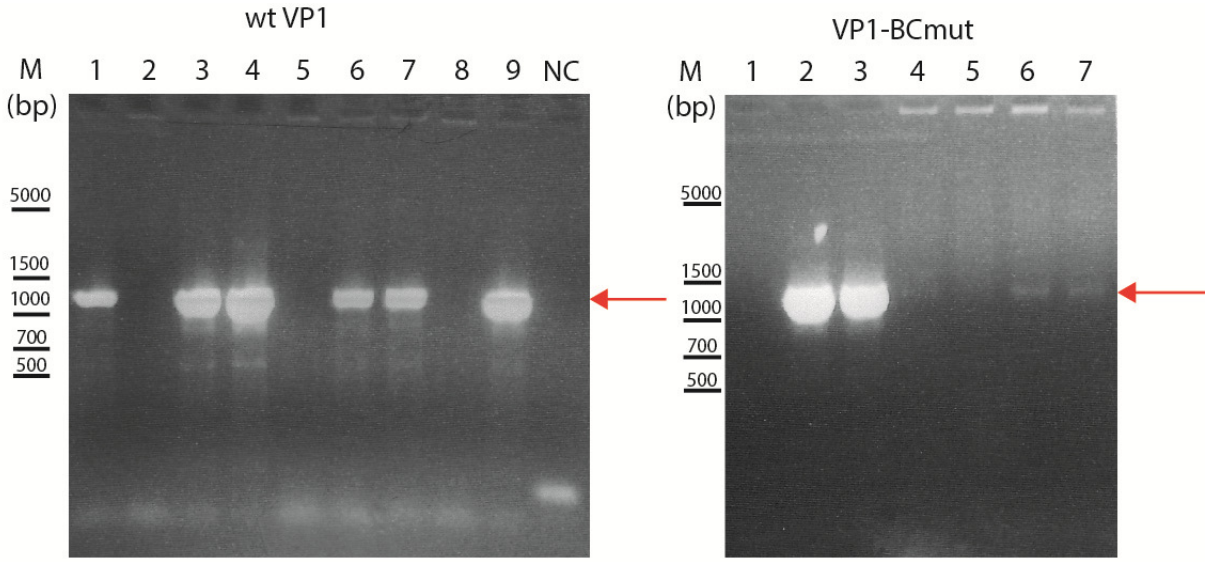

Figure 5.1.5: Colony PCR of transformed Stellar™ cells colonies
The colonies were analyzed using colony PCR to detect if the inserted *VP1* sequence is present using primers MPyV VP1_1F and MPyV VP1_Sal-Rw. In control *wtVP1* transformation there were 6 positive colonies, 1, 3, 4, 6, 7 and 9 with PCR product of approx. 1200 bp (red arrow). There were positive colonies in *VP1-BCmut* transformation as well, namely 2, 3, 6, 7 and 4 which had a very weak signal of approx. 1200 bp long PCR product. NC is a negative control PCR mixture without the template DNA.

The plasmids were isolated from *VP1-BCmut* positive colonies using GenElute™ Plasmid Miniprep Kit (Sigma-Aldrich). The plasmid quality was then controled using agarose electrophoresis, all of them were intact. To make sure the change was present in the BC-loop of *VP1* sequence, the plasmids were digested with NheI restriction enzyme and analyzed using agarose electrophoresis. All of the plasmids were digested (not shown). Plasmids from colonies 4, 6 and 7 were chosen for the sequencing analysis. The sequencing confirmed that all three plasmids carry *VP1* gene with modified BC loop. Thus we prepared *VP1* construct with modified BC loop called *VP1-BCmut* in donor plasmid pFastBac1 for Bac-to-Bac® baculovirus expression system. The map of the construct pFastBac1_noBamHI_VP1-BCmut is shown in figure 5.1.6.

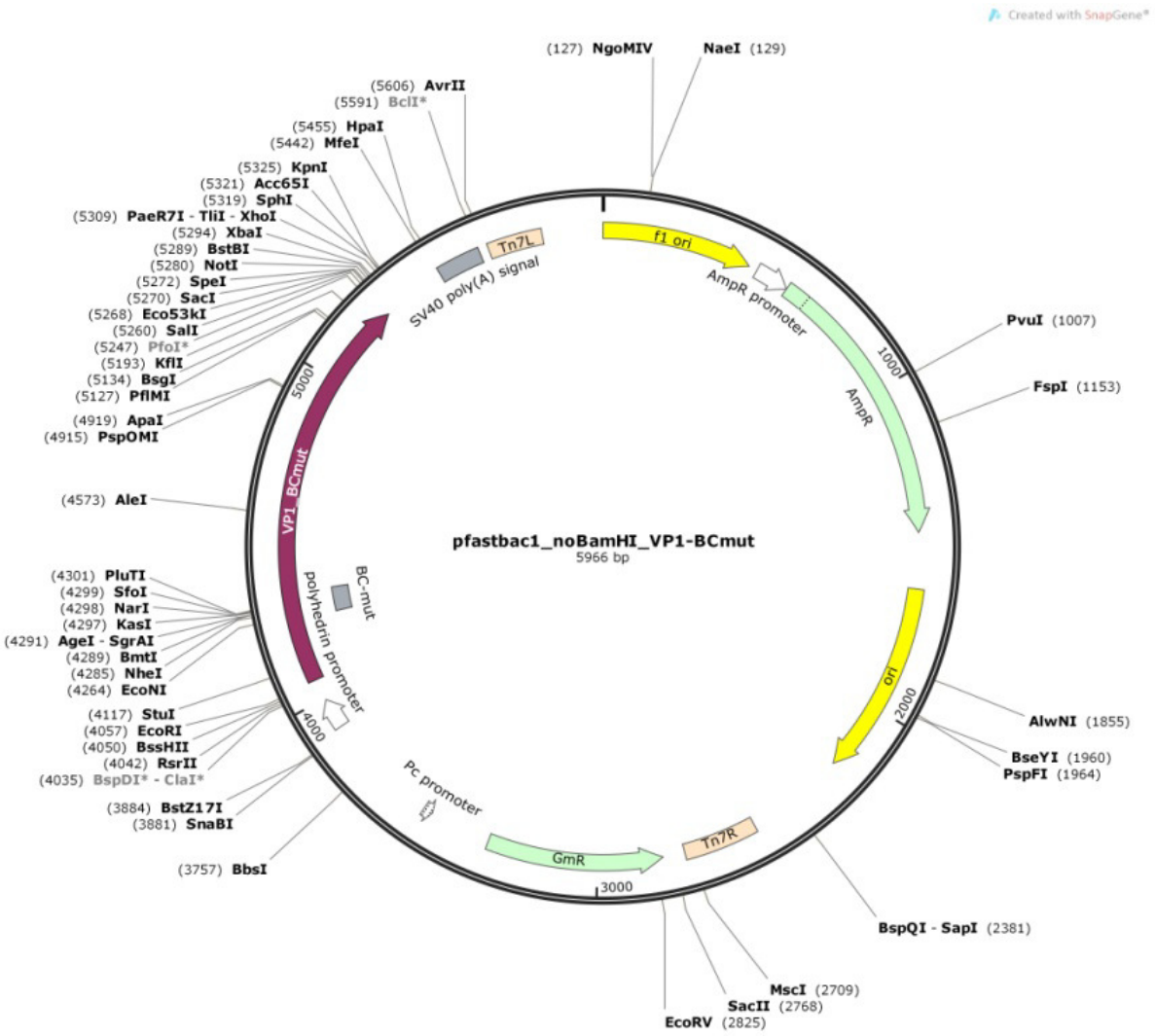

Figure 5.1.6: Map of pFastBac1_noBamHI_VP1-BCmut construct
The *VP1* gene with modified BC loop (*VP1-BCmut*) is inserted in pFastBac1 plasmid with deleted BamHI restriction site in the multiple cloning site. The *VP1* gene is inserted under polyhedrin promoter, which allows VP1 expression in baculovirus expression system.

5.1.2 Preparation of MPyV *VP1* modified DNA sequence with restriction sites in BC and DE loop (*VP1-BCmut+DE7less*)

We also decided to combine previously prepared construct with modified DE loop with restriction site BamHI called *VP1-7less* (Kojzarová, 2011) with *VP1-BCmut* to prepare *VP1* sequence with restriction sites in both BC and DE loop.

5.1.2.1 Construction design

As pFastBac1_noBamHI_VP1-BCmut has the restriction site in the BC loop and the *VP1* sequence is surrounded by EcoRI and SalI restriction site, we decided to simply replace the *VP1 long* fragment with *VP1-7less long* fragment.

5.1.2.2 Molecular cloning

First the *VP1-7less long* fragment was prepared using PCR. We used BC-RSins-FW and MPyV_VP1_SalI_Rw primers and pFastBac1_noBamHI_VP17less (Kojzarová, 2011) as a template. The PCR product was purified using High Pure PCR Product Purification Kit (Roche) and controlled on agarose electrophoresis (figure 5.1.7).

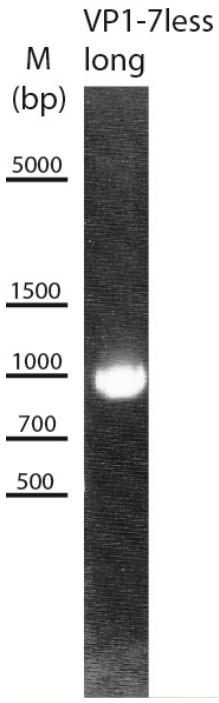

Figure 5.1.7: Preparation of *VP1-7less long*, an electrophoretic control of PCR product
We prepared *VP1-7less long* fragment which has BamHI restriction site in DE loop using PCR. We visualized the PCR product on agarose electrophoresis. *VP1-7less long* was successfully produced.

After, the *VP1-7less long* fragment and the pFastBac1_noBamHI_VP1-BCmut vector were digested with AgeI and SalI restriction endonucleases. After enzymes inactivation, DNA fragments were separated using agarose electrophoresis (figure 5.1.8). The fragments of expected sizes were isolated from the gel using Nucleospin® kit. This way we obtained linearized pFastBac1_noBamHI_VP1-BCmut with missing *VP1 long* fragment.

VP1-7less long fragment was ligated into the vector in 3:1 molar ends ratio and the Stellar™ cells were transformed with the ligation mixture as described in the manual. We obtained many colonies on ampicillin plates from which we picked several and restriped them on fresh ampicillin plates and used them for colony PCR analysis. We obtained 8 positive colonies from which we chose 4 to isolate plasmid using GenElute™ Plasmid Miniprep Kit.

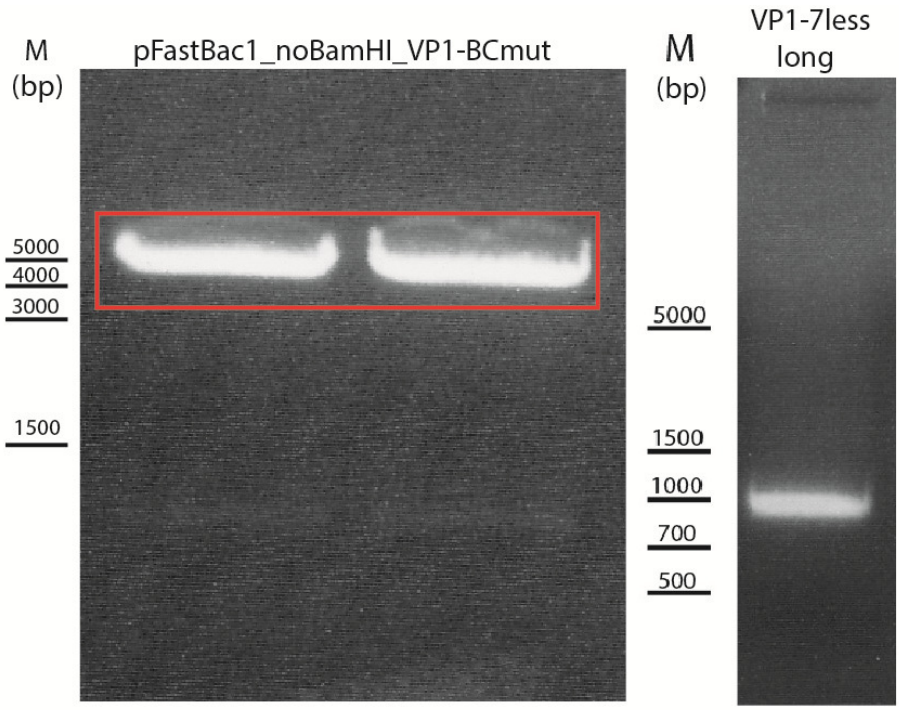

Figure 5.1.8: Purification of fragments from agarose electrophoresis
pFastBac1_noBamHI_VP1-BCmut and PCR product *VP1-7less long* digested with AgeI and SalI were separated using agarose electrophoresis. The products of expected size were cut out of the gel and purified. The size of *VP1-7less long* was approx. 1000 bp. There were two fragments in pFastBac1_noBamHI_VP1-BCmut digestion, the shorter fragments represents *VP1 long fragment*. Only the longer fragment of digested vector of approx 5000 bp (red rectangle) was isolated from the gel.

The isolated plasmids were analyzed using agarose electrophoresis, all of them were intact. Also the presence of restriction sites in both BC and DE loop was controlled using restriction endonucleases NheI and EcoRV for BC-loop control and BamHI and EcoRV for DE-loop. All four plasmids contained both NheI and BamHI restriction site (not shown). Finally, the sequencing analysis confirmed that we prepared new *VP1* construct with modified BC and DE loops (*VP1-BCmut+DE7less*) cloned in pFastBac1 vector, a donor vector for Bac-to-Bac® baculovirus expression system. We call this construct pFastBac1_noBamHI_VP1-BCmut+DE7less (figure 5.1.10).

Both pFastBac1_noBamHI_VP1-BCmut+DE7less and pFastBac1_noBamHI_VP1-BCmut constructs were prepared as part of this diploma thesis but its further use is not documented herein. It was prepared as a universal vector for various applications in the Laboratory of Virology.

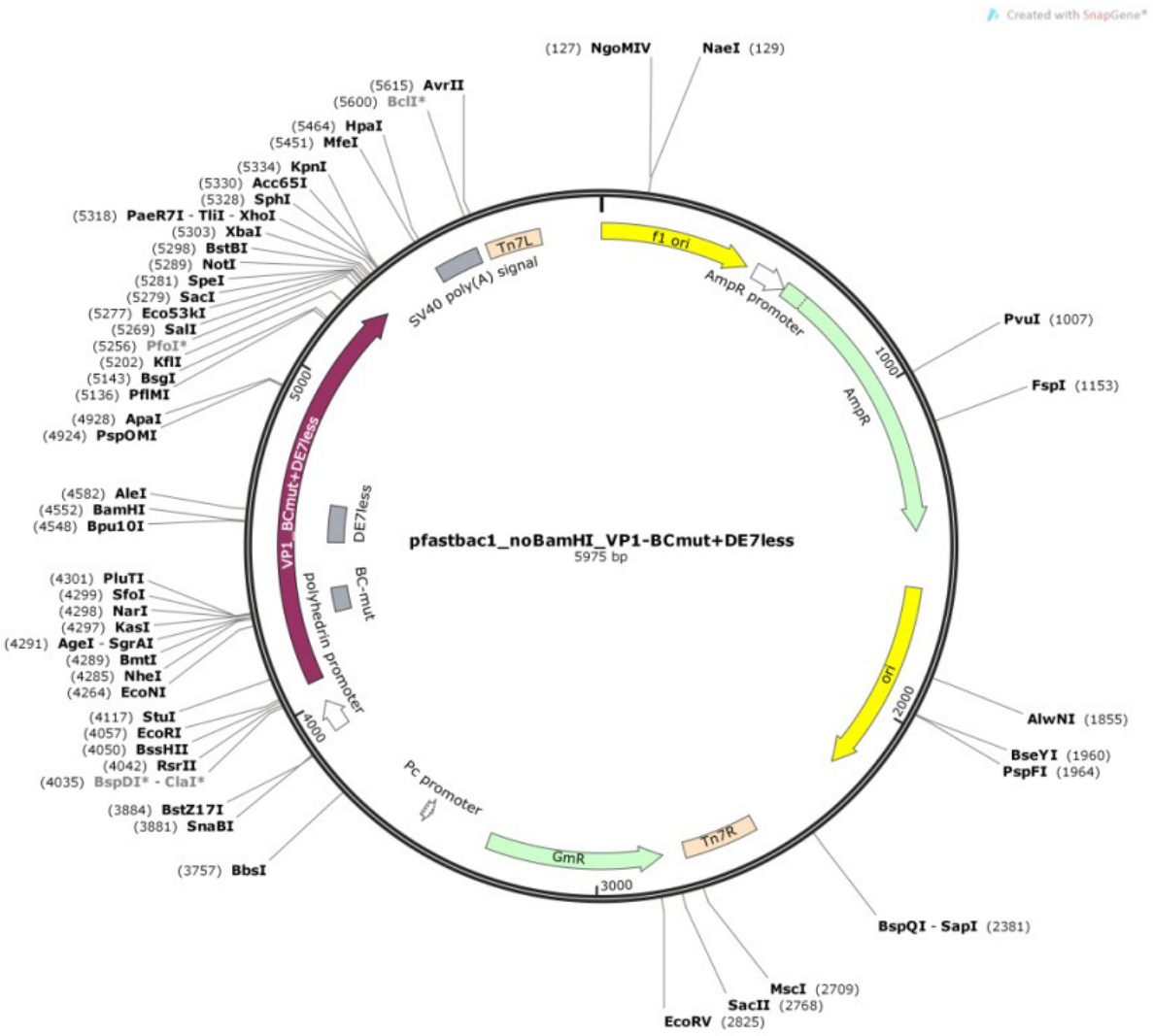

Figure 5.1.9: Map of pFastBac1_noBamHI_VP1-BCmut+DE7less construct
The *VP1* gene with modified BC loop and DE loop is inserted in pFastBac1 plasmid with deleted BamHI restriction site in the multiple cloning site. The *VP1* gene is inserted under polyhedrin promoter, which allows VP1 expression in the baculovirus expression system.

5.2 Cargo encapsidation

The MPyV VLPs composed of VP1 protein self-assemble intracelullarly when expressed in recombinant baculovirus expression system. In addition, we are able to disassemble and reassemble them successfully *in vitro* (chapter 2.2.2). In order to use MPyV VP1-VLPs as a delivery system for various cargos we wanted to prove that the selected cargos can be encapsidated or at least make a stable association with VLPs during reassembly. Finally we wanted to observe VLPs and cargo entry into the mammalian cells.

5.2.1 Encapsidation of cargo into the VP1-VLPs

We selected two different cargos for encapsidation into VLPs. First selected was a small molecule, fluorescently labeled β-cyclodextrin modified by two fluorescein isothiocyanate molecules (FITC) and five gadolinium complexes (as the product was prepared to be further

used in magnetic resonance imaging, MRI, figure 5.2.1) (Kotková et al., 2010). The abbreviation CD is used for this modified cyclodextrin throughout this work. For encapsidation, CD alone or together with DNA was used. DNA is a natural cargo of VLPs and may help stabilization of CD in the particles as beta cyclodextrins were found to interact with DNA (Alves et al., 2015). pmaxGFP (AMAXA) control plasmid coding for green fluorescent protein was used as the helper DNA molecule. The second cargo was a fluorescently labeled antibody GαM Atto594 (AB) because antibodies are small enough to fit the lumen of VLPs.

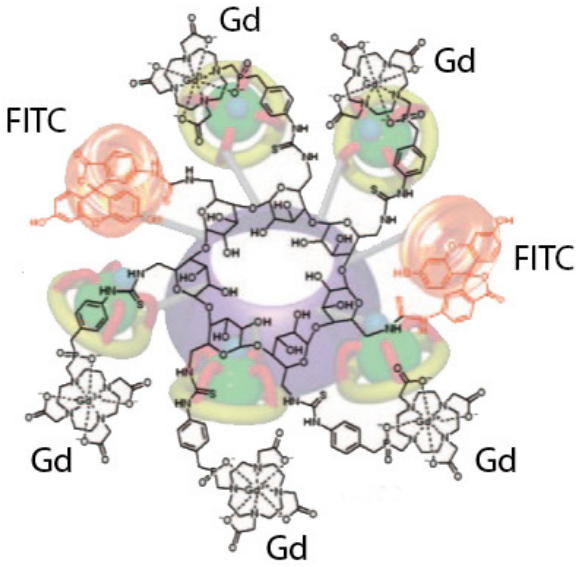

Figure 5.2.1: Structure of labeled cyclodextrin cargo (CD)
Cyclodextrin modified by two fluorescein isothiocyanate molecules (FITC) and five gadolinium complexes (Gd) was used as a small molecule cargo for encapsulation into MPyV VP VLPs. Gd is a contrast agent for magnetic resonance imaging (MRI) and FITC is a fluorescent molecule. Modified according to (Kotková et al., 2010).

We used VP1 particles which were produced using recombinant baculovirus expression system and by CsCl gradient centrifugation (chapters 4.1.11, 4.2.4.1 – 4.2.4.6, figure 5.2.2A). Previously optimized disassembly and reassembly protocol was followed (chapter 4.2.4.11). We first disassembled the VLPs, separated pentamers and mixed them with cargo before reassembly and dialysis into buffer B. The reassembly reactions are listed in table 5.2.1.

Reassembly reactions in the presence of cargo				
Reaction (400 µl)	Pentamers	CD	DNA	AB
CD	1.5 µM (140 µg)	0.4 mM	-	-
CD+DNA	1.5 µM (140 µg)	0.4 mM	28 µg DNA	-
AB	1.5 µM (140 µg)	-	-	140 µg
Control (NC)	1.5 µM (140 µg)	-	-	-

Table 5.2.1: Reassembly reactions for cargo encapsulation
We prepared the reassembly reactions using purified pentamers after disassembly and selected cargo. CD is FITC-conjugated cyclodextrin, AB is fluorescently labeled goat anti mouse antibody Atto594. NC is a reassembly control without cargo.

Samples for electron microscopy were prepared in each step (figure 5.2.2). We managed to disassemble the VLPs and separate the VP1 pentamers (figure 5.2.2C) from aggregated material (figure 5.2.2B). Also the reassembly of all samples and the negative control was successful (figure 5.2.2D-G) although there was still a significant amount of pentamers in the reassembly with antibody (figure 5.2.2G). We named the VLPs reassembled with CD "CD-VLPs", with CD and DNA "CD+DNA-VLPs", with fluorescent antibody "AB-VLPs" and the control reassembled VLPs "NC-VLPs".

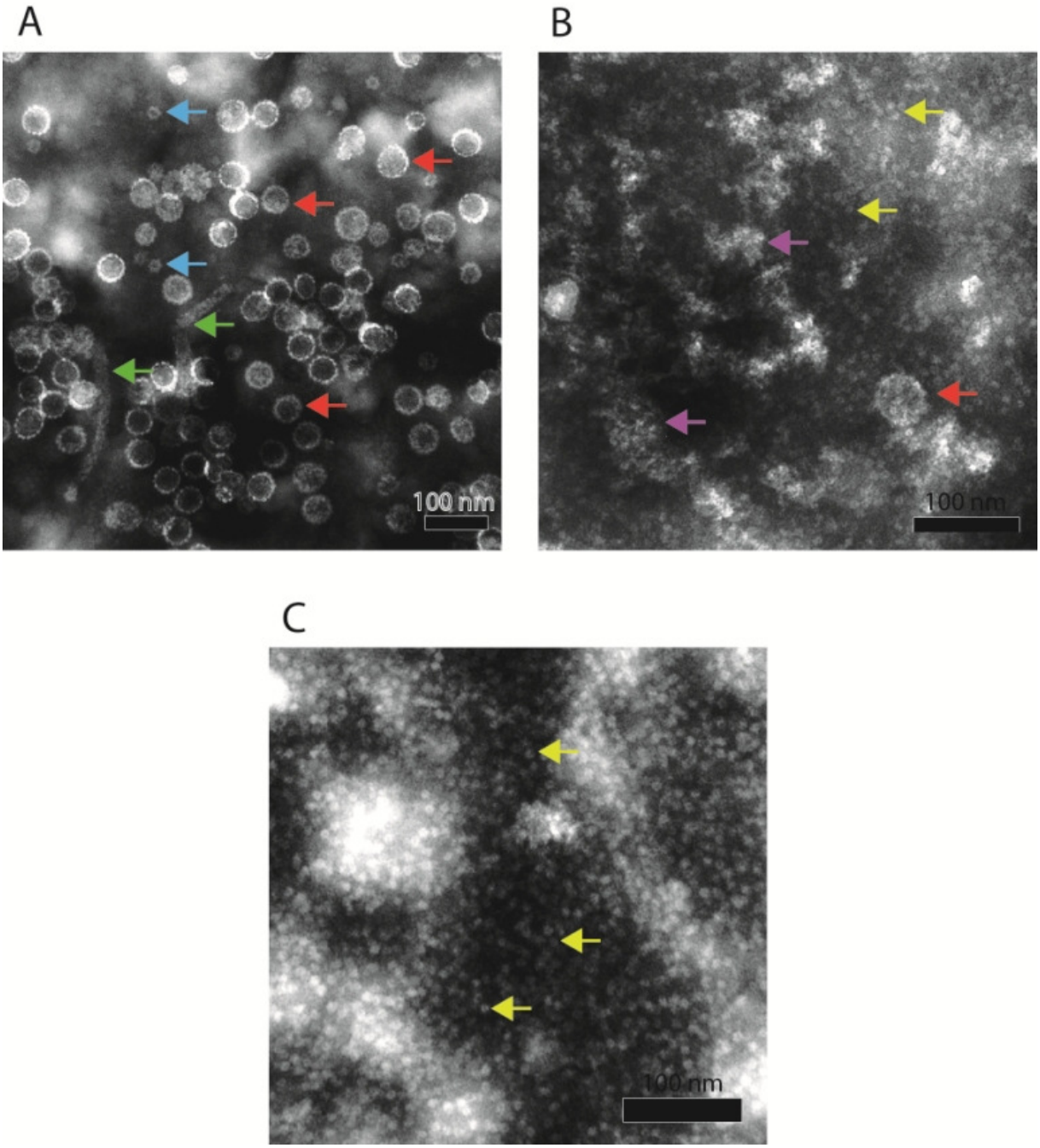

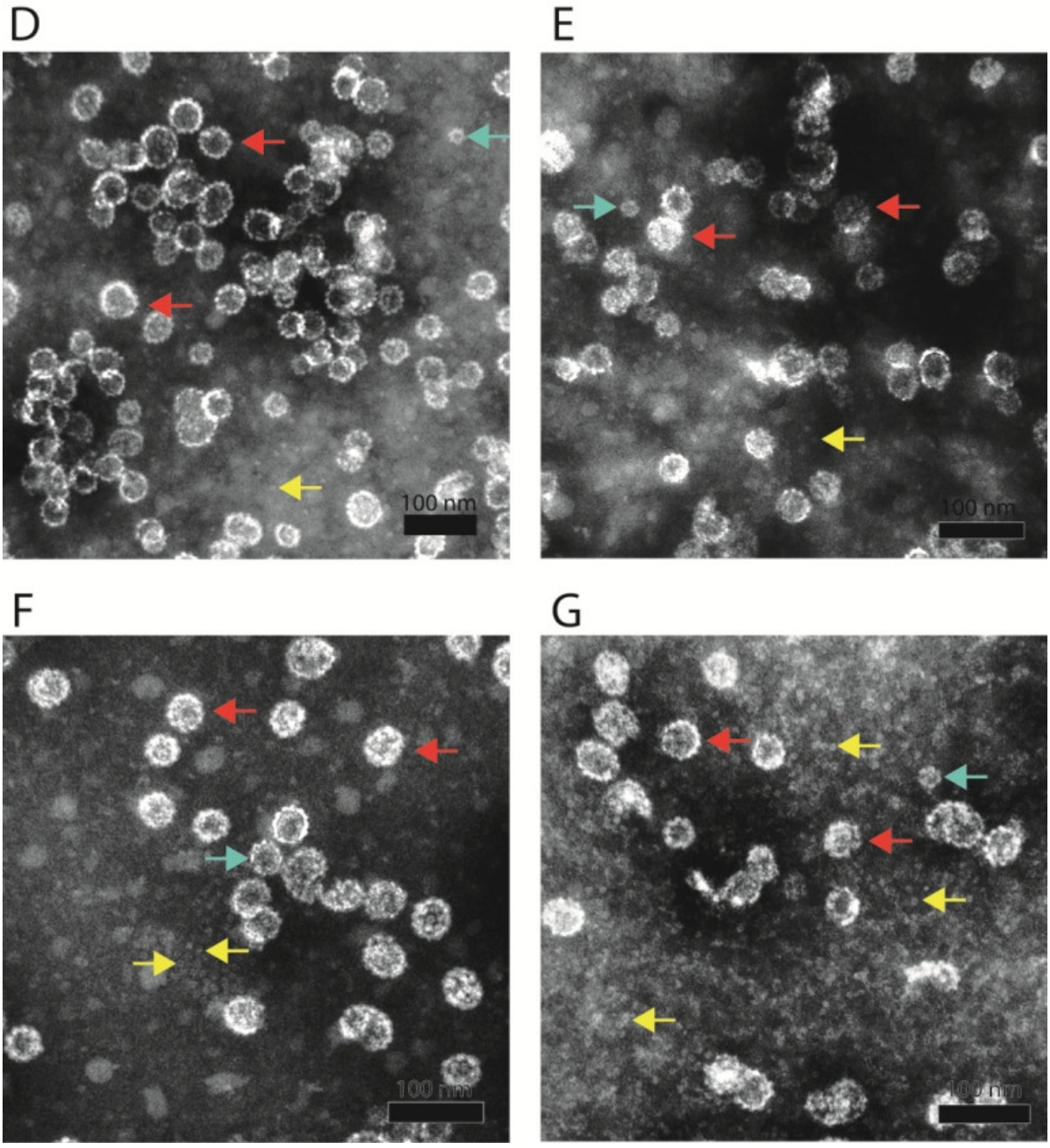

Figure 5.2.2: Electron microscopy images of the disassembly and reassembly process (negative staining)
We prepared samples for electron microscopy in every step of the disassembly and reassembly with cargo. **A:** MPyV VP1 particles used for disassembly. The sample contained 45nm VLPs (red arrows), smaller VLPs (turquoise arrows) and tubular structures (green arrows). **B:** The aggregates. The samples were centrifuged after disassembly to pellet not properly disassembled material with pentamers (yellow arrows), VLPs (red arrow) and aggregates (purple arrows). **C:** The pentamers. We obtained pure VP1 pentamers in the supernatant after disassembly and centrifugation (yellow arrows). **D-G:** Samples after reassembly and dialysis into buffer B. We observed reassembled 45nm VLPs (red arrows), smaller particles (turquoise arrows) and not assembled material – VP1 pentamers (yellow arrows marking small white circles) in all of the samples. **D:** NC-VLPs. **E:** CD-VLPs. **F:** CD+DNA-VLPs. **G:** AB-VLPs.
Images: Mgr. Jiřina Suchanová

The samples were purified using sucrose gradient centrifugation (chapter 4.2.4.2) to remove all of the unbound material and pentamers. The collected gradient fractions were analyzed using

immuno-dot blot (dot blot followed by immunodetection using chemiluminescence, chapters 4.2.3.2 and 4.2.3.6) for the presence of VP1 protein, FITC and AB (figure 5.2.3). VP1 protein was present in most fractions with some peaks in fractions 12-14 and 17-18 (figure 5.2.3A), the highest CD signal was in fractions 11-13 of CD-VLPs and 13-15 in CD+DNA-VLPs (figure 5.2.3B) and highest AB signal in fractions 13-15 and 19-20 (figure 5.2.3D). We also denatured the dot blot in 1% SDS for 10 min at 37°C before immunodetection to try if we can detect the encapsidated cargo (figure 5.2.3C, E). We observed a shift of the highest signal in CD+DNA-VLPs to fractions 10-12 (figure 5.2.3C). However we could not conclude if the signal after denaturation was increased.

In addition, we used Biorad Molecular imager to control the fluorescence of CD-VLPs, CD+DNA-VLPs and AB-VLPs fractions. The fluorescence signal corresponded with the one observed with immuno-dot blot (not shown). We also measured the refractive index (table 5.2.2).

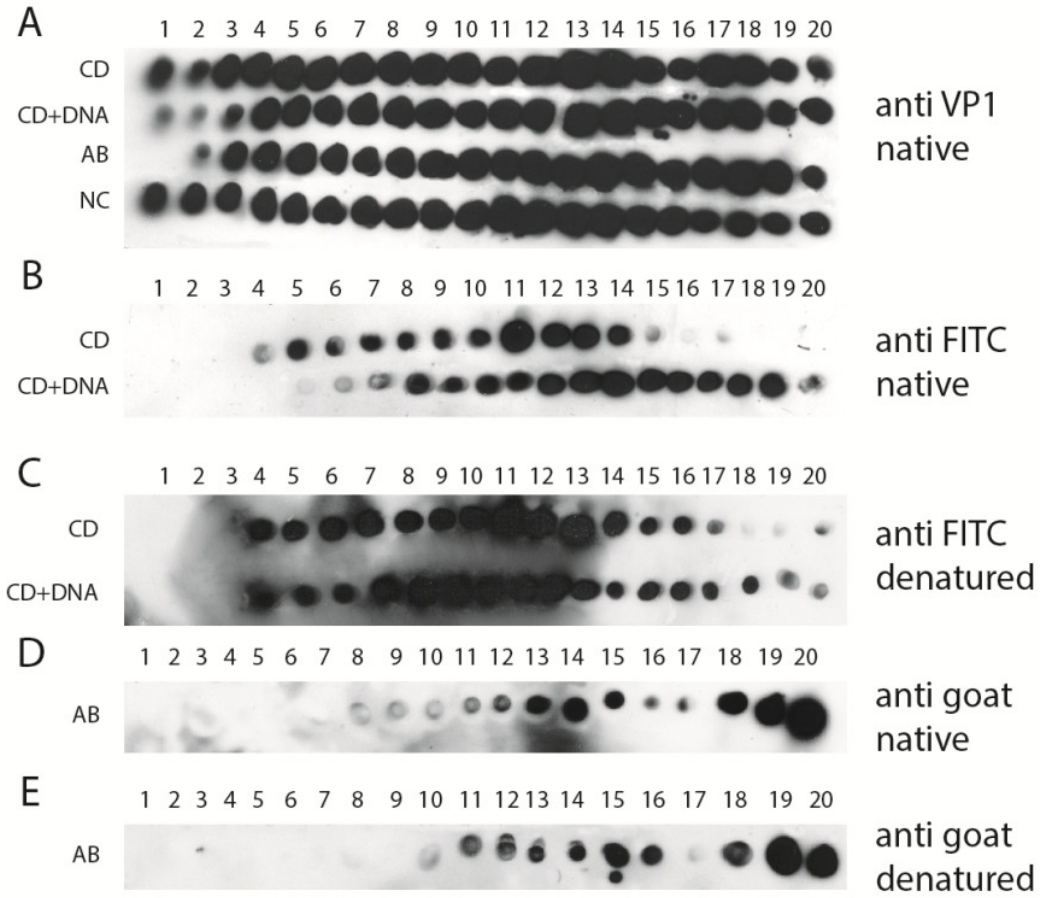

Figure 5.2.3: Immuno-dot blot detection of VP1 protein, FITC and AB in sucrose gradient fractions of reassembly with cargo

A: Detection of VP1 protein with MαVP1-D4 antibody. The results were used for combining the fractions for dialysis into buffer B. **B:** Detection of CD in native VLPs with GαFITC antibody. **C:** Detection of CD in denatured VLPs. **D:** Detection of fluorescently labeled mouse antibody in native VLPs directly with secondary antibody. **E:** Detection of fluorescently labeled mouse antibody in denatured VLPs. CD are CD-VLPs fractions, CD+DNA are CD+DNA-VLPs fractions, AB are AB-VLPs fractions and NC are control NC-VLPs.

Refractive index of sucrose gradient fractions of reassembled VLPs in the presence of cargo				
Fraction	CD	CD+DNA	AB	NC
1	1.398	1.398	1.396	1.396
2	1.401 CD F-I	1.400 CD+DNA F-I	1.400 AB F-I	1.401 NC F-I
3	1.400	1.397	1.399	1.399
4	1.395	1.392	1.394	1.394
5	1.3895 CD F-II	1.388 CD+DNA F-II	1.388 AB F-II	1.389 NC F-II
6	1.384	1.384	1.385	1.385
7	1.381	1.381	1.3815	1.381
8	1.378	1.378	1.378	1.378
9	1.374 CD F-III	1.375 CD+DNA F-III	1.375 AB F-III	1.375 NC F-III
10	1.372	1.373	1.372	1.373
11	1.371	1.371	1.371	1.371
12	1.368 CD F-IV	1.369	1.370	1.369
13	1.367	1.367 CD+DNA F-IV	1.367	1.3675 NC F-IV
14	1.366	1.366	1.366 AB F-IV	1.366
15	1.363	1.364	1.364	1.364
16	1.360	1.362	1.3625	1.361
17	1.359 CD F-V	1.360	1.360	1.359
18	1.3555	1.359 CD+DNA F-V	1.357 AB F-V	1.357 NC F-V
19	1.352	1.357	1.356	1.352
20	1.3505	1.355	1.349	1.348

Table 5.2.2: Refractive index of sucrose gradient fractions of reassembled VLPs in the presence of cargo
The refractive index of sucrose gradient fractions of reassembly mixtures was measured. The fractions were connected for dialysis based on the immuno-dot blot results and the refractive index. We prepared five separate dialysis fractions for each reassembly (colored boxes).

We selected several fractions with the highest dot blot signal of the cargo after sucrose gradient and prepared samples for electron microscopy. We observed pure VLPs in all selected fractions except for fraction 19 from reassembly with AB which contained only few VLPs (figure 5.2.4).

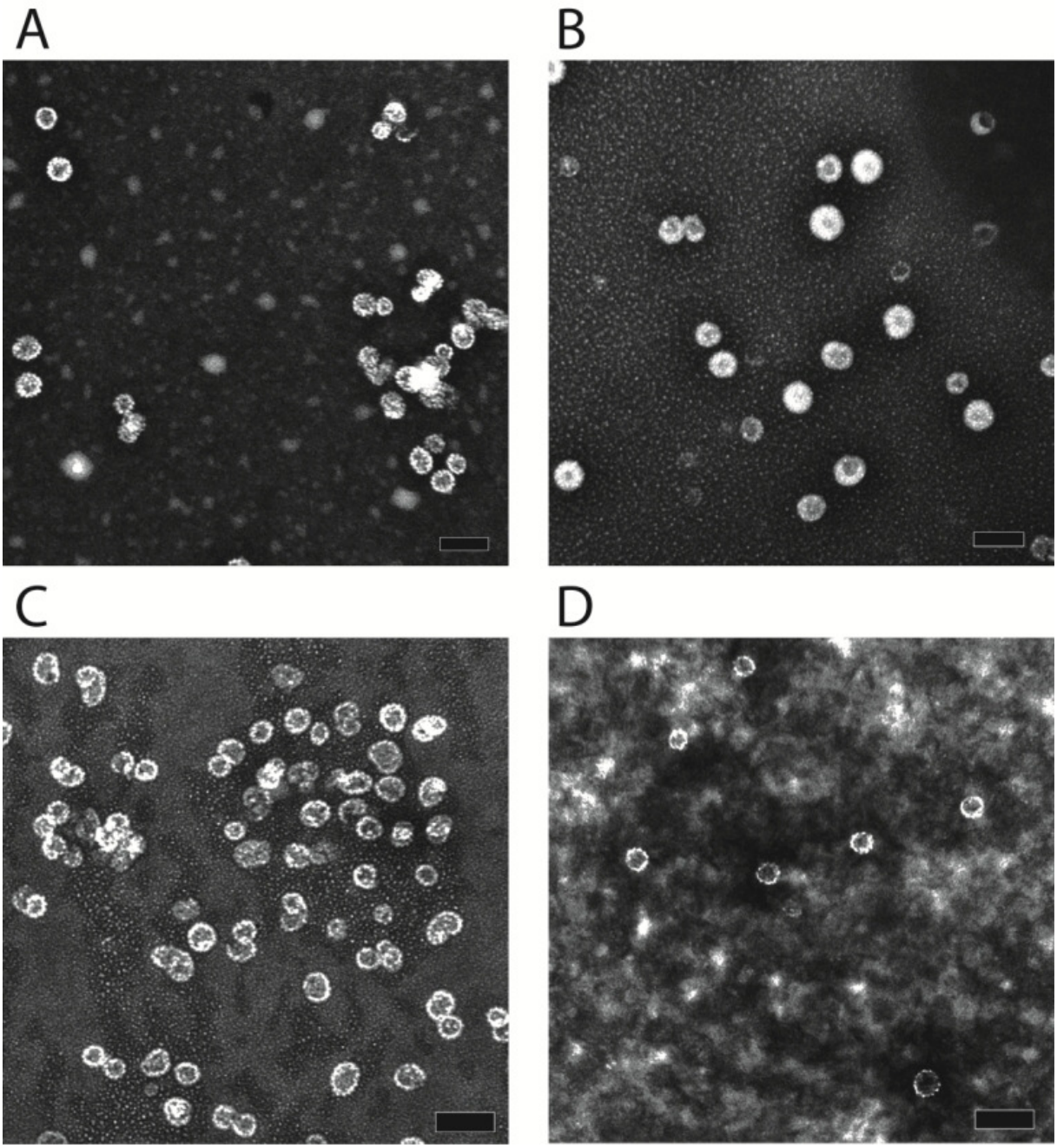

Figure 5.2.4: Electron microscopy images of selected fractions of reassembled VLPs after sucrose gradient (negative staining)
A: CD-VLPs fraction 11. **B:** CD+DNA-VLPs fraction 14. **C:** AB-VLPs fraction 14. **D:** AB-VLPs fraction 19. Black rectangles represent 100 nm. Lower quality of images was caused by the sucrose which complicates the focusing.
Images: Mgr. Jiřina Suchanová

We combined the fractions based on the immuno-dot blot and refractive index into 5 fractions for each cargo molecule sample (F-I to F-V, table 5.2.2). After overnight dialysis against buffer B, we reduced the volume of fractions F-I and F-II of each reassembly reaction using PEG 20 000 (these fractions were not further analyzed as the signal on immuno-dot blot was weak) and fractions F-III, F-IV and F-V of each reassembly reaction using 20% sucrose cushion centrifugation. The pellets were dissolved in buffer B and the protein concentration of fractions

F-III, F-IV and F-V was measured using Quibit fluorometer (table 5.2.3). The presence of VP1, CD and AB in both pellet and supernatants was again verified by immuno-dot blot detection (figure 5.2.6) and quality of samples in pelleted material was verified by electron microscopy (figure 5.2.5).

Protein concentrations of reassembly reactions	
Sample and fraction	Protein concentration
all F-III fractions	under detection limit
CD F-IV	61.5 µg/ml
CD+DNA F-IV	96.0 µg/ml
AB F-IV	95.0 µg/ml
NC F-IV	105.0 µg/ml
CD F-V	under detection limit
CD+DNA F-V	152.0 µg/ml
AB F-V	75.0 µg/ml
NC F-V	75.2 µg/ml

Table 5.2.3: Protein concentrations of reassembly reactions after sucrose cushion centrifugation

The protein concentrations of fractions that contained higher VP1 signal (FIV and FV) on dot blot were mostly measurable although quite low (table 5.2.3). The big material loss is a part of the disassembly and reassembly process as well as the purification steps.

The electron microscopy figures revealed that we successfully produced VLPs that were present in fractions F-IV of all samples (figure 5.2.5). Fractions F-V also contained some VLPs, especially in CD+DNA isolations (not shown). Assembled VLPs of 45 nm in diameter as well as smaller VLPs were predominant structures in the material from CD (figure 5.2.5A), CD+DNA (figure 5.2.5B) and control reassembly without cargo (figure 5.2.5D). When the pentamers were reassembled with the fluorescent antibody they formed VLPs of various sizes but a lot of pentamers were present (figure 5.2.5C) even though they were not observed in fractions after sucrose gradient (figure 5.2.4C). This suggests that the AB-VLPs were unstable.

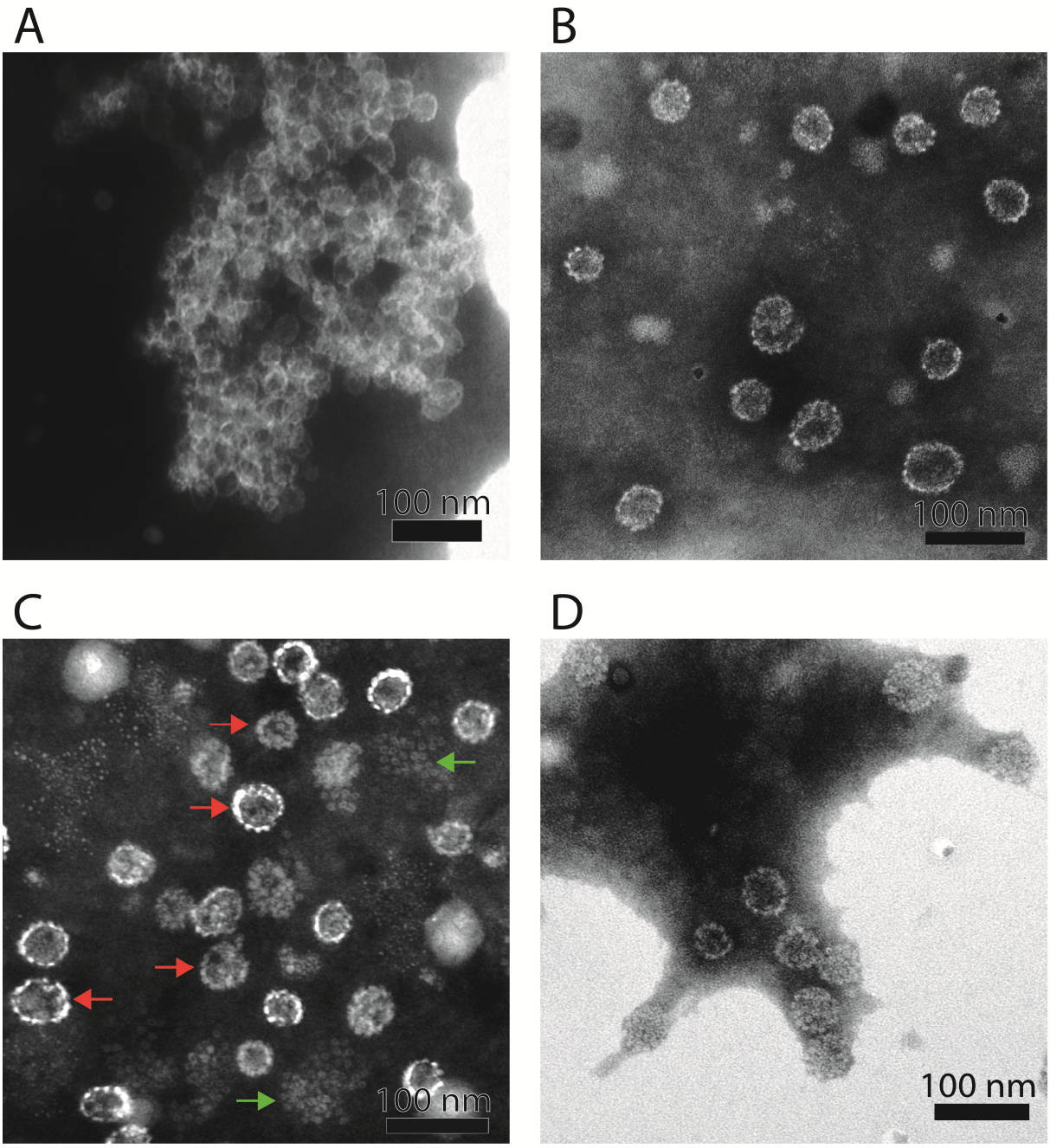

Figure 5.2.5: Electron microscopy images of the purified VLPs reassembled in the presence of cargo (negative staining)

The samples of fractions F-IV were taken after dialysis and final purification and concentration by centrifugation through 10% sucrose cushion. **A:** CD-VLPs. The VLPs seems to be aggregated that can be due the preparation of the negative staining sample **B:** CD+DNA-VLPs had various sizes including approx. 45 nm in diameter. **C:** AB-VLPs had various sizes including 45 nm in diameter (red arrows) but also lots of pentamers (green arrows). **D:** NC-VLPs reassembled in absence of cargo.

Images: Mgr. Jiřina Suchanová

Finally, to detect if the cargo was stably associated with the VLPs, we performed immuno-dot blot of both isolated VLPs after sucrose cushion centrifugation and the supernatants (figure 5.2.6). The supernatants should contain any free material not stably bound to the VLPs.

In agreement with the electron microscopy, most of the VP1 signal was present in fractions F-IV of CD-, CD+DNA- and AB-VLPs. Some signal was present also in fractions F-III and F-V (figure

5.2.6A). No VP1 signal was detectable in supernatants except for a weak signal in the fraction F-IV of AB-VLPs (figure 5.2.6 D). CD was present in F-IV and F-V of CD- and CD-DNA VLPs and a very weak signal could be detected in F-III. AB had weak signal in F-IV of AB-VLPs (figure 5.2.6B). When we checked the presence of CD and AB in the supernatants, we detected strong signal of CD in the fractions F-V of CD-VLPs and CD+DNA VLPs as expected, because this was the least concentrated part of the sucrose gradient where the unbound small molecules were supposed to accumulate. Also strong antibody signal was detected in fraction F-V of AB-VLPs supernatant (figure 5.2.6E).

In attempt to study if we can detect cargo encapsidated into the VLPs, we also denatured the samples on nitrocellulose membrane by incubation in 1% SDS at 37°C for 10 minutes before the immunodetection. We observed an increase of CD signal in the fractions F-III of CD-VLPs and CD+DNA-VLPs; however, the signal from F-IV and F-V was mostly unchanged. Similarly the signal of AB in F-IV of AB-VLPs remained weak (figure 5.2.6C).

To conclude, we successfully reassembled MPyV VP1-VLPs in the presence of cargo. The reassembled VLPs in presence of cargo did not significantly differ from the ones reassembled without cargo. CD was stably associated with VLPs even after extensive purification. Even though CD was clearly attached also on the surface of the VLPs based on the immuno-dot blot results, the association was stable and it is highly probable that the cargo was also encapsidated inside the VLPs. We did not notice any significant difference between CD-VLPs and CD+DNA-VLPs. On the contrary we did not manage to encapsidate the antibody into the VLPs as the antibody signal associated with VLPs was very weak and a significant amount of antibody remained in the supernatant after the final purification. In addition, AB-VLPs seemed to be unstable as there was significant amount of disassembled material present after the final purification.

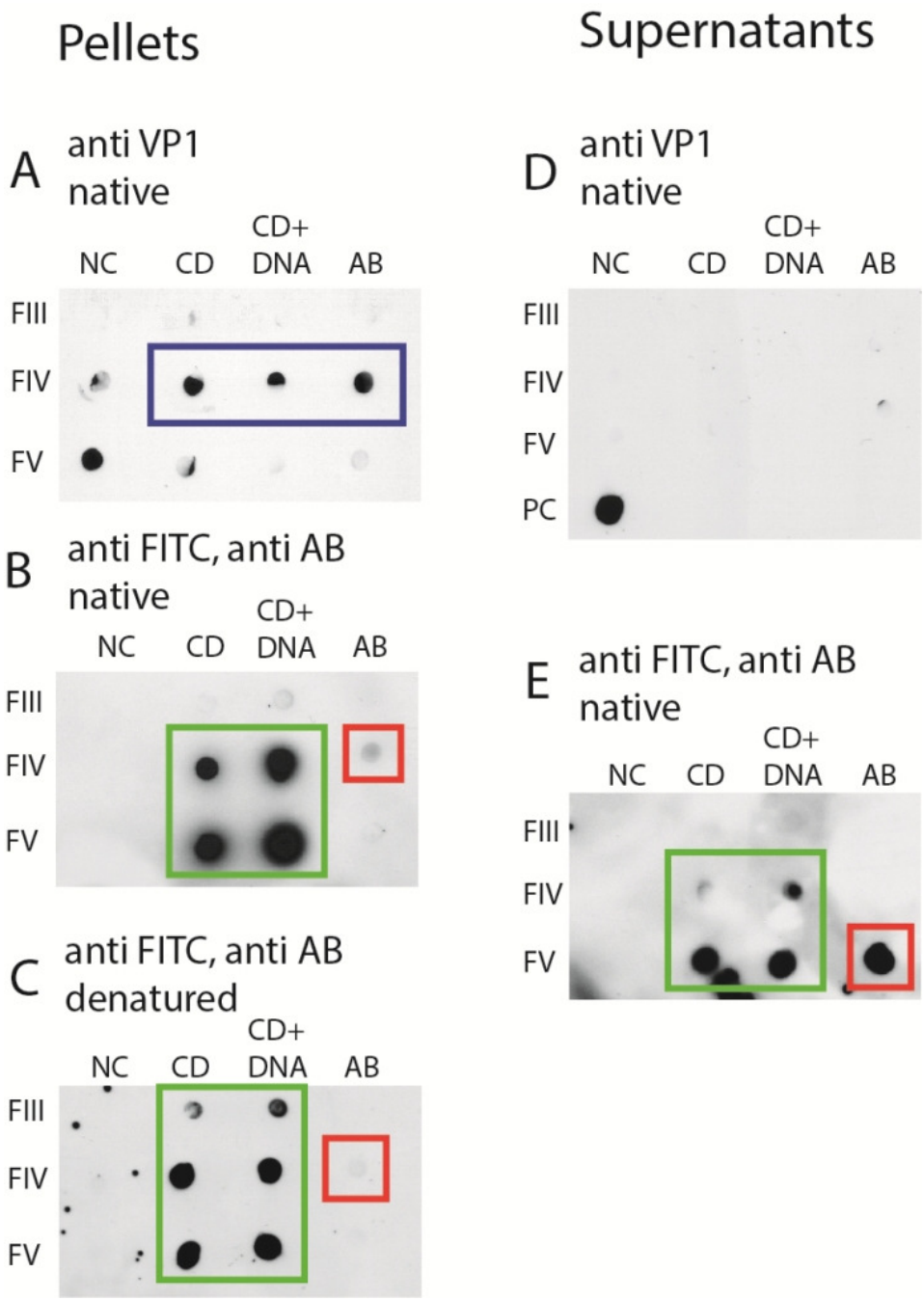

Figure 5.2.6: Verification of presence of cargo molecules in purified reassembled VLPs (immuno-dot blot detection)

A: VP1 protein detected with MαVP1-D4 antibody in pellets dissolved in buffer B. We detected most of the VP1 signal in F-IV of CD, CD+DNA and AB reassembly (blue rectangle) whereas the highest VP1 signal of NC reassembly was in F-V. **B:** CD and AB detected in pellets. CD was detected with goat anti FITC antibody. The fluorescent goat anti mouse antibody was detected directly with horseradish peroxidase conjugated donkey anti goat antibody which was also the secondary antibody for CD detection. There was a strong signal of CD in F-IV and F-V of CD-VLPs and CD+DNA-VLPs (green rectangle). There was a weak signal of AB in F-IV in AB reassembly (red square). **C:** CD and AB detected in denatured pellets. The signal of CD in F-III both CD and CD-DNA was seemed to be higher than before denaturation (green rectangle). There was a slight decrease of the signal of AB in F-IV (red square). **D:** VP1 protein detected in supernatants. VP1 signal was not present in the supernatants except for a weak signal in F-IV of AB reassembly. VP1 VLPs were used as a positive control (PC). **E:** CD and AB detected in supernatants. There was almost no CD in the supernatants of FIV whereas in FV there was a strong signal of CD (green rectangle). There was a strong signal of the fluorescent AB in FV supernatant (red square). CD is CD-VLPs, CD+DNA is CD+DNA-VLPs, AB is AB-VLPs and NC is control NC-VLPs.

5.2.2 VLPs and cargo entry into the mammalian cells

To prove that we can deliver the cargo inside cells using MPyV VP1-VLPs we observed the fate of cargo in 3T6 mouse fibroblast cells by immunofluorescent microscopy. 3T6 cells are a permissive cell line for MPyV infection thus are a suitable tool for studying VLPs entry.

Before the pseudoinfection with VLPs and the indirect immunofluorescence staining, several control experiments were performed. We tested optimal time, antibodies dilution and CD fluorescence. We realized that CD itself does not enter the cells very efficiently. After 2 hrs of incubation most of the CD seemed to be in proximity to the surface of the cells. It entered some vesicles when observed after 6.5 hrs (figure 5.2.7B). In addition, CD fluorescence was quite weak and FITC fluorescence was described to decrease in acidic conditions (Geisow, 1984). Thus we used anti FITC antibody for CD in all experiments. In control experiments we added FITC conjugated swine anti mouse antibody (FITC-AB), usually used as secondary antibody, to the cells. Surprisingly the FITC-AB was endocyted into vesicles inside the cells and stained the endosomes (figure 5.3.6C). Thus we used FITC-AB further as a control and we also included it into our second project studying the endosome escape of histidine modified VLPs (chapter 5.3.9.2).

We passaged $5x10^4$ 3T6 cells on 24-well dish on glass cover slips and pseudoinfected them after 24 hours (chapter 4.2.6.6). We pseudoinfected the cells as described in the table 5.2.4 for 6.5 hrs.

Pseudoinfection sample preparation		
Sample	Inoculum (in serum-free medium)	Figure
CD-VLPs	2.5 µg/well CD-VLPs	5.2.7E, F (anti FITC), 5.2.8E,D, 5.2.9B (anti FITC, anti VP1)
CD-DNA VLPs	2.5 µg/well CD+DNA-VLPs	5.2.7G, H (anti FITC)
NC-VLPs	2.5 µg/well NC-VLPs	5.2.7D, 5.2.8F, 5.2.9A (anti FITC, anti VP1),
FITC-AB	5 µl/well FITC-AB	5.2.7C (anti FITC)
CD	0.5 µl/well 40mM CD	5.2.7B, 5.2.8B (anti FITC)
VLPs	2.5 µg/well VP1 VLPs	5.2.8C, 5.2.9C, D (anti VP1)
NC	serum-free medium	5.2.7A, 5.2.8A (anti FITC, anti VP1)

Table 5.2.4: The pseudoinfection experiment scheme
To observe the cargo and VLPs entry into the mammalian cells we pseudoinfected the 3T6 mouse fibroblasts with CD-VLPs, CD+DNA-VLPs and NC-VLPs. As additional control we used normal, not reassembled, VP1-VLPs (VLPs). We pseudoinfected the cells with control VLPs alone. We also added FITC-AB or CD alone to the cells. Serum-free medium was added to the cells as a non infected negative control (NC).

After, we fixed and permeabilized the cells and performed the immunofluorescence staining (chapters 4.2.6.7 and 4.2.6.8). We visualized CD with GαFITC and green fluorescent antibody and VLPs with RbαVP1 and red fluorescent antibody.

We observed that after 6.5 hrs CD partially entered the cells in vesicles but it was also localized on or under the surface of the cell in stripe-like structures (figure 5.2.7B). FITC-AB entered the cells in vesicles as expected and labeled them green (figure 5.2.7C). We observed some green signal that appeared to be inside the cells in CD-VLPs (figure 5.2.7E, F) and CD+DNA-VLPs pseudoinfection (figure 5.2.7G, H). We usually observed one or two large green spots per cell in CD-VLPs and CD+DNA-VLPs (figure 5.2.7H) but we could also find few cells with several spots in both pseudoinfections (figure 5.2.7E-G).

In order to verify colocalisation of FITC and VP1 we decided to repeat the experiment for confocal microscopy (figure 5.2.8). We got similar results. There was usually one or two spots where VP1 and CD colocalized in the cells incubated with CD-VLPs (5.2.8D, E). Such spots were localized close to the nuclei and these spots were larger when compared to VP1 only positive vesicles. Taken together we confirmed that CD can be delivered by VLPs into the eukaryotic cells but we expected more extensive colocalization of CD and VP1 during internalization process. Our results will need further investigations to characterize the fate of CD in the cell.

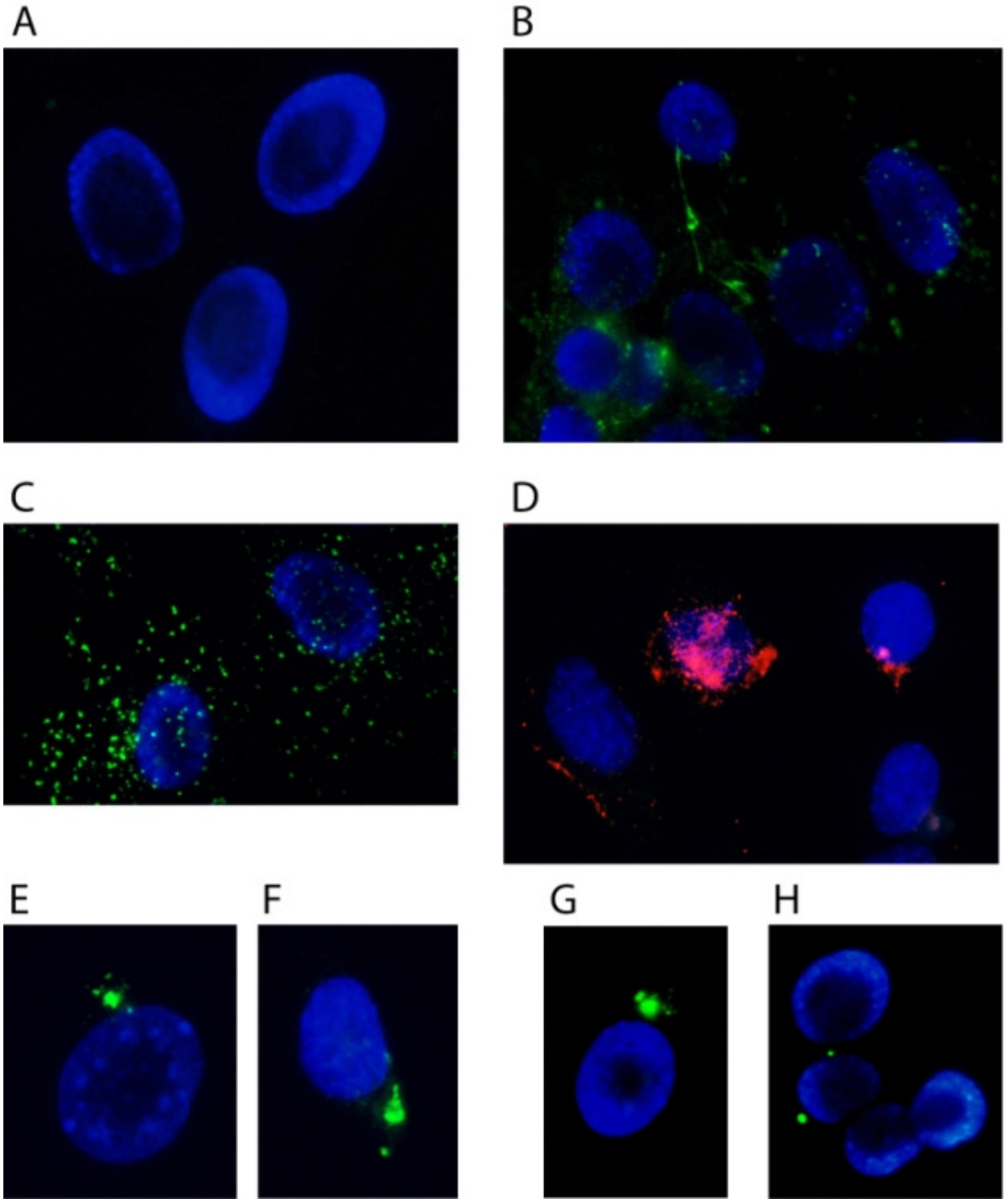

Figure 5.2.7: Pseudoifnection of 3T6 mouse fibroblast 6.5 hrs p.i. with CD-VLPs and CD+DNA VLPs, immunofluorescent staining observed with fluorescent microscope

To determine if we can deliver cargo into the cells using MPyV VP1-VLPs we used reassembled particles with CD (CD-VLPs) and CD and DNA (CD+DNA-VLPs). We performed indirect immunofluorescence staining with GαFITC antibody and green fluorescent antibody to better visualize CD (green; B, C, E-H). We also stained VP1 protein with RbαVP1 antibody and red fluorescent antibody (red; A, D). The nuclei were visualized with DAPI (blue). **A:** Negative control, uninfected cells (anti FITC and anti VP1). **B:** Pure CD entered some vesicles but also maintained some diffuse pattern more prevalent earlier p.i. (anti FITC). **C:** Pure FITC-AB was endocyted and stained the vesicles (anti FITC). **D:** NC-VLPs pseudoinfection (anti FITC, anti VP1). VLPs entered the cells, similar pattern and amount of VLPs was observed also in CD-VLPs and CD+DNA-VLPs (not shown). **E, F:** CD-VLPs pseudoinfection. One or few green spots localized close to the nuclei of pseudoinfected cells were present (anti FITC). **G, H:** CD+DNA-VLPS pseudoinfection. The pattern was the same as in CD-VLPs, one or few green spots close to the nuclei (anti FITC).

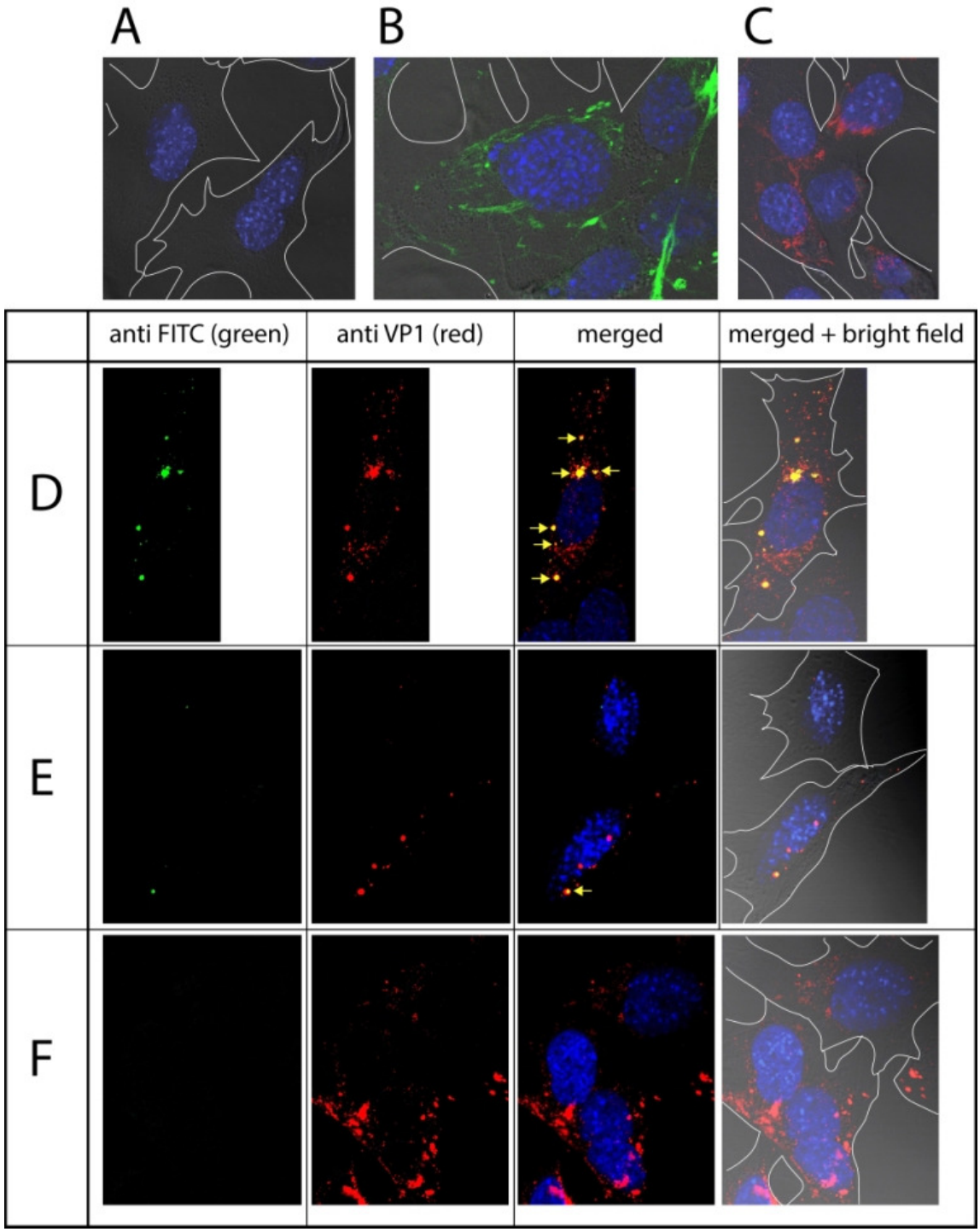

Figure 5.2.8: Pseudoifnection of 3T6 mouse fibroblasts 6.5 hrs p.i. with CD-VLPs, immunofluorescent staining observed with confocal microscope

We used the same antibodies as in figure 5.2.6 to detect CD and VP1. Nuclei are stained with DAPI (blue), VP1 in red and CD in green. White lines depict the borders of cells as observed in bright field. All of the images represent one selected thin section under confocal microscope. **A:** Uninfected cells were used as a negative control. **B:** CD alone made fiber-like structures inside the cells. **C:** Control VP1-VLPs added in excess on the cells appear to enter the cells and were observed in cytoplasm with a few in nuclei. **D, E:** CD-VLPs entered the cells and were observed inside the cytoplasm as well as in nuclei. However the green signal appeared and colocalized with VP1 only in big spots of VP1, possibly some vesicles (yellow arrows). Usually there were only one or two spots of CD and VP1 colocalization per cell localized close to the nuclei. **F:** NC-VLPs were used as a control. The pattern of entry resembled the entry of CD-VLPs. VP1 was observed in cytoplasm and nuclei.

Images: Mgr. Ondřej Šebesta and Dr. Jozef Janda

Even though we aimed for adding the same amount of VLPs based on the protein concentration, the observable amount (evaluated by the intensity of VP1 signal) of non reassembled VLPs seem to be larger than of reassembled VLPs. Consequently, we observed that the pattern of entering VLPs differed between control VP1-VLPs (possibly added in excess) and reassembled VLPs (CD-VLPs and NC-VLPs; figure 5.2.8 C, D, E, F, figure 5.2.9). VP1 immunofluorescent signal from reassembled VLPs appeared amorphous, concentrated in larger spots (possibly vesicles) and wase more frequently observed in the nuclei (figure 5.2.9A, B). The non reassembled VLPs appeared to enter cells in distict smaller dots; however, the majority of VP1 material was localized on the cell periphery in fiber-like configuration (figure 5.2.9C, D). The cells with VP1 signal in larger spots tended to have VP1 signal inside the nuclei (figure 5.2.9 C) whereas in cells with fiber-like VP1 signal no nuclear VP1 was observed (figure 5.2.9 D).

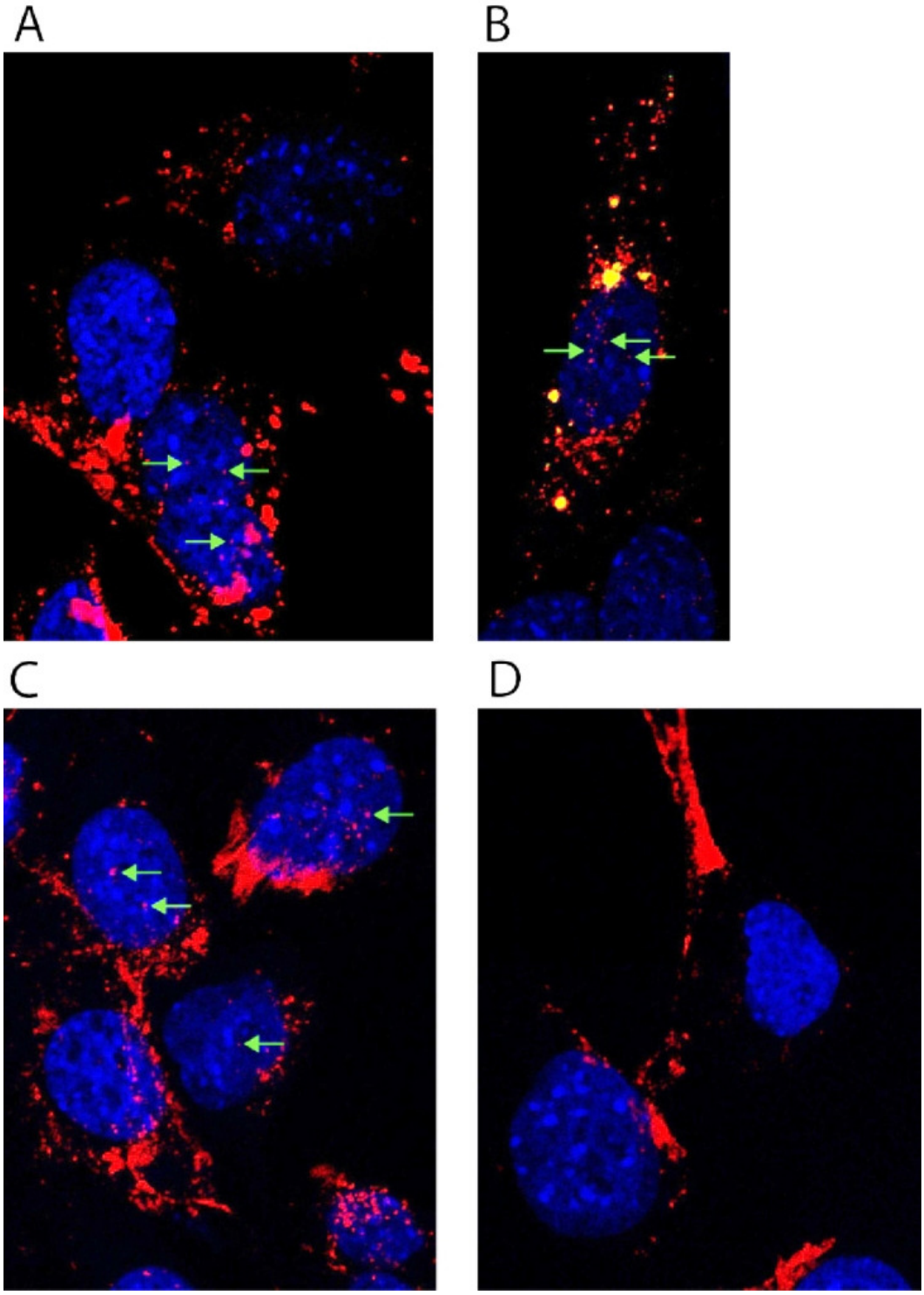

Figure 5.2.9: VP1 signal observed in nuclei of 3T6 mouse fibroblasts pseudoifnected with MPyV VP1-VLPs 6.5 hrs p.i., immunofluorescent staining observed with confocal microscope

We observed VP1 signal nuclear localization in cells pseudoinfected with CD-VLPs and control VLPs. The same antibodies were used as in figures 5.2.6 and 5.2.7. Nuclei were stained with DAPI (blue), VP1 is red and CD green. **A:** NC-VLPs entered cells in larger spots and localized inside the cytoplasm and nuclei (green arrows). **B:** CD-VLPs followed the same pattern as the NC-VLPs. **C, D:** Non disassembled VP1-VLPs appered to be added in excess of other variants of VLPs and two entry patterns were observed **C:** The cells with VP1 signal that appeared to be more in spots than fiber tended to have VP1 inside the nuclei. **D:** Some cells had very strong VP1 signal in the periphery of the cell and the VP1 spots were smaller and closer to the cell surface often in fiber-like structures with no VP1 inside the nuclei.

Images: Mgr. Ondřej Šebesta and Dr. Jozef Janda

5.3 Preparation of histidine modified MPyV VP1-VLPs (His-VLPs) and determination of their endosome escape properties

In attempt to prepare MPyV-derived VLPs with enhanced endosome escape properties, we decided to insert multiple histidines into DE loop of VP1 protein. Such modification should not affect the receptor binding (Kojzarová, 2011). The histidine modification was selected because of its low pH dependent endosome escape potential investigated on various synthetic delivery systems (chapter 2.3.2).

We used Bac-to-Bac® baculovirus expression system for His-VLPs production (chapter 4.1.11) which is a well established method in our laboratory. It allows modification of the *VP1* sequence in a donor plasmid and then such modified plasmid can be used in the same manner as the original one for VLPs production to obtain modified VP1-VLPs.

5.3.1 Construction design

We used previously prepared construct of *VP1* sequence with modified DE loop containing BamHI restriction site surrounded with flexible glycine serine linker called *VP1-7less* under strong polyhedrin promoter in pFastBac1 donor vector with deleted BamHI site (pFastBac1_noBamHI_VP1-7less, Kojzarová 2011).

We designed a pair of phosphorylated oligonucleotides that encode for histidine tag that is 6 histidines long (His_6, chapter 4.1.6). The oligonucleotides were designed so they anneal in the complementary His_6-coding sequence and have 5'-overhangs that pair with BamHI digested vector. Additionally the BamHI sequence encodes for glycine and serine which form a flexible linker (figure 5.3.1B). At the end we had to design a new set of oligonucleotides because we made a mistake and the first set of oligonucleotides resulted in blunt ends when annealed (figure 5.3.1A). However, we were able to get one construct with the incorrectly designed old oligonucleotides as well.

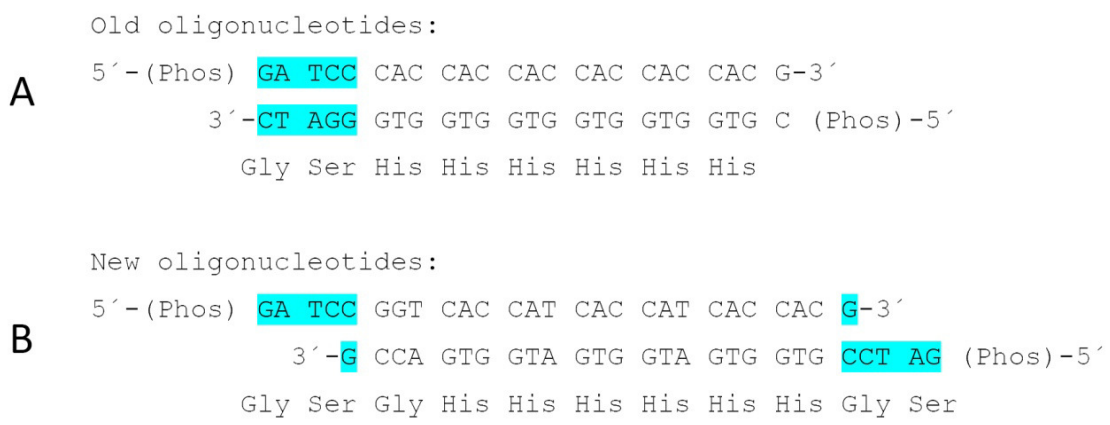

Figure 5.3.1: His_6 coding phosphorylated oligonucleotides design
A: The first set of oligonucleotides (old oligonucleotides) was wrongly designed and instead of 5'-overhangs pairing with BamHI digested vector they formed blunt ends after annealing. However this construct also encodes for six histidines. **B:** The second set of oligonucleotides (new oligonucleotides) anneals correctly with 5'-overhangs pairing with BamHI digested vector. It encodes for six histidines surrounded with glycine and serine after insertion into the vector.

As there is only one restriction site in DE loop of *VP1-7less*, the ligation of vector and oligonucleotides is not oriented. On the other hand it allows insertion of multiple oligonucleotides resulting in more than just one His_6 in the DE loop. Such longer insertions could have stronger endosome escape properties that we wanted to examine.

5.3.2 Insertion of His_6-coding oligonucleotides into *VP1-7less* DE loop in pFastBac1 plasmid

We first had to anneal each pair of complementary oligonucleotides in order to get double stranded DNA insert. We mixed the oligonucleotides in 1:1 ratio and annealed them as described in chapter 4.2.2.3. We verified the result on agarose electrophoresis using 4% agarose gel because the oligonucleotides were 24 and 27 bp long (figure 5.3.2).

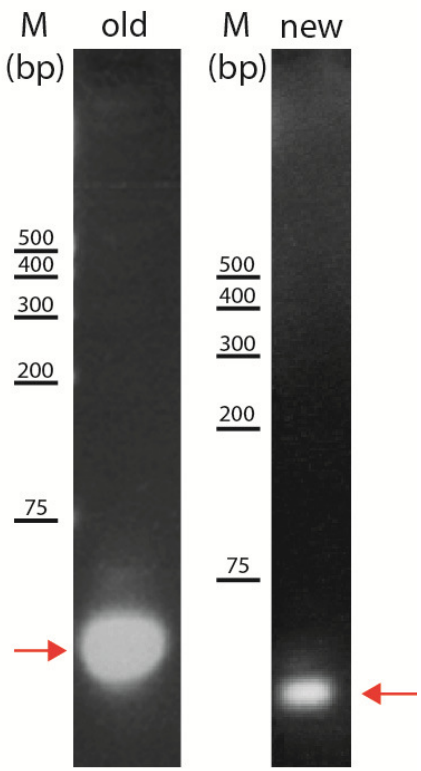

Figure 5.3.2: Insert preparation – an electrophoretic control of annealed oligonucleotides
Designed complementary oligonucleotides were mixed in 1:1 ratio. The mixture was denatured and cooled down from 95 °C to 25 °C for 5 hrs for the annealing. We checked the oligonucleotides annealing using agarose electrophoresis (4% agarose). Annealed products of expected size were detected (red arrows).

The pFastBac1_noBamHI_VP1-7less construct was linearized with BamHI restriction endonuclease and dephosphorylated to prevent its recircularization. Annealed His_6 coding oligonucleotides were then ligated into *VP1-7less* construct in 3:1, 10:1 and 50:1 molar ratios of the ends. We hoped that the big excess of oligonucleotides would result in multiple insertions. Stellar™ cells were then transformed with the ligation mixtures as well as control uncut pFastBac1_noBamHI_VP1-7less. We selected several colonies from each transformation grown on ampicillin plates, restriped them on fresh ampicillin plates and performed colony PCR with primers MK(BG)2 and MK(BG)3 to detect the insertion in DE loop (chapter 4.1.6). We visualized the results of colony PCR using agarose electrophoresis. We were already able to distinguish colonies that differed from unmodified *VP1-7less* control as the PCR products with insertion were slightly larger (figure 5.3.3A). To make sure that the insert is really present the PCR products were digested with BamHI endonuclease and visualized the result using agarose electrophoresis. The control *VP1-7less* digestion resulted in two fragments, approx. 450 bp and 100 bp long. When the insert was present, there was at least one additional shorter fragment (figure 5.3.3B).

A

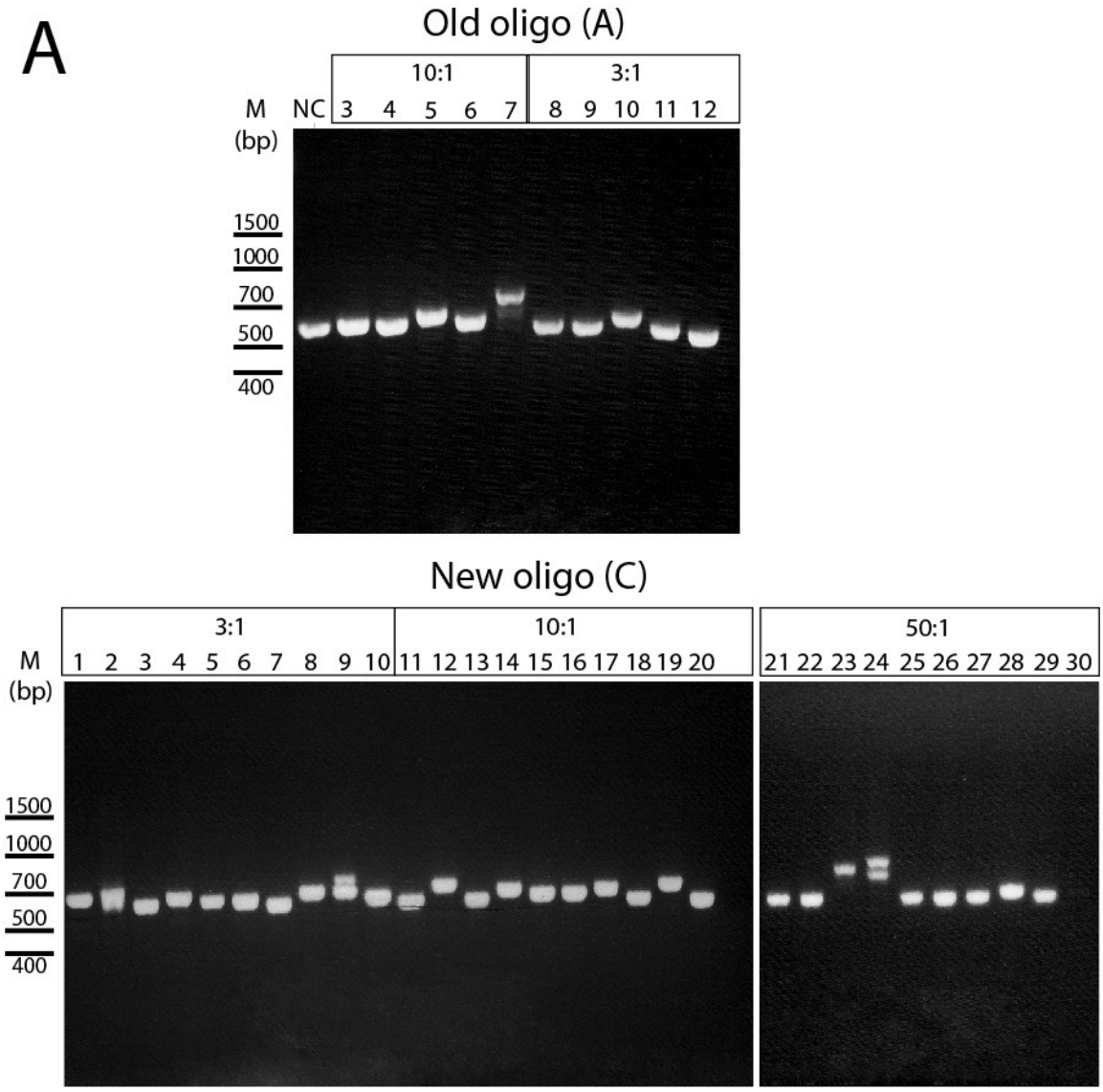
Old oligo (A)
10:1
3:1
M NC 3 4 5 6 7 8 9 10 11 12
(bp)
1500
1000
700
500
400
New oligo (C)
3:1
10:1
50:1
M 1 2 3 4 5 6 7 8 9 10 11 12 13 14 15 16 17 18 19 20 21 22 23 24 25 26 27 28 29 30
(bp)
1500
1000
700
500
400

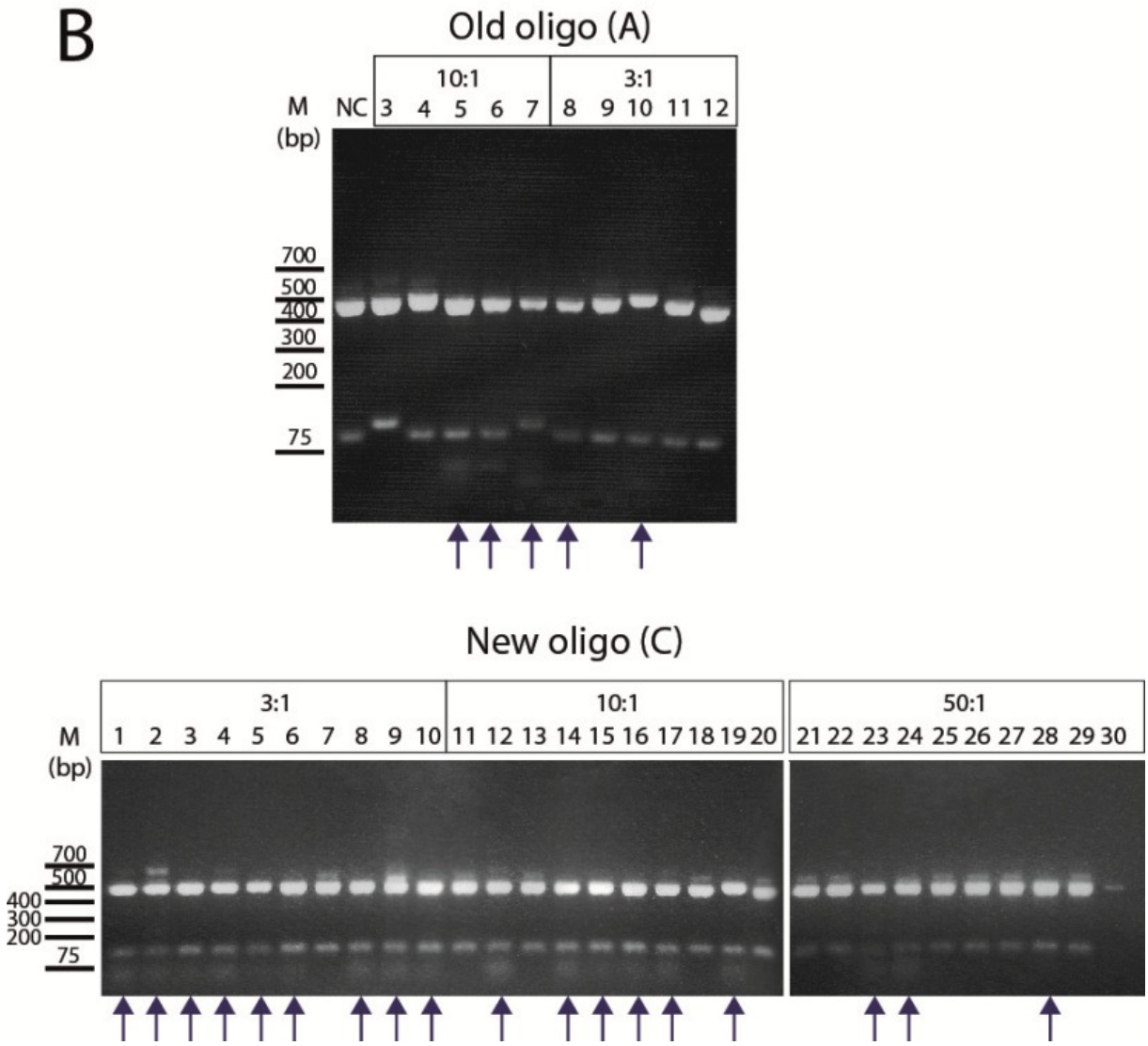

Figure 5.3.3: Electrophoretic detection of Stellar™ *E.coli* colonies containing His_6-oligonucleotides insertion in DE loop of *VP1*

The insertion of His_6 coding oligonucleotides into the *VP1* in transformed Stellar™ cells was validated using two methods. **A:** The results of colony PCR. The "negative control, NC" is colony PCR from Stellar™ cells transformed with vector with unchanged *VP1-7less*. The colonies with probable insertion resulted in slightly longer PCR product. **B:** BamHI endonuclease digestion of colony PCR products. The "negative control, NC" resulted in two fragments whereas the colonies with insertion had at least three fragments after BamHI digestion. Colonies with inserted His-oligonucleotides are marked with blue arrows. The ratios above samples describe the ligation ratios of oligonucleotides and the vector.

All the positive colonies were cultivated, the plasmid was isolated from the culture using High Pure Plasmid Isolation Kit (Roche) and the *VP1* insert was sequenced. As the ligation was non oriented many of the colonies did not encoded only His_6 or its multiples. However we were able to isolate plasmids with *VP1* with inserted His-tag coding sequence, *His-VP1*. Although we hoped the excess of oligonucleotides in the ligation mixture would result in increased number of inserted oligonucleotides, it only reduced the ligation efficiency as there were much less colonies with insert from 50:1 ligation than the optimal 3:1 reaction. We prepared *His-VP1* with one

inserted His-tag coding sequence, two inserted His-tag coding sequences and four inserted His-tag coding sequences (table 5.3.1). The latter is the result of old, incorrectly designed oligonucleotides and it lacks the 3'-terminal BamHI.

Senquencing analysis of *His-VP1* constructs	
Colony	**Insert**
C5	BamHI-His_6 oligo-BamHI
C6	BamHI-His_6 oligo-BamHI
C8	BamHI-His_6 oligo-BamHI-His_6 oligo-BamHI
C10	BamHI-His_6 oligo-BamHI
C14	BamHI-His_6 oligo-BamHI-His_6 oligo-BamHI
C15	BamHI-His_6 oligo-BamHI
C28	BamHI-His_6 oligo-BamHI
A7 (old oligo)	BamHI-His_6 oligo-BamHI-His_6 oligo-BamHI-His_6 oligo-BamHI-His_6 oligo

Table 5.3.1 List of colonies with inserted His_6 coding sequence in DE loop of *VP1*
Isolated plasmids were sequenced to determine which have His_6-oligonucleotides inserted in the correct orientation so they translate into histidines. The sequencing analysis revealed that we prepared three different types of consturcts. We obtained *His-VP1* with once inserted His_6 coding sequence surrounded by BamHI restriction sites (C5, C6, C10, C15 and C28), *His-VP1* with twice inserted His_6 coding sequence surrounded with BamHI restriction sites (C8 and C14) and *His-VP1* with four times inserted His_6 coding sequence surrounded with BamHI restriction sites although the last BamHI is missing because this is the result of incorrectly designed oligonucleotides with blunt ends (A7). We chose C5, C14 and A7 plasmids for further work.

5.3.3 Preparation of His-VP1 bacmids

Next step in Bac-to-Bac® baculovirus expression system is the production of bacmids for which the previously prepared donor plasmids are needed. We followed the manual "Bac-to-Bac® instruction manual" (Invitrogen) for bacmid production. We transformed the electrocompetent DH10Bac *E.coli* with plasmid isolated from C5, C14 and A7 colonies (1xHis_6, 2xHis_6, 4xHis_6) and after cultivation the bacmid was isolated from selected colonies.

We then controlled the quality of bacmids using agarose electrophoresis. Finally, we determined if the insert is trully present using PCR with bacmid specific primers (chapter 4.1.6) and visualised the products using agarose electrophoresis. The PCR fragments were of expected size 3500 bp, thus we concluded the inserts were present (data not shown).

5.3.4 Preparation of His-VP1 recombinant baculovirus

Sf9 insect cells were transfected in a 6-well dish with prepared bacmids as described in Cellfectin® II Reagent protocol. The bacmids A7, C5 and C14 were used for the transfection. We collected the medium 3 days post infection (d.p.i) that is designated as P1 inoculum and stored at 4 °C. We multiplied the baculovirus inocula by two reinfections (chapter 4.2.6.2). We used the cells from one of the passages for detection of VP1 and His_6. Non-infected cells were used as a negative control. We lysed the collected cells (chapter 4.2.3.1) and performed immuno-dot blot

to check the presence of VP1 protein and His_6 in the lysate. We detected both VP1 and His_6 in all isolations (figure 5.3.4), that means we successfully prepared recombinant bacmid that allows production of His-VP1 protein.

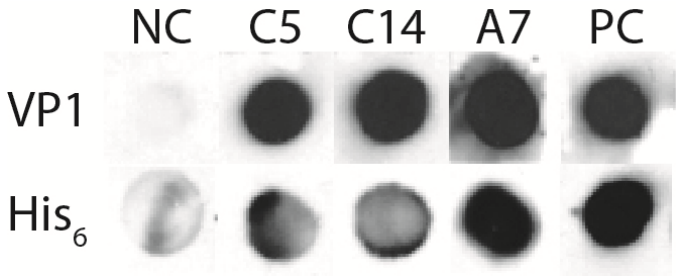

Figure 5.3.4: Immuno-dot blot of cell lysates after recombinant baculovirus infection.
Immuno-dot blot analysis of cell lysates was performed after infection of Sf9 cell with recombinant baculovirus inocula collected after transfection with prepared bacmids. We used MαVP1-A and MαHis. Because the signal was detected for both VP1 and His_6, we concluded we produced recombinant baculoviruses that allow His-VP1 production. Cell lysate from uninfected cells was used as a negative control (NC), MPyV VP1-VLPs as a positive control (PC) for VP1 detection and histidine-rich protein Yin Yang 1 as a positive control for His_6 detection.

To verify the formation of VLPs we performed small scale isolation of VLPs. Infected cells from one of the baculovirus multiplication steps were used. Standard protocol for VLPs isolation was used (sonication and CsCl gradient centrifugation, chapter 4.2.4.5). CsCl fractions were analyzed using immuno-dot blot to determine VP1 positive fractions (not shown). We dialyzed the selected fractions against buffer B, concentrated the samples using PEG 20000 and prepared electron microscopy samples. We confirmed that there were VLPs present in C14 isolations and very few in C5 (figure 5.3.5). We did not perform this preliminary experiment for A7 inoculum.

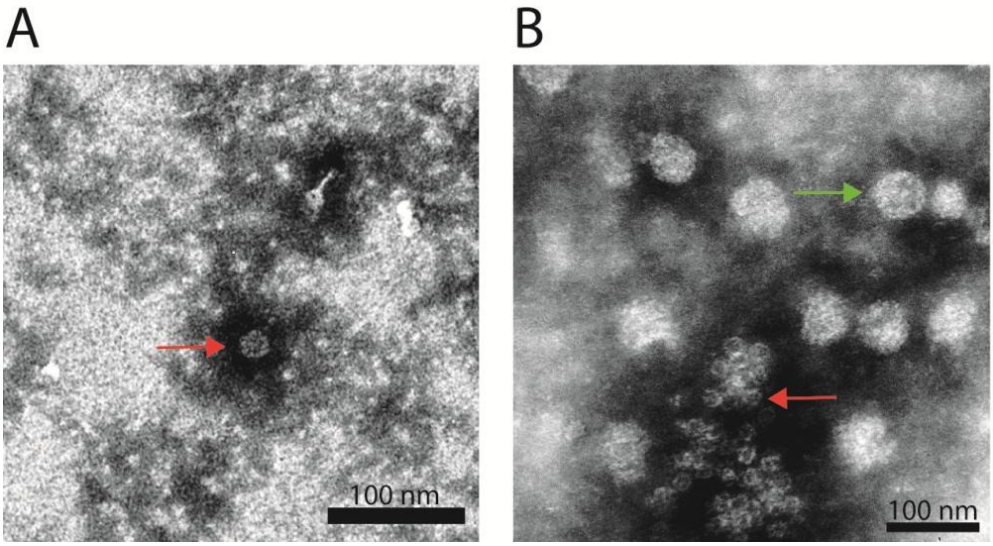

Figure 5.3.5: Electron microscopy from small scale VLPs isolation (negative staining)
To prove that VLPs are forming in His-VP1 recombinant baculovirus infected cells we performed smalls scale VLPs isolation. **A:** Few 20nm VLPs (red arrow) were observed in C5 isolation. **B:** Both 45nm VLPs (green arrow) and 20nm VLPs were observed in C14 isolation. The isolation for A7 was not performed.
Images: Mgr. Jiřina Suchanová

The small scale isolation confirmed that VLPs assembled in His-VP1 recombinant baculovirus infected cells. To obtain pure monoclonal inocula for further infections we performed plaque assay with multiplied inocula (chapter 5.2.6.3). We selected the plaques and dissolved in serum-free medium 8 d.p.i. We used these inocula for further infection of Sf9 cells to obtain monoclonal recombinant baculovirus inocula. We passaged the inocula two times to get sufficient amount for large scale infections.

5.3.5 Production of His-VLPs and other His-VP1 nanomaterial

The production of His-VLPs and other His-VP1 nanomaterial was a very challenging part of this project. First we used the standard for polyomavirus VLPs isolation (sonication of infected cells, centrifugation in CsCl gradient, separation of fractions, dialysis to buffer B and centrifugation through 10% sucrose cushion chapters 4.2.4.1, 4.2.4.3-4.2.4.5). The fractions from CsCl gradient were analyzed using immuno-dot blot to confirm the presence of VP1. The fractions were combined based on the dot blot signal (figure 5.3.6) and refractive index of the fractions (table 5.3.2).

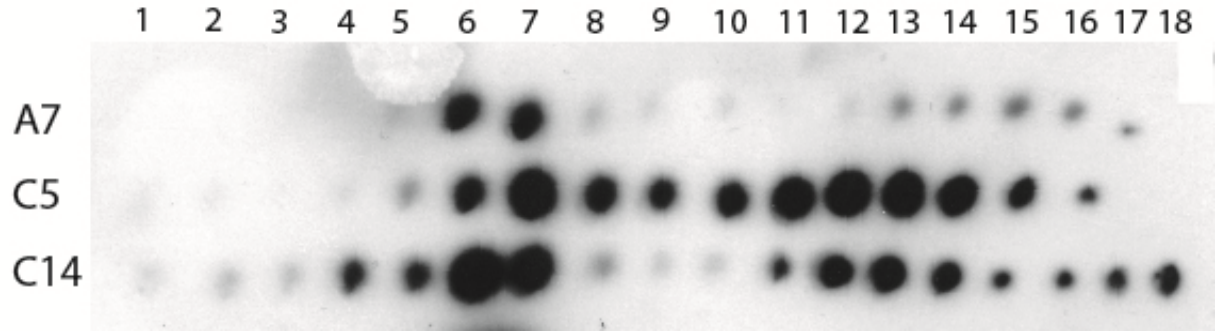

Figure 5.3.6: Immuno-dot blot of VP1 protein in CsCl gradient fractions (sonication protocol)
The presence of VP1 protein was determined in CsCl gradient fractions using immuno-dot blot using MαVP1-A antibody.

Refractive index of CsCl fractions of small scale isolation of His-VLPs			
fraction	C5	C14	A7
1	1.372	1.373	1.375
2	1.372	1.373	1.373
3	1.370	1.371	1.370
4	1.368	1.368	1.368
5	1.366	1.3665	1.367
6	1.3645 C5 F-I	1.366 C14 F-I	1.3655 A7 F-I
7	1.364	1.364	1.3645
8	1.3635	1.364	1.364
9	1.363	1.3635	1.364
10	1.363	1.363	1.364
11	1.362 C5 F-II	1.363 C14 FII	1.363
12	1.362	1.3625	1.363
13	1.3605	1.362	1.362 A7 F-II
14	1.360	1.361	1.361
15	1.359	1.360	1.360
16	1.357	1.359	1.359
17		1.358	1.357
18		1.357	

Table 5.3.2: Refractive index of CsCl gradient fractions (sonication protocol)
We measured the refractive index of CsCl gradient fractions. The fractions for dialysis were combined based on immuno-dot blot results and the refractive index. We made two separate fractions for each sample (colored boxes).

After the whole isolation we prepared electron microscopy samples. The results were quite surprising. There were very few VLPs in both fractions of C5 isolation (which is His-VP1 with one His_6 insert). The material was mostly disorganized clumps (figure 5.3.7A) thus we did not continue further experiments with C5 inoculum. The fractions of A7 (four His_6 inserts) differed. There were no VLPs in fraction F-I the material looked sort of disorganized in net-like structures probably composed of VP1 pentamers (figure 5.3.7B). There were some structures in fraction F-II that resembled VLPs (not shown). However, the most striking result brought C14 isolation (two His_6 inserts). The majority of the material formed highly organized planar structures that looked like composed from monomeric VP1 instead of usual VP1 pentamers. We decided to name the planar structures "nano-jumpers" as they resemble the pattern of knitted fabric (figure 5.3.7). We also found VLPs and tubular structures in the C14 isolation (figure 5.3.7D).

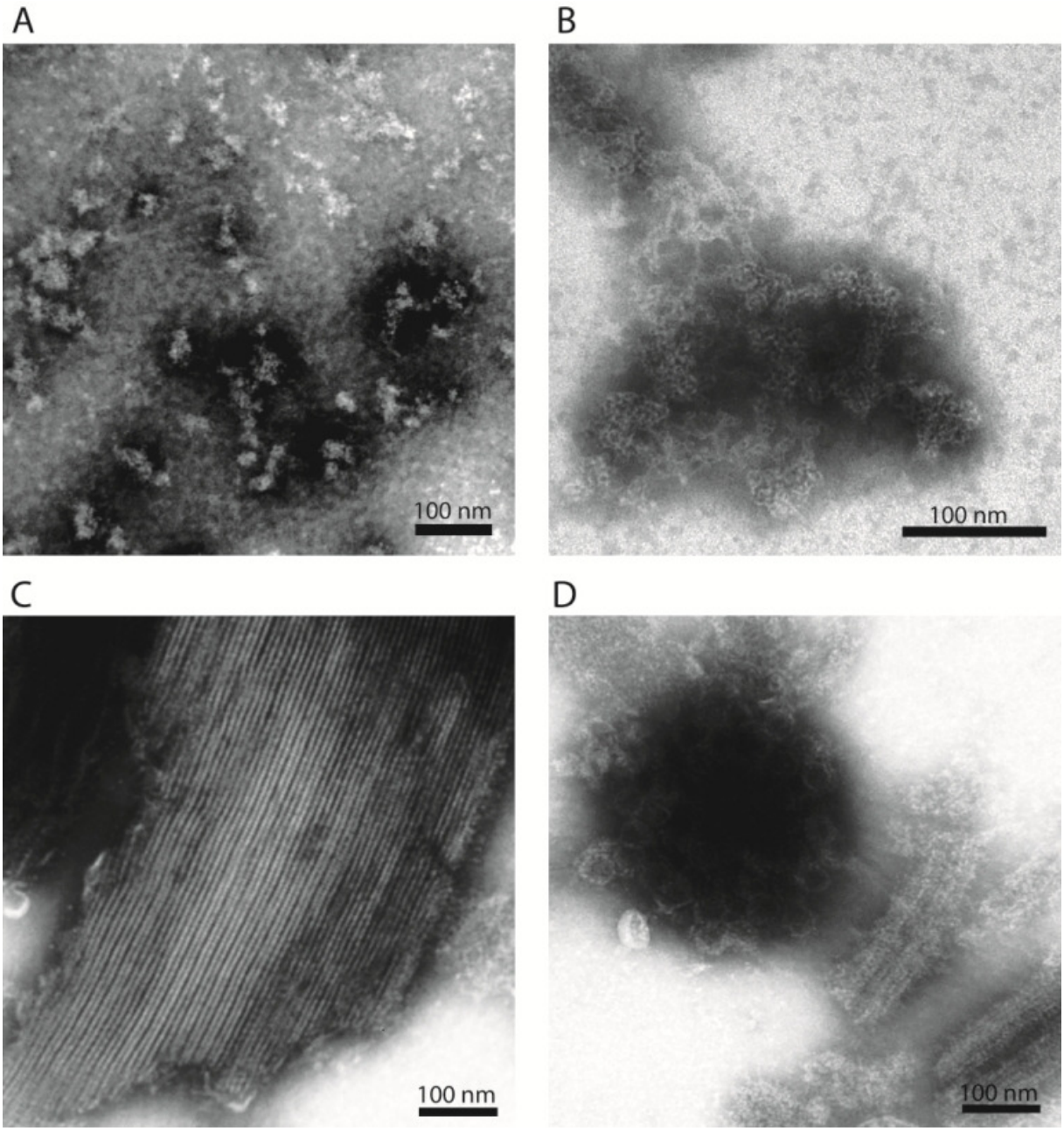

Figure 5.3.7 Electron microscopy images of His-VP1 isolation, sonication protocol (negative staining)
The electron microscopy images revealed the structure of produced His-VP1. **A:** C5 isolation. The material was mostly disorganized clumps with very few VLPs. **B:** A7 F-I contained disorganized net-like structures probably composed of VP1 pentamers. **C, D:** The material in C14 isolations was in diverse structures. **C:** Most of the material organized in highly regular planar structures without typical pentamers **D:** Both VLPs and tubular structures composed of VP1 pentamers were also observed in C14 isolation.
Images: Mgr. Jiřina Suchanová

The protein concentration was surprisingly low compared to the dot blot signal and input material, especially in C5 and C14 isolations (table 5.3.3). Our idea was that His_6 changes the binding properties of VLPs to plastic and other material used during the isolation resulting in low yield of nanostructures. Thus we continued with optimization.

Protein concentration of His-VLPs	
Fraction after dialysis	Protein concentration
A7-4 FI	128 µg/ml
A7-4 FII	49.4 µg/ml
C14-1 FI	62.3 µg/ml
C14-1 FII	157 µg/ml
C5-1 FI	51.3 µg/ml
C5-1 FII	121 µg/ml

Table 5.3.3: Protein concentration of His-VLPs isolations measured by Quibit Fluorimeter

The first attempt to increase the yield of His-VLPs isolation was to perform the standard isolation in acidic conditions together with detergent Triton X-100 (chapter 4.2.4.7). We reasoned that detergent can help to liberate material from membranes and low pH can help to charge the surface of nanostructures (as histidine acquires positive charge in acidic conditions) and influence aggregation and stickiness of material. Unfortunately this approach did not bring a positive result. We obtained neither VLPs nor other nano-structures, and there was a lot of cellular material, especially lipid membranes, in the isolation (data not shown).

Next we tried the isolation based on affinity of histidine to metal ions such as nickel and cobalt. First we used small scale isolation using magnetic beads based on cobalt chemistry (Dynabeads® for His-Tag Isolation, chapter 4.2.4.8). Our first attempt was quite successful. We obtained VLPs, nano-jumpers and tubular structures in both C14 and A7. The only problem was that the material was associated with membranous cellular material. We decided to scale up the affinity isolation. We tried nickel based HisTrap FF crude 1ml column and His-select® Nickel Affinity Gel (Sigma-Aldrich) for His-VLPs isolation with no positive result. The most of His-VP1 material remained in the flow through and wash fractions as analyzed on immuno-dot blot or SDS-PAGE followed by western blot.

As a result, we tried the magnetic beads again. This time we also analyzed the flow through and wash fractions. We also tried different amounts of the infected cells. We were not able to repeat the results of the first Dynabeads® experiment. The isolations were much more contaminated with cell debris. Moreover, the most of His-VP1 material remained in the flow through and wash fractions. Also the signal was still present on the beads even after multiple elution steps. This suggests the His-VLPs and His-VP1 nanomaterial do not bind to the beads very specifically. Also the His-VLPs and nanostructures bind nonspecifically to the cellular material, especially membranes.

Finally we decided to try another common method for VLPs isolation which is cell lysis with Triton X-100, Benzonase® treatment and salt precipitation followed by standard protocol with CsCl gradient centrifugation and other steps as in isolation with sonication (chapter 4.2.4.6). We performed immuno-dot blot detection of VP1 and His_6 (figure 5.3.8). We combined the fractions

for dialysis after CsCl gradient based on the immunodetection and refractive index as shown in table 5.3.4.

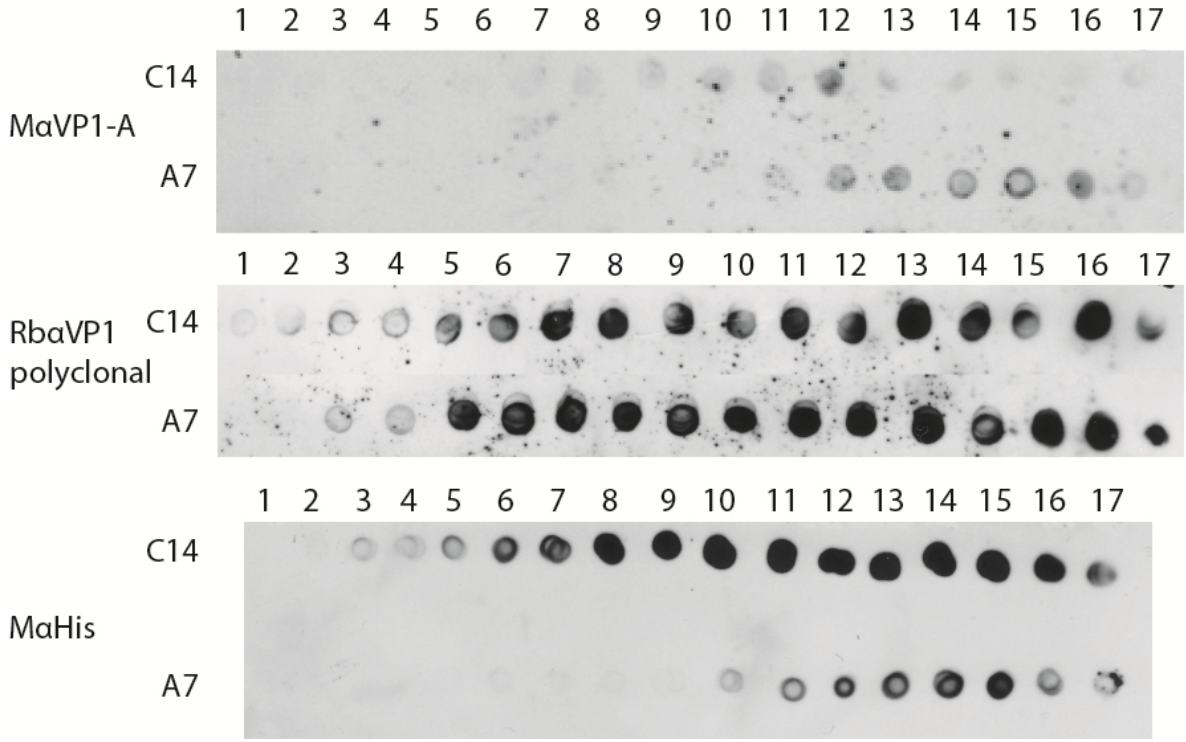

Figure 5.3.8: Immuno-dot blot of VP1 protein and His_6 in CsCl gradient fractions (lysis protocol)
We checked the presence of VP1 protein in CsCl gradient fractions using immuno-dot blot. VP1 was detected first with MαVP1-A antibody as in all previous experiments. For reasons that are not clear the signal was very weak. Thus we detected VP1 again with RbαVP1 antibody and His_6 with MαHis antibody. We combined the fractions for dialysis based on the result and refractive index of fractions (table 5.3.5).

Refractive index of CsCl gradient fractions, lysate protocol				
Fraction	C14		A7	
1	1.374		1.3725	
2	1.3725		1.373	
3	1.370	C14 F-I	1.371	A7 F-I
4	1.168		1.368	
5	1.367		1.367	
6	1.366		1.3655	
7	1.365		1.365	A7 F-II
8	1.364	C14 F-II	1.364	
9	1.364		1.364	
10	1.364		1.363	
11	1.3635		1.363	
12	1.363		1.363	
13	1.3625		1.362	A7 F-III
14	1.362	C14 F-III	1.3615	
15	1.361		1.361	
16	1.360		1.359	
17	1.358		1.357	

Table 5.3.4: Refractive index of CsCl gradient fractions (lysate protocol)
We measured the refractive index of CsCl gradient fractions. The fractions were combined for dialysis based on the dot blot results and the refractive index. We made three separate fractions for each sample (colored boxes).

After the isolation we prepared the electron microscopy samples. Fraction F-III of A7 isolation contained long tubular structures and small VLPs of approx. 20 nm (figure 5.3.9A, B). As in previous experiments we obtained mainly nano-jumpers in C14 isolation (5.3.9D), this time in sufficient concentration. Also tubular structures or VLPs could be found (5.3.9C). The nano-jumpers were enriched in the fraction F-III whereas fraction F-I was almost empty and fraction F-II had mostly disorganized structures or tubules (not shown).

Taken together, we managed to optimize to protocol for His-VP1 nanostructures isolation. We prepared C14 His-VP1 with twice inserted His_6 sequence separated by glycine-serine linkers. C14 forms a novel nanostructure which we called nano-jumpers. We also prepared A7 His-VP1 with four times inserted His_6 sequence separated by glycine-serine linkers. A7 forms long tubules and small VLPs of approx. 20 nm in diameter. We further investigated both constructs in following experiments.

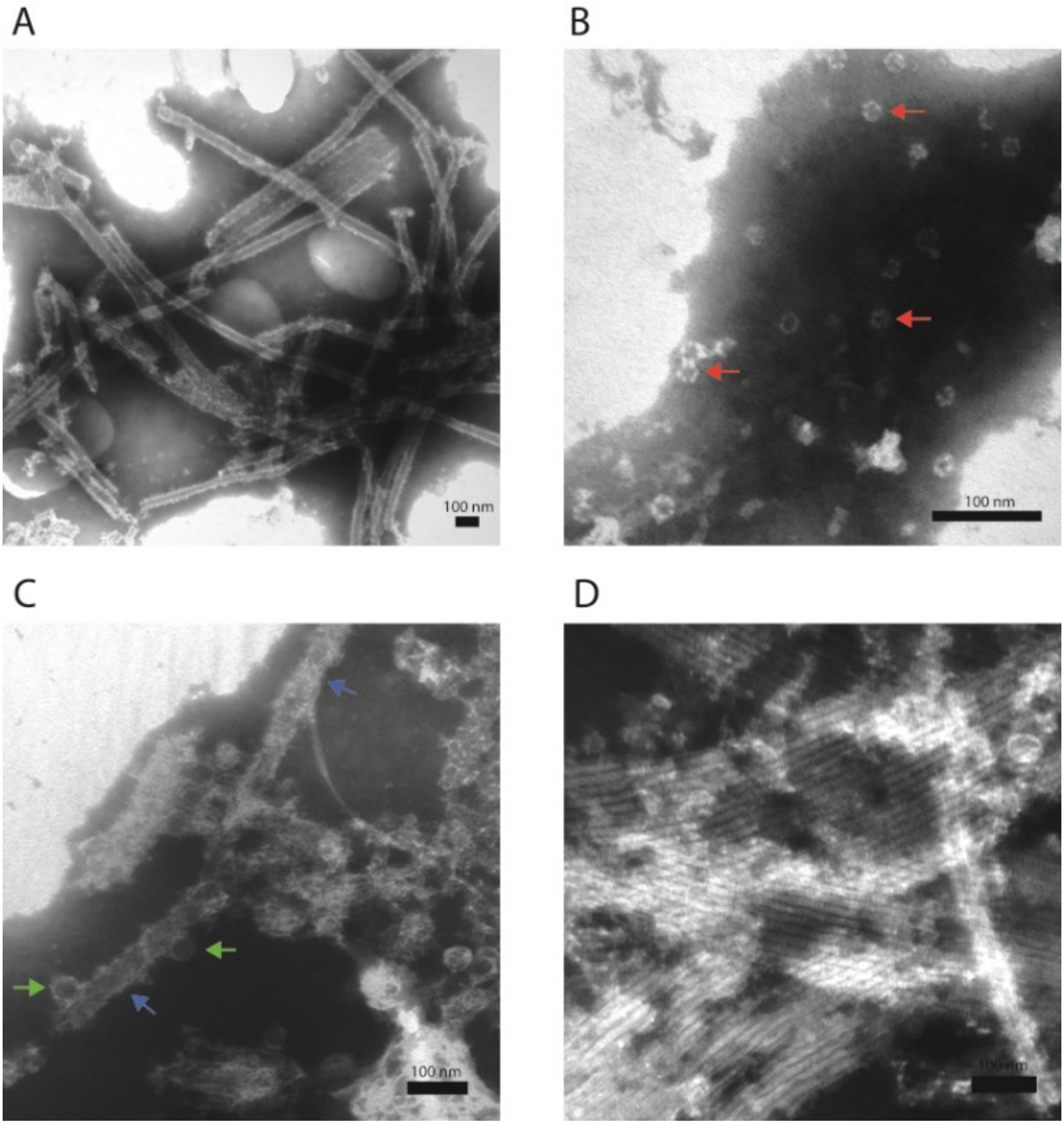

Figure 5.3.9: Electron microscopy images of His-VP1 isolation, lysate protocol (negative staining)
The electron microscopy revealed that the His-VLPs and nano-structures isolation using cell lysis was successful. **A:** His-VP1 in A7 isolation formed long tubules composed of VP1 pentamers. **B:** A7 His-VP1 also formed small VLPs of approx. 20 nm in diameter (red arrows). **C, D:** His-VP1 in C14 isolation formed many structures. **C:** We could find tubular structures (blue arrows) and VLPs (green arrows), but **D:** the nano-jumpers were the predominant structures. Images: Mgr. Jiřina Suchanová

5.3.6 Morphology of His-VP1 recombinant baculovirus infected cells

During production of recombinant baculovirus inocula and His-VP1 we noticed an interesting morphology of A7 His-VP1 recombinant baculovirus infected Sf9 cells. The nuclei of such cells appeared donut-shaped or as they had some kind of large central invagination (figure 5.3.10A). We did not observe such morphology in uninfected Sf9 (figure 5.3.10C) cells or wild type VP1 recombinant baculovirus infected Sf9 cells (figure 5.3.10B).

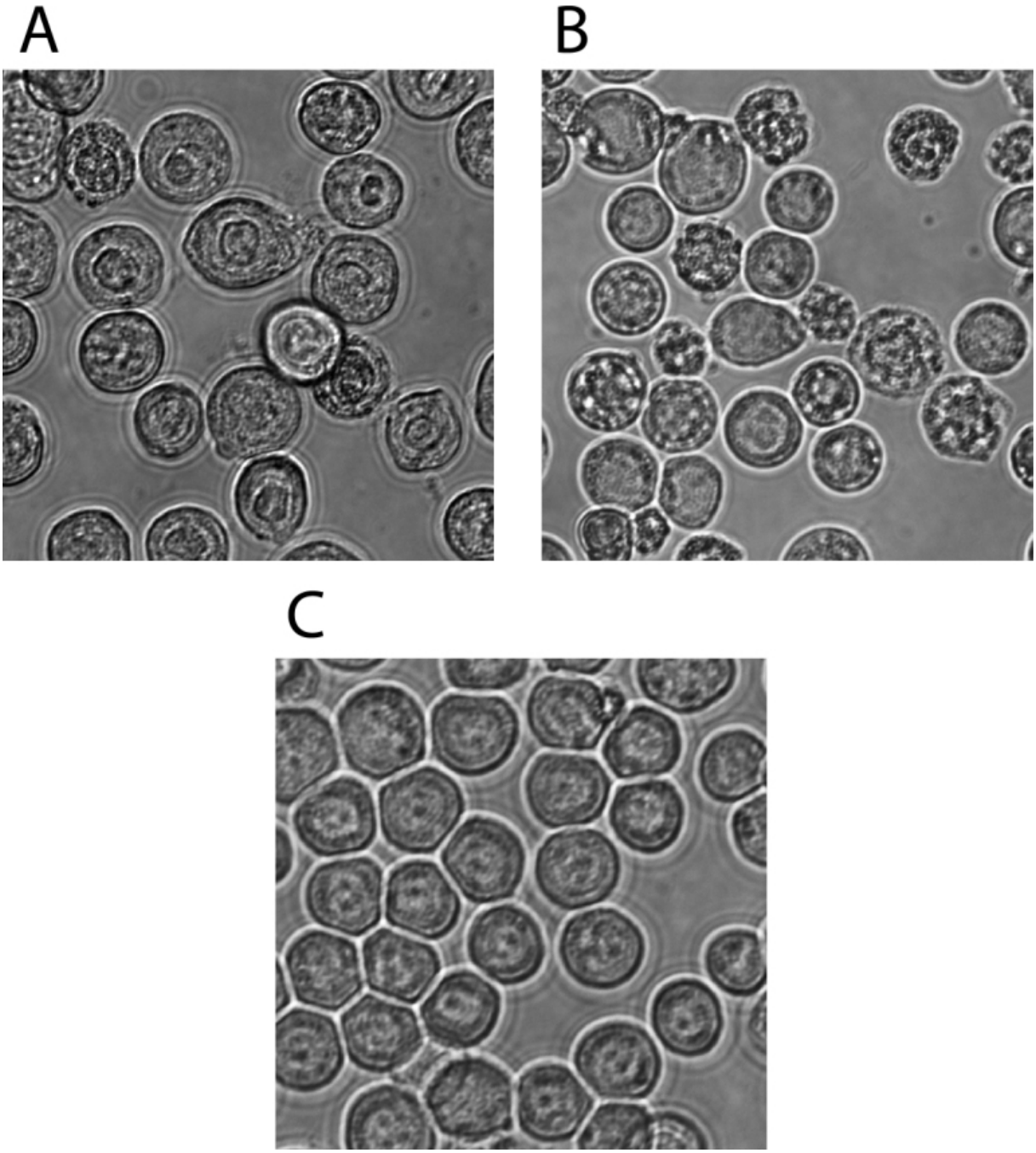

Figure 5.3.10: The morphology of A7 His-VP1 recombinant baculovirus infected Sf9 cells observed using light microscopy.
A: We noticed an unusual nuclei morphology of A7 His-VP1 recombinant baculovirus infected Sf9 cells. The nuclei looked donut shaped or somewhat invaginated. **B:** No such feature was observed in wtVP1 recombinant baculovirus infected Sf9 cells. **C:** No such feature was observed in uninfected Sf9 cells.

We were also curious if the nano-jumpers were present already inside the infected cells or if the assembly occurred during isolation. Thus we asked our colleague Mgr. Martin Fraiberk to prepare ultrathin sections for electron microscopy. We observed two types of cell morphology in both A7 and C14 infected Sf9 cells. There were cells with granular structures inside the nuclei (figure 5.3.11A) and cells with fiber-like structures inside the nuclei (figure 5.3.11B). When we

looked at the details, the granular structures were composed of clumps of material that appeared striped, possibly nano-jumpers (figure 5.3.11C). Other granular structures were organized in structures that resembled VLPs (figure 5.3.11D, red arrows). The nuclear fiber-like structures were long, branched and also had horizontal stripes suggesting that these could be nano-jumpers as well (figure 5.3.11E, F). In addition the fibers had different width as if it was a planar structure with a twist. We concluded that the nano-jumpers and other nanostructures are present already inside the cell nuclei thus are not the result of isolation.

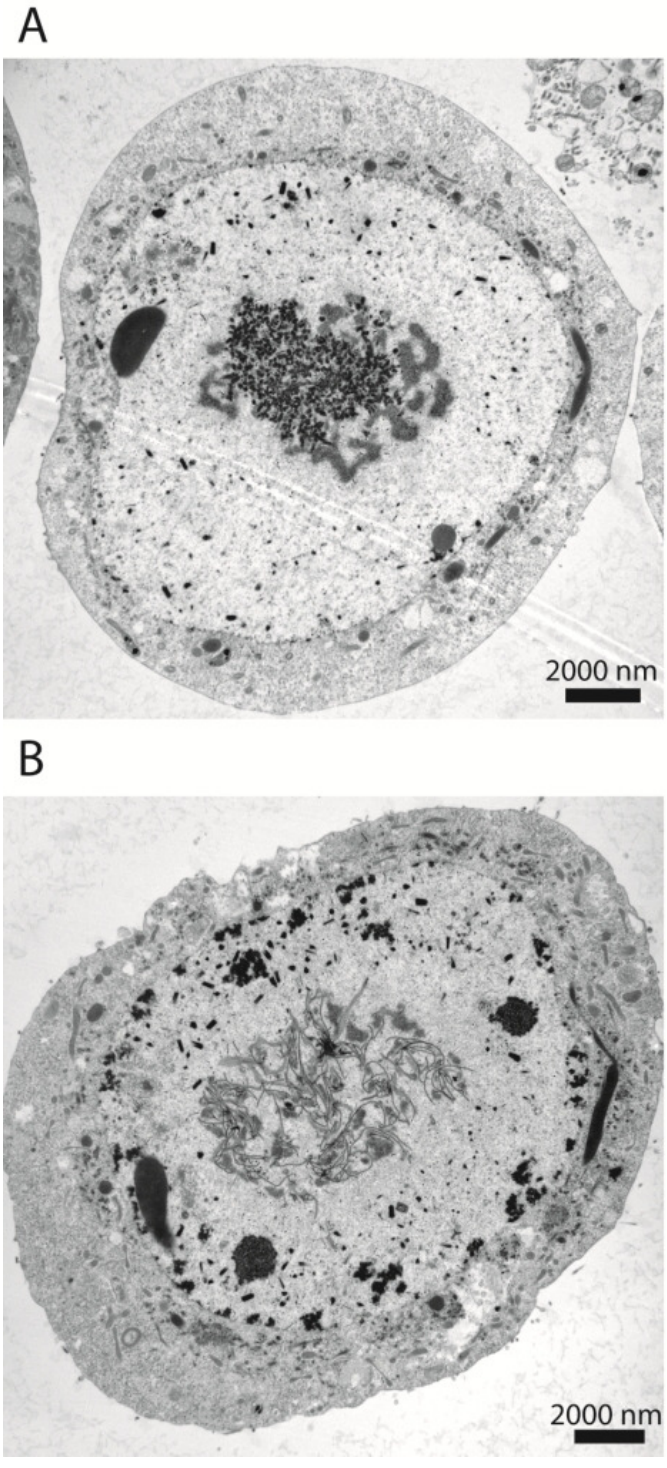

C

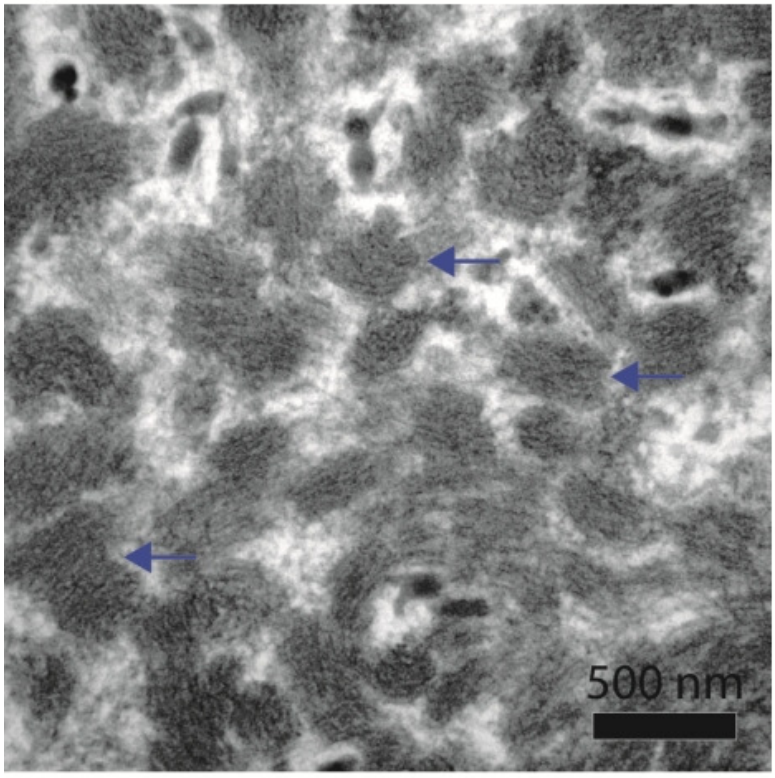

D

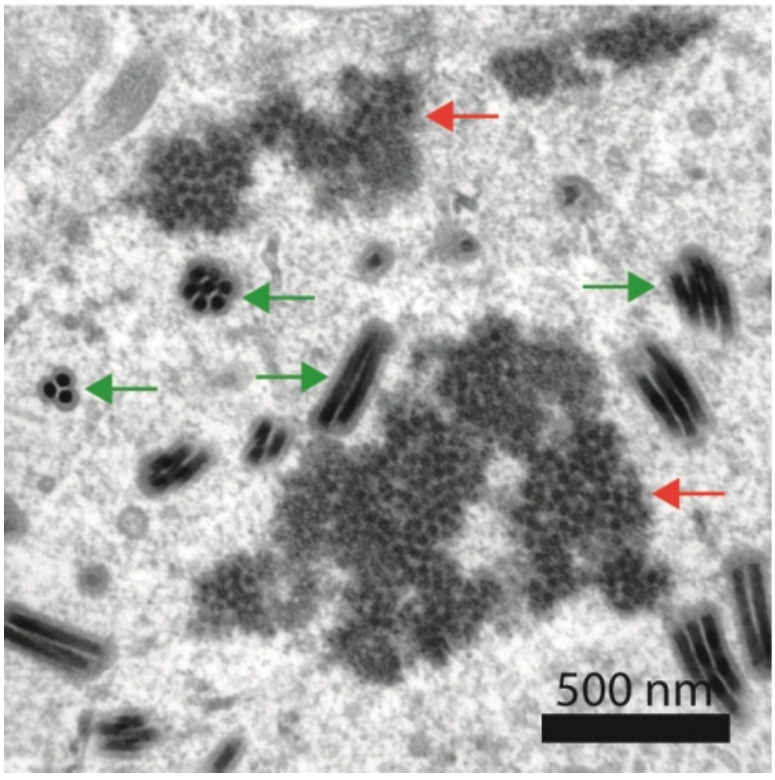

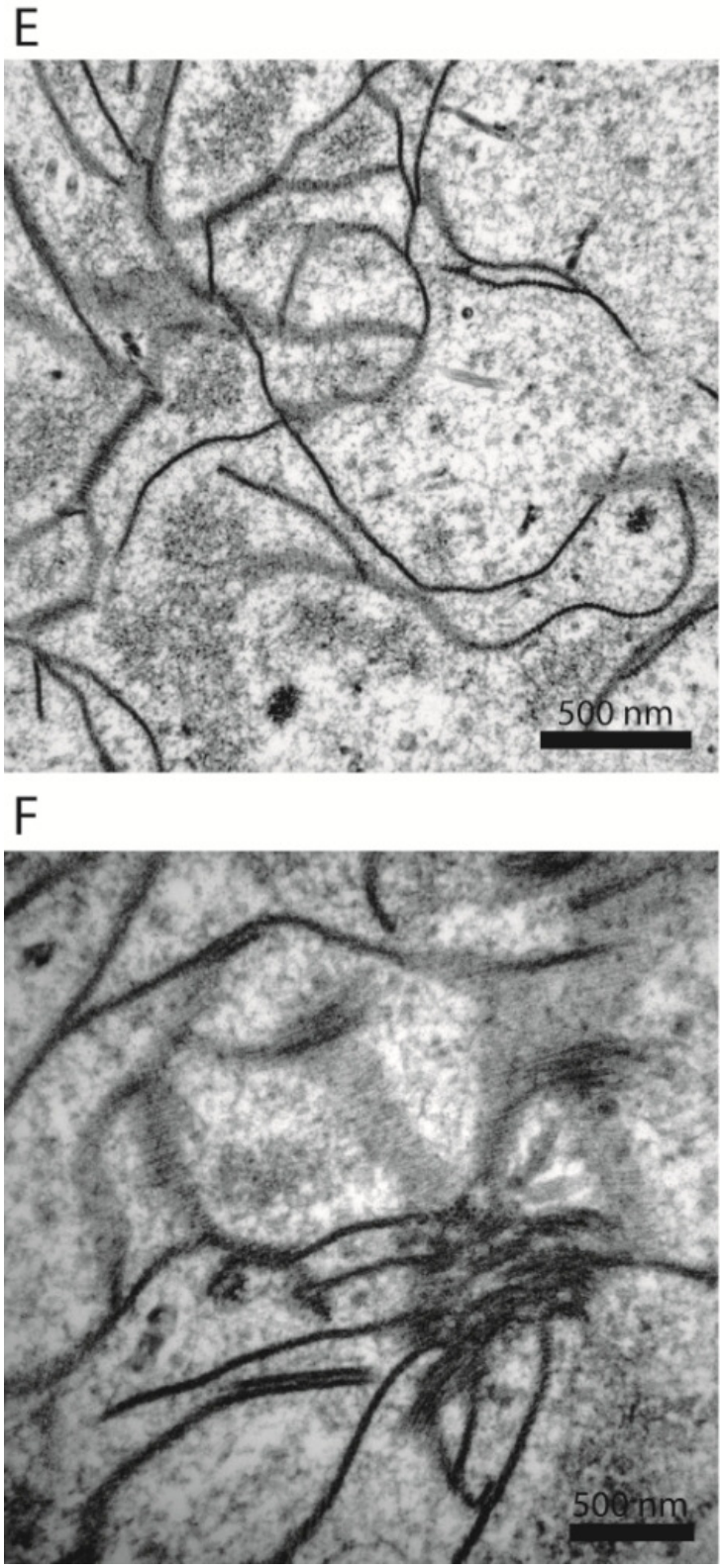

Figure 5.3.11: Electron microscopy of ultrathin sections of His-VP1 baculovirus infected Sf9 cells
Ultrathin sections of the His-VP1 recombinant baculovirus infected cells were prepared to investigate if His-VP1 nano-jumpers were present already inside the infected cells or were a result of the isolation. There were two types of nuclear morphology of the infected cells. **A:** Granular structures and **B:** fiber-like structures. **C:** The detail of the granular structures resembling nano-jumpers (blue arrows). **D:** The detail of other granular structures resembling forming VLPs (red arrows), also forming baculovirus virions are present (green arrows). **E, F:** The details of fiber-like structures resembling nano-jumpers.
Preparation of samples and images: Mgr. Martin Fraiberk

5.3.7 Nano-jumpers disassembly and reassembly

Although we were excited about the novel structure of nano-jumpers we still wanted to get VLPs because one of our future perspectives was to use His-VLPs for drug delivery into the cells. For that the nano-jumpers do not seem suitable.

Thus we tried the disassembly and reassembly protocol which we used for unmodified VP1-VLPs with success (chapters 4.2.4.11, 5.2.1). We used the C14 material isolated using sonication protocol (figure 5.3.7C, D). We managed to disassemble the material into pentamers (figure 5.3.12A), however, after reassembly the material formed only disorganized clumps (figure 5.3.12B).

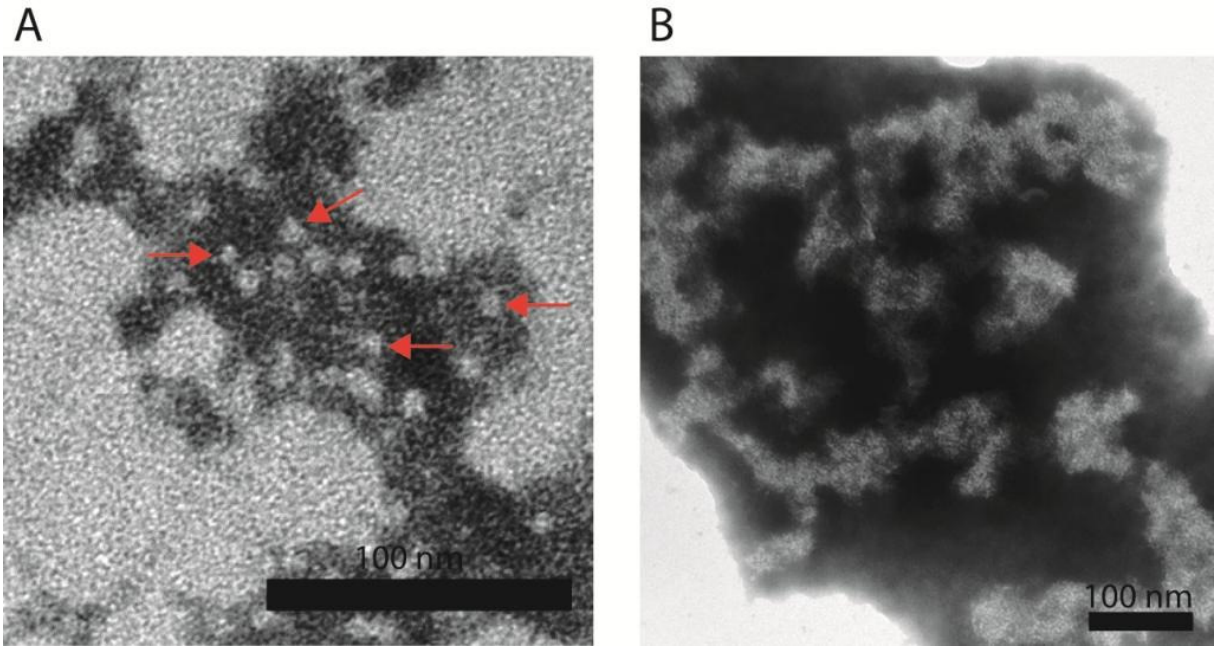

Figure 5.3.12: Electron microscopy images of C14 nano-jumpers disassembly and reassembly (negative staining)

In attempt to obtain His-VLPs from nano-jumpers we tried to disassemble and reassemble the C14 material. **A:** After dialysis in disassembly buffers and centrifugation to separate aggregates from pentamers we observed that VP1 pentamers were present (red arrows). **B:** However, after incubation of pentamers in the reassembly buffer, we did not obtain any VLPs. The material aggregated into disorganized clumps.

Images: Mgr. Jiřina Suchanová

We concluded that insertion of two His_6 sequences into the DE loop of VP1 influenced VP1 self-assembly properties and the yield of VLPs cannot be increased by in vitro methods. Nonetheless, the nano-jumpers are still attractive structures for diverse applications which we want to further explore.

A7 His-VP1 formed VLPs, even though of smaller diameter than MPyV virions, so we later used it for the testing of His-VLPs endosome escape properties (chapter 5.3.9.2).

5.3.8 Choosing the endosome escape assay

To investigate the endosome escape properties of the His-modified VP1-VLPs and other nanostructures we had to choose a suitable assay.

5.3.8.1 Fluorescent dextran assay

Fluorescent dextran assay was previously described in literature as a method to monitor escape of endocyted material from endosome to cytoplasm (Salomone et al., 2012; Suikkanen et al., 2003). We used FITC labeled dextran of 3000 Da (Dx, Sigma-Aldrich). We intended to perform co-endocytosis of VLPs with Dx and observe the effect of VLPs modification on endosome leakage. We first tested staining of endosomes with Dx in 3T6 cell line. We cultivated cells in media with Dx in the final concentration 3 mg/ml for different time periods, washed cells with DPBS and observed the cells under fluorescent microscope. Unfortunately, we were not able to detect specific fluorescent signal of Dx in the cells due to a very high fluorescent background (Dx was probably attached to the dish surface). Therefore we attempted to perform co-endocytosis of Dx and MPyV VP1-VLPs and detect both in the same compartments in fixed cells.

We passaged $5x10^4$ of 3T6 cells on cover slips in 24-well dish (chapter 4.2.6.4) and after 24 hrs we applied Dx with or without VP1-VLPs on the cells (chapter 4.2.6.6). Pure VP1-VLPs and non infected cells were used as controls. We used Dx in the final concentration 3 mg/ml and approx. 10^4 VP1-VLPs per cell in 500 μl of serum-free medium per well. The cells were incubated with the inocula for 30 min, 3hrs, 4 hrs and 22 hrs. After, they were fixed, permeabilized and immunofluorescence staining was performed (chapters 4.2.6.7 and 4.2.6.8). We noticed in experiments with FITC-labeled cyclodextrin (chapter 5.2.2) that FITC fluorescence in the cells is quite weak, so we used immunofluorescent detection of FITC because it enhanced the signal. Thus we stained Dx samples with GαFITC and green fluorescent antibody and VLPs with MαVP1-D4 and red fluorescent antibody.

We observed that Dx did not follow VP1-VLPs in endosomes (figure 5.3.13F, G). It looked like it accumulated in one distinct spot in a cell. In 22 hrs post infection (p.i.) the spot was usually one per cell (figure 5.3.13E, G). Earlier, after 30 min (figure 5.3.13C), 3 hrs (figure 5.3.13D) and 4 hrs p.i. (figure 5.3.13F) the spots were smaller and there were sometimes more than one per cell. The spots were also much smaller and less visible after 30 min than in 3 hrs suggesting the spots enlarge and finally merge into one.

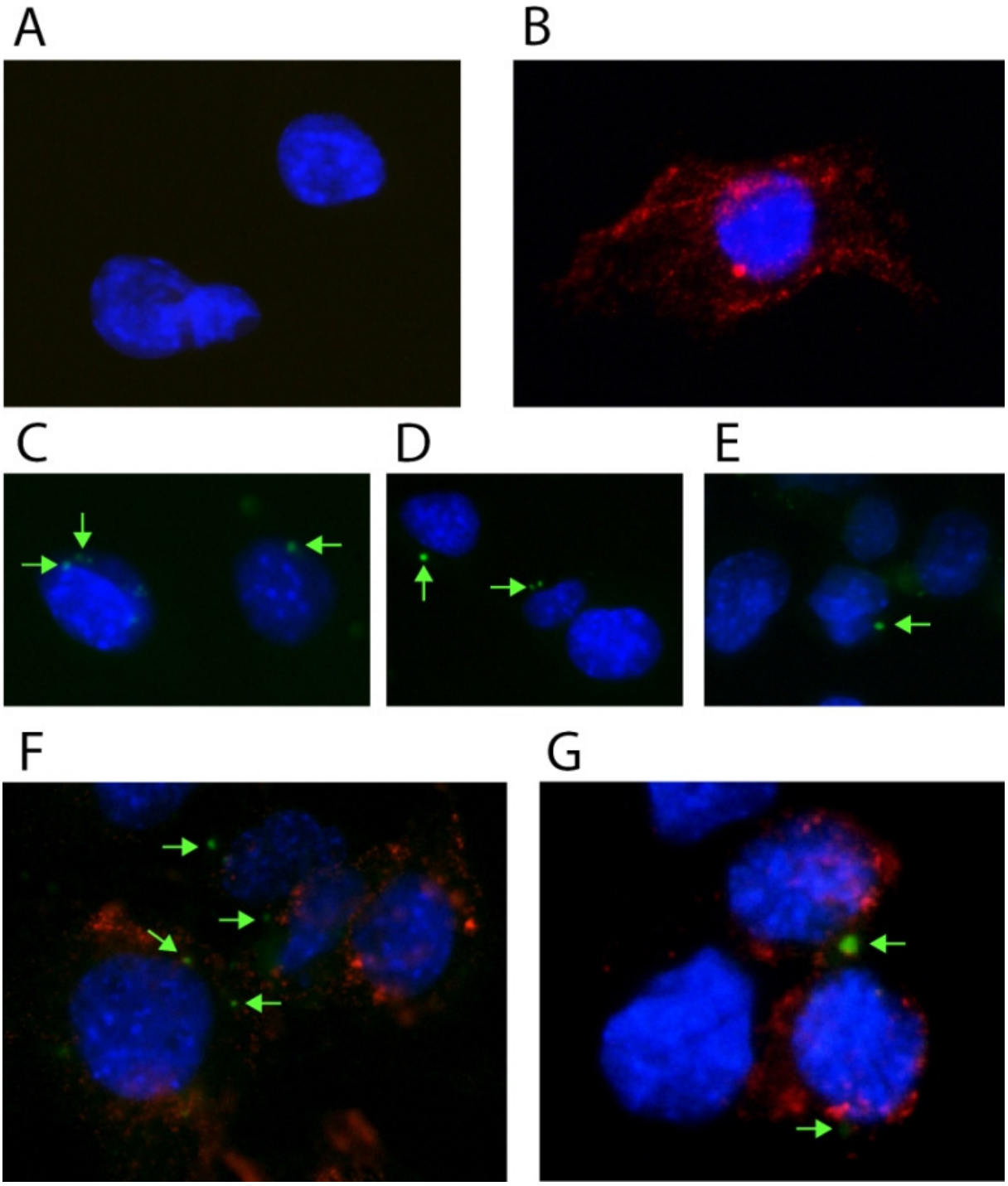

Figure 5.3.13: Fluorescent dextran testing on 3T6 mouse fibroblast, immunofluorescent staining observed with fluorescent microscope

To test if dextran assay is suitable for endosome escape testing we applied Dx on 3T6 cells alone (C-E) or together with MPyV VP1-VLPs (F, G). Dx (green) was visualized using GαFITC and green fluorescent antibody to enhance the signal. VP1 (red) was visualized using MαVP1-D4 and red fluorescent antibody. Nuclei were stained with DAPI (blue). **A:** Negative control, no Dx, no VLPs. **B:** VP1-VLPs without Dx. **C:** Dx, 0.5 hr p. i. Weak green spots close to the nuclei started to appear (green arrows). There were usually several smaller spots per cell. **D:** Dx, 3 hrs p. i. Green spots close to nuclei were more visible and there were usually several spots per cell. **E:** Dx, 22 hrs p. i. One or two large green spots close to the nuclei were observed. **F:** Dx and VP1-VLPs, 4 hrs. p. i. Several green spots close to the nuclei were observed (similar to 3 hrs p. i.). The VLPs were endocyted but they did not appear to be in the same compartments as Dx. **G:** Dx and VP1-VLPs, 22 hrs p. i. One or two large green spots close to the nuclei were observed. The VLPs moved to the perinuclear area but they did not appear to be in the same compartments as Dx.

Taken together, we observed that Dx entered the cells and stained some distinct structures localized close to nuclei. However there were very few Dx positive structures in comparison to VP1 positive vesicles. In addition Dx positive structures were distinct from the ones positive for VP1. As the results differed from previously published works (Salomone et al., 2012) we suppose that fluorescent dextran we obtained was wrongly manufactured.

5.3.8.2 Fluorescent antibody assay

When optimizing the antibodies for the cargo encapsidation we noticed that FITC conjugated swine anti mouse antibody was endocyted by 3T6 cells and stained the endocytic vesicles very efficiently (chapter 5.2.2, figures 5.2.6C and 5.3.16B). Thus we decided to use it instead of Dx in further experiments (chapter 5.3.9.2)

5.3.8.3 SNAP-Trap assay

Another method for endosome escape detection is the SNAP-Trap assay (chapter 4.1.12). We prepared control lysates of 293TT cells expressing SNAP in cytoplasm and we modified A7 sample of His-VLPs and nanostructures (further referred to as His-VLPs), normal VP1-VLPs and with SNAP substrate benzylguanine (BG-GLA-NHS). We incubated the modified samples with the control cell lysate and performed SDS PAGE and western blot to prove successful modification of samples (figure 5.3.14). We confirmed the modification with BG-GLA-NHS for both VP1-VLPs and His-VLPs. Modified VLPs are called BG-VP1-VLPs and BG-His-VLPs respectively.

Next, the endosome escape experiment was performed as described in chapter 4.1.12. Cells transfected with $pSNAP_f$ plasmid were pseudoinfected with inocula described in table 5.3.5. PEI and histidine-rich peptide $KH_{27}K$ (lysine – 27 histidine residues – lysine) were used with BG-VP1-VLPs for comparison because of their endosome escape properties (chapter 5.3.9).

Inocula for SNAP-Trap assay	
Inoculum per well (300 μl)	Preparation
VP1-VLPs	1 μg/well of unmodified VP1-VLPs in serum-free DMEM
BG-VP1-VLPs	1 μg/well of BG-modified VP1-VLPs in serum-free DMEM
BG-VP1-VLPs + PEI	1 μg/well of BG-modified VP1-VLPs and 50μM PEI in serum-free DMEM, incubated rocking for 10 minutes
BG-VP1-VLPs + $KH_{27}K$	1 μg/well of BG-modified VP1-VLPs and 20μM $KH_{27}K$ in serum-free DMEM, incubated rocking for 30 minutes
BG-His-VLPs	1 μg/well of BG-modified His-VLPs in serum-free DMEM
uninfected	uninfected cells, 300 μl of serum-free DMEM
uninfected mock	uninfected, mock transfected cells

Table 5.3.5: Inocula preparation for SNAP-Trap assay
All samples were used on $pSNAP_f$ transfected 293TT cells except for uninfected mock sample which were mock transfected cells.

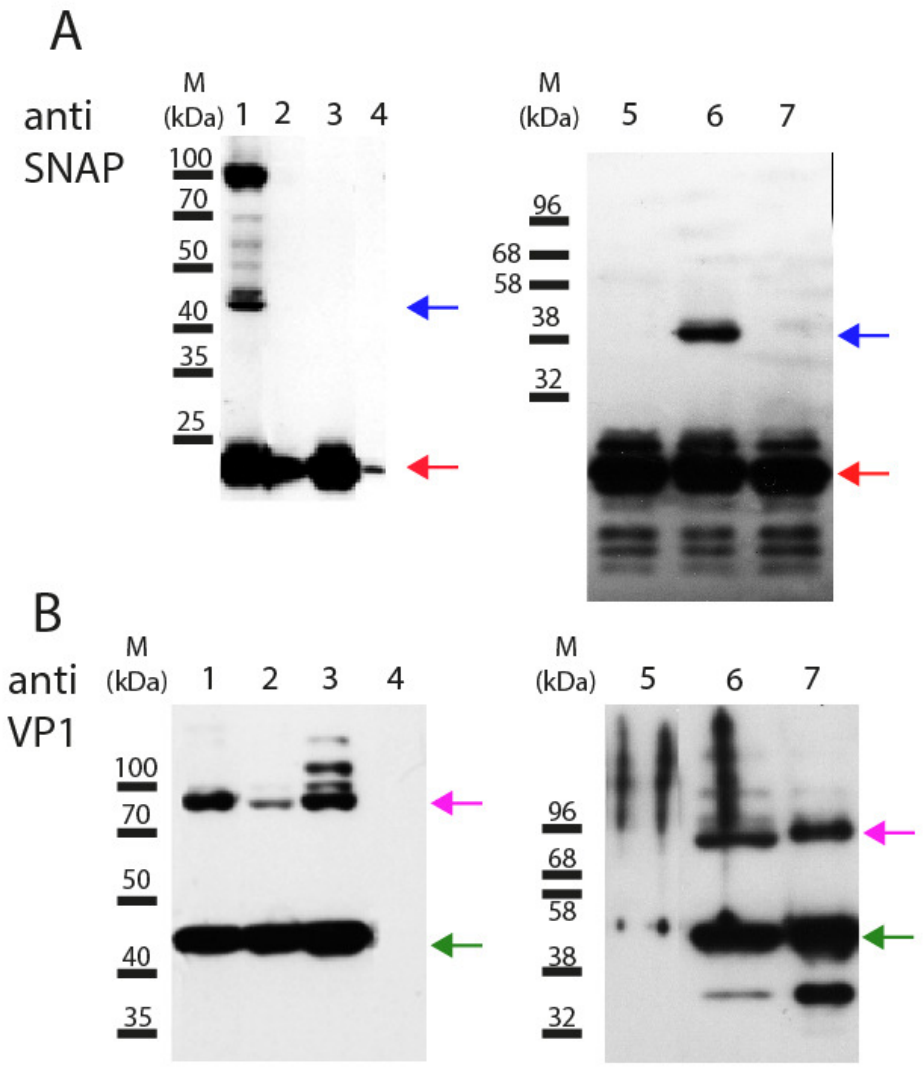

Figure 5.3.14: Control of modification of VLPs with BG-GLA-NHS
VP1-VLPs and His-VLPs were modified with BG-GLA-NHS and the modification was controlled by mixing with cell lysate with expressed SNAP-tag. The samples were analyzed using SDS-PAGE and western blot with immunodetection. SNAP was detected with RbαSNAP antibody and VP1 with MαVP1-A. **A:** Free SNAP-tag has approx. 20 kDa (red arrows), SNAP bound to VP1 was between 40 and 50 kDa and it is the proof of VLPs modification with BG-GLA-NHS (blue arrows). **B:** VP1 monomer is approx 45 kDa (green arrows) and VP1 dimers between 70 and 100 kDa (purple arrows). **1:** BG-VP1-VLPs + SNAP lysate, **2:** BG-VP1-VLPs + mock lysate (weak SNAP signal in mock lysate is caused by diffusion from SNAP samples), **3:** VP1-VLPs + SNAP lysate, **4:** mock lysate, **5:** SNAP lysate, **6:** His-VLPs + SNAP lysate, **7:** VP1-VLPs + SNAP lysate

The pseudoinfection lasted 6 hrs, after, the samples for SDS-PAGE were prepared (chapter 4.1.12) and analyzed using SDS-PAGE and western blot followed by immunodetection (chapters 4.2.3.3, 4.2.3.5 and 4.2.3.6). The only significant interaction of VP1 and SNAP was in the case of BG-His-VLPs (figure 5.3.15, anti SNAP, sample 4) which means that BG-His-VLPs and nanostructures successfully escaped the endosomes into cytoplasm. Addition of endosome escape enhancing agents PEI and histidine-rich peptide did not have any effect on BG-VP1-VLPs release into cytoplasm (figure 5.3.15, anti SNAP, samples 1, 2 and 3).

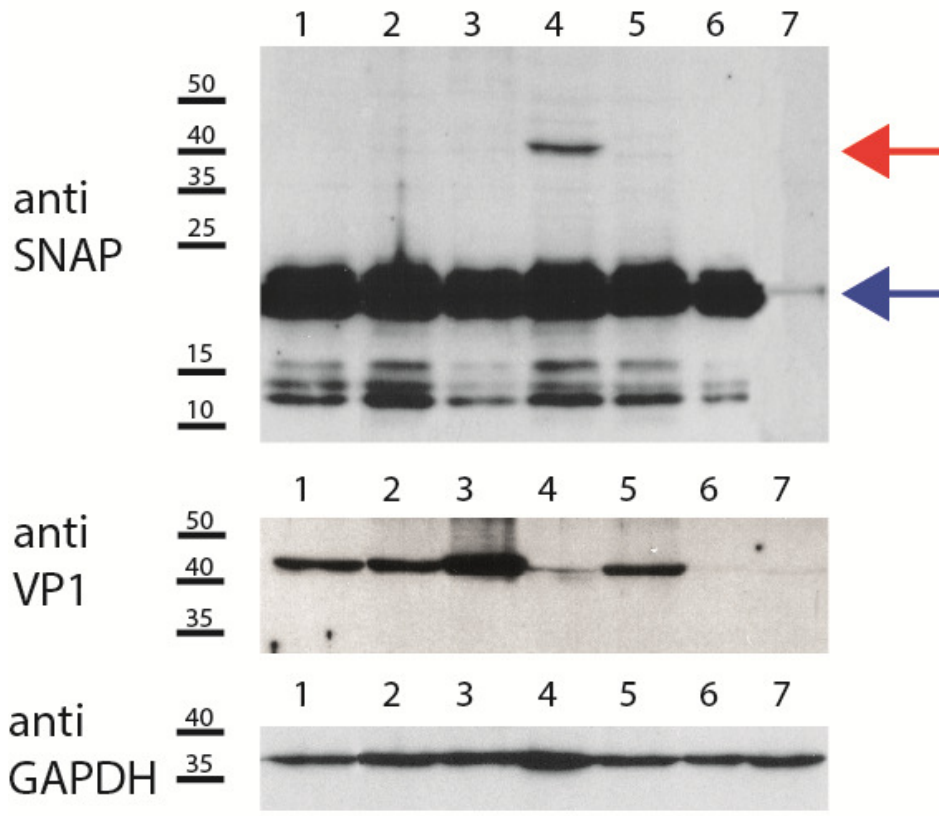

Figure 5.3.15: SNAP-Trap assay for endosome escape detection
The results of SNAP-Trap assay of endosome escape experiment analyzed using SDS-PAGE followed by western blot and immunodetection. SNAP-tag was detected with RbαSNAP antibody, VP1 with RbαVP1 polyclonal antibodies and GAPDH was detected as a sample amount control using RbαGAPDH antibody. **1:** BG-VP1-VLPs in SNAP-transfected cells, **2:** BG-VP1-VLPs + PEI in SNAP-transfected cells, **3:** BG-VP1-VLPs + $KH_{27}K$ in SNAP-transfected cells, **4:** BG-His-VLPs in SNAP-transfected cells, **5:** VP1-VLPs in SNAP-transfected cells, **6:** uninfected SNAP-transfected cells **7:** uninfected mock-transfected cells.

Even though we applied similar amount of cellular material into all samples (figure 5.3.15, anti GAPDH), the VP1 signal in BG-His-VLPs was very weak (figure 5.3.15, anti VP1, sample 4). Moreover, the detection had to be done using RbαVP1 polyclonal antibodies instead of previously used MαVP-A monoclonal antibody anti C-terminal sequence epitope, because there was no VP1 signal (not shown). However, SNAP signal was present in the expected size of VP1+SNAP (figure 5.3.15, anti SNAP, sample 4), thus VP1 clearly had to be present. The reasons for the problematic detection of VP1 may be due to combined effect of histidine insertions and SNAP binding that might prevent proper antibody binding. The VP1 C-terminus might have been cleaved in the cells as there was no problem with VP1 detection using MαVP1-A in *in vitro* testing (figure 5.3.14).

Taken together we prepared His-VP1-VLPs and nanostructures with enhanced endosome escape properties by insertion of 4 His_6 sequences separated by glycine and serine moieties into DE loop of MPyV VP1 protein.

5.3.9 Effects of histidine-rich peptide

To proof the concept that His-rich peptides have proposed effect on endosome escape we compared the effect of histidin-rich peptide ($KH_{27}K$) and known endosome disrupting agent polythylenimine (PEI, chapter 2.3.1). We investigated the effect of PEI and $KH_{27}K$ on MPyV infectivity and we also observed the effect on transition of FITC conjugated antibody (FITC-AB) from endocytic vesicles (chapter 5.3.8.2).

5.3.9.1 Effect of histidine-rich peptide and endosome disrupting agent on MPyV infectivity

We first tested the effect of histidine-rich peptide on infectivity of MPyV. MPyV is supposed to enter the cells in endocytic vesicles and later needs to escape from some vesicle of the endocytic pathway or endoplasmic reticulum into the cytoplasm to be able to reach the nucleus. We hypothesized that endosome disrupting agents could help release MPyV from endocytic vesicles and increase its infectivity.

$5x10^4$ of 3T6 cells passaged on 24-well dish with cover slips (chapter 4.2.6.4) were cultivated at 37 °C and 5% CO_2 for 24 hrs. We prepared the inocula of MPyV with PEI, $HK_{27}K$ or alone. The inocula are described in table 5.3.6.

Inocula for MPyV infectivity testing	
Inoculum per well (150 µl)	Preparation
wt	1 µg MPyV in serum-free DMEM
PEI	1 µg MPyV + 50 µM PEI in serum-free DMEM, mixed and incubated 10 minutes rocking in room temperature
peptide	1 µg MPyV + 20 µM $HK_{27}K$ in serum-free DMEM mixed and incubated 30 minutes rocking in room temperature
NC	negative control, 150 µl serum-free DMEM

Table 5.3.6: Inocula preparations for MPyV infectivity test in presence of PEI and $HK_{27}K$
The infection was performed with 1 µg of virus with theoretical moi= 0,5 FU/cell (fluorescence units).

The cells were infected with the inocula for 1 hour, then the inocula were removed and the cells were washed with serum-fee DMEM. We added DMEM with FBS and antibiotics and incubated for 24 hrs at 37°C, 5% CO_2 (chapter 4.2.6.6.). After the cells were fixed and permeabilized and stained with primary antibody anti MPyV LT (large T antigen) followed by green fluorescent secondary antibody to visualize the infected cells using indirect immunofluorescence (chapters 4.2.6.7 and 4.2.6.8). We observed the samples under fluorescent microscope and counted the percentage of infected cells (figures 5.3.16 and 5.3.17). There were approx. 7 % of infected cells in samples with MPyV only, 25 % of infected cells when PEI was added in the infection and 50 % of infected cells when histidine-rich peptide $KH_{27}K$ was added. That was 3.6 and 7.2 times

increase of infectivity when PEI or $KH_{27}K$ peptide was added respectively. In addition, the intensity of LT fluorescence was higher in cells infected with PEI or peptide than in cells infected MPyV without these agents. These results showed that histidine-rich peptide had an enhancing effect on MPyV infection which may be associated with endosome disrupting properties of histidine-rich sequences.

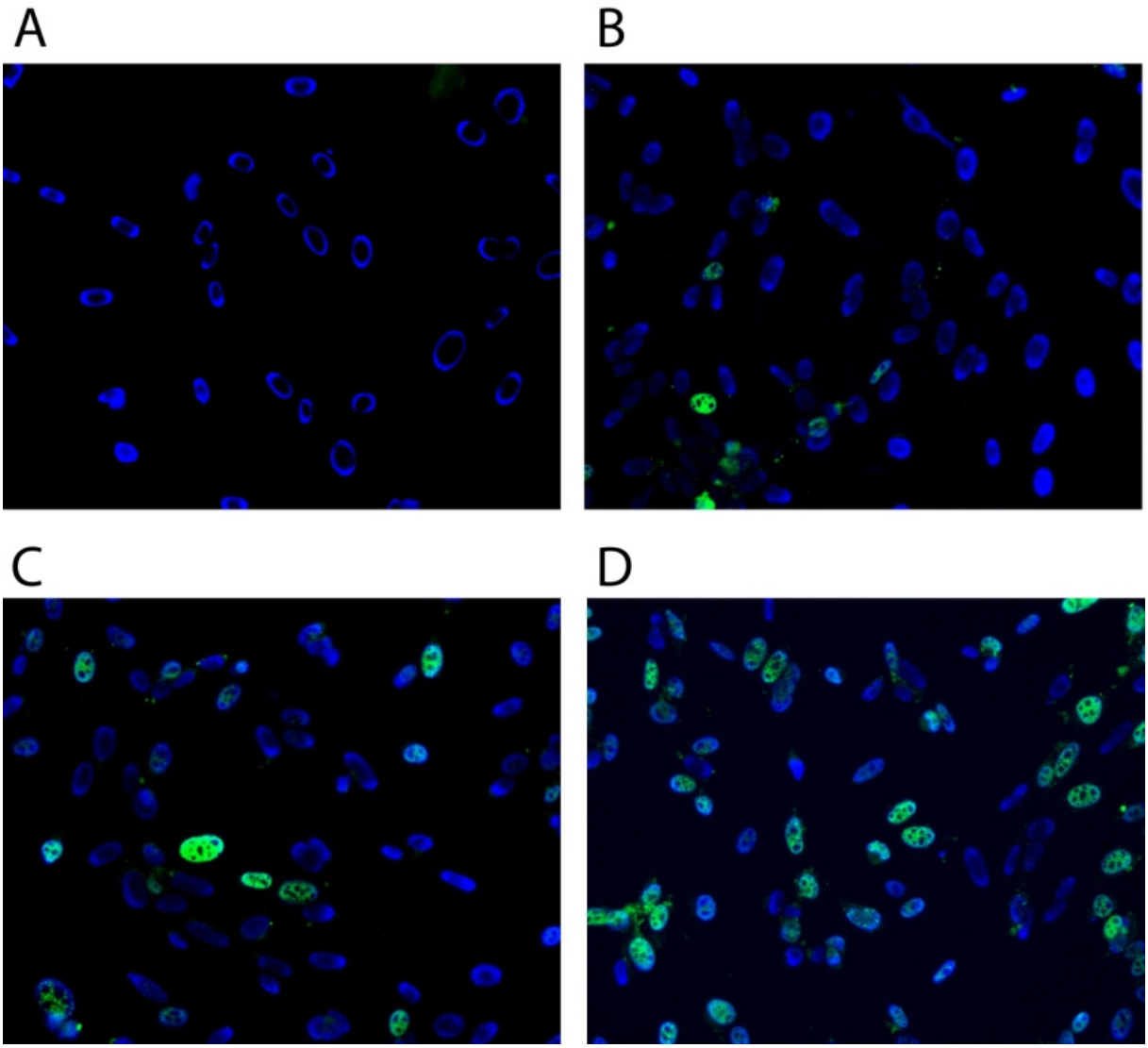

Figure 5.3.16: The effect of histidine-rich peptide on MPyV infectivity, immunofluorescent staining observed with fluorescent microscope

To test the histidine-rich peptide effect on MPyV infectivity we compared 3T6 cells infected with MPyV alone, with known endosome disruption agent 50μM polyethylenimine (PEI) and with 20μM $KH_{27}K$ histidine-rich peptide. Infected cells were detected by MPyV large T antigen (LT, green), nuclear marker of early infection. We visualized LT using RαLT-1 and green fluorescent antibody. Nuclei were stained with DAPI (blue). **A:** Uninfected cells. **B:** MPyV only infection. **C:** MPyV infection with PEI. **D:** MPyV infection with $KH_{27}K$. We also counted the infected cells (figure 5.3.17).

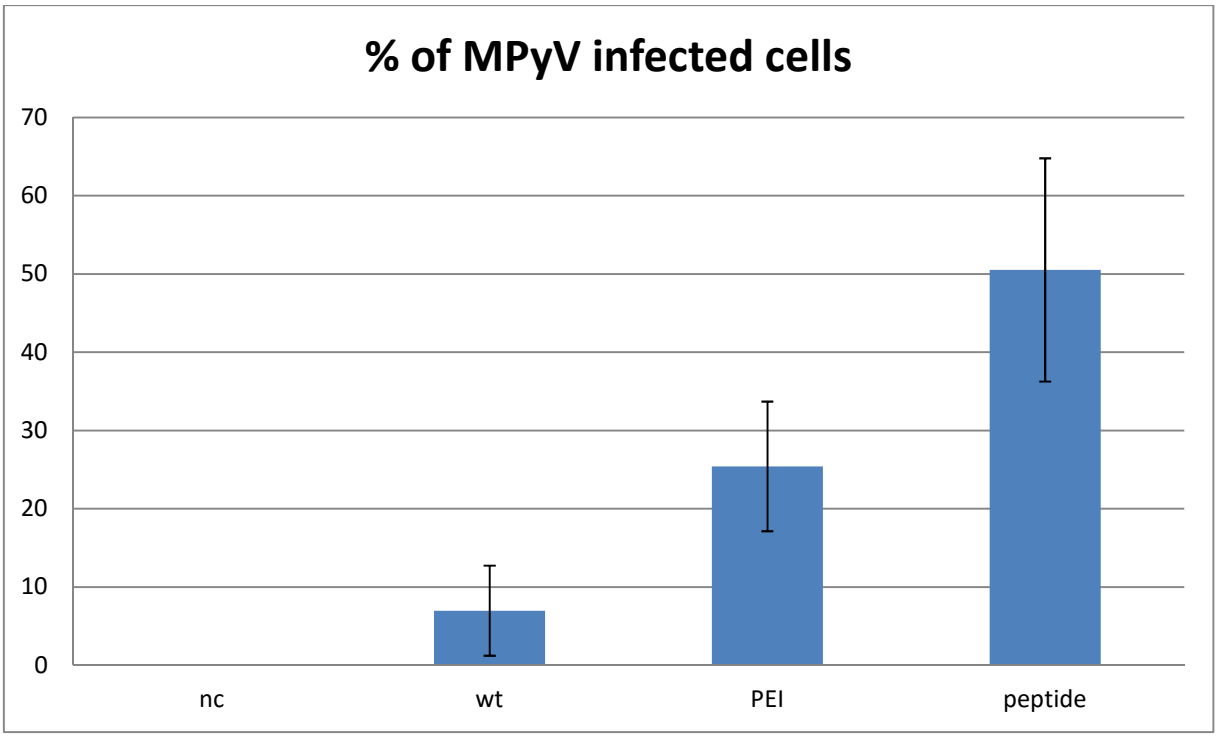

Figure 5.3.17: The effect of histidine-rich peptide on MPyV infectivity
The data show percentage of infected cells (the average of 20 images with standard deviations) as described in legend of figure 5.3.16. At least 1000 cells were counted for each sample.

5.3.9.2 Effect of histidine-rich peptide and PEI on transition of fluorescent antibody from endocytic vesicles

Because the results of histidine-rich peptide effect on MPyV infectivity were promising we were wondering if we can observe some change in endosomal system. For this we wanted to use FITC conjugated antibody appeared to be endocyted and it labeled the endocytic vesicles.

We incubated 3T6 cells on cover slips in 24-well dish with FITC-AB alone, FITC-AB mixed with $KH_{27}K$ and FITC-AB mixed with PEI for 75 min (the inocula are described in table 5.3.7). After, the inocula were removed, the cells were washed with serum-free medium and incubated in medium with FBS and antibiotics for 2 hrs (chapter 4.2.6.6). Then the cells were fixed, permeabilized and stained with goat anti FITC primary antibody followed by green fluorescent antibody to enhance the signal (chapters 4.2.6.7 and 4.2.6.8)

Inocula preparations for endosome disruption test	
Inoculum per well (150 µl)	Preparation
AB	5 µl of FITC-conjugated swine anti mouse antibody in serum free medium
PEI	5 µl of FITC-conjugated swine anti mouse antibody, 50µM PEI in serum free medium, mixed and incubated for 10 minute while rocking
peptide	5 µl of FITC-conjugated swine anti mouse antibody, 20µM $KH_{27}K$ in serum free medium, mixed and incubated for 30 minute while rocking
NC	Negative control, 150 µl serum-free medium

Table 5.3.7: Inocula preparations for endosome disruption test in presence of PEI and $HK_{27}K$

FITC-AB without added PEI or peptide stained vesicles, supposedly endosomes, as observed in previous experiment (chapter 5.2.2, figures 5.2.6C and 5.3.17B). When PEI was added, the staining became diffused with some vesicles still visible (figure 5.3.17C). The same effect was observed when histidine-rich peptide $HK_{27}K$ was added (figure 5.3.17D). This result suggests that FITC-AB is a suitable tool to study endosome disruption and that histidine-rich peptide has endosome disruption properties similar to those of polyethylenimine.

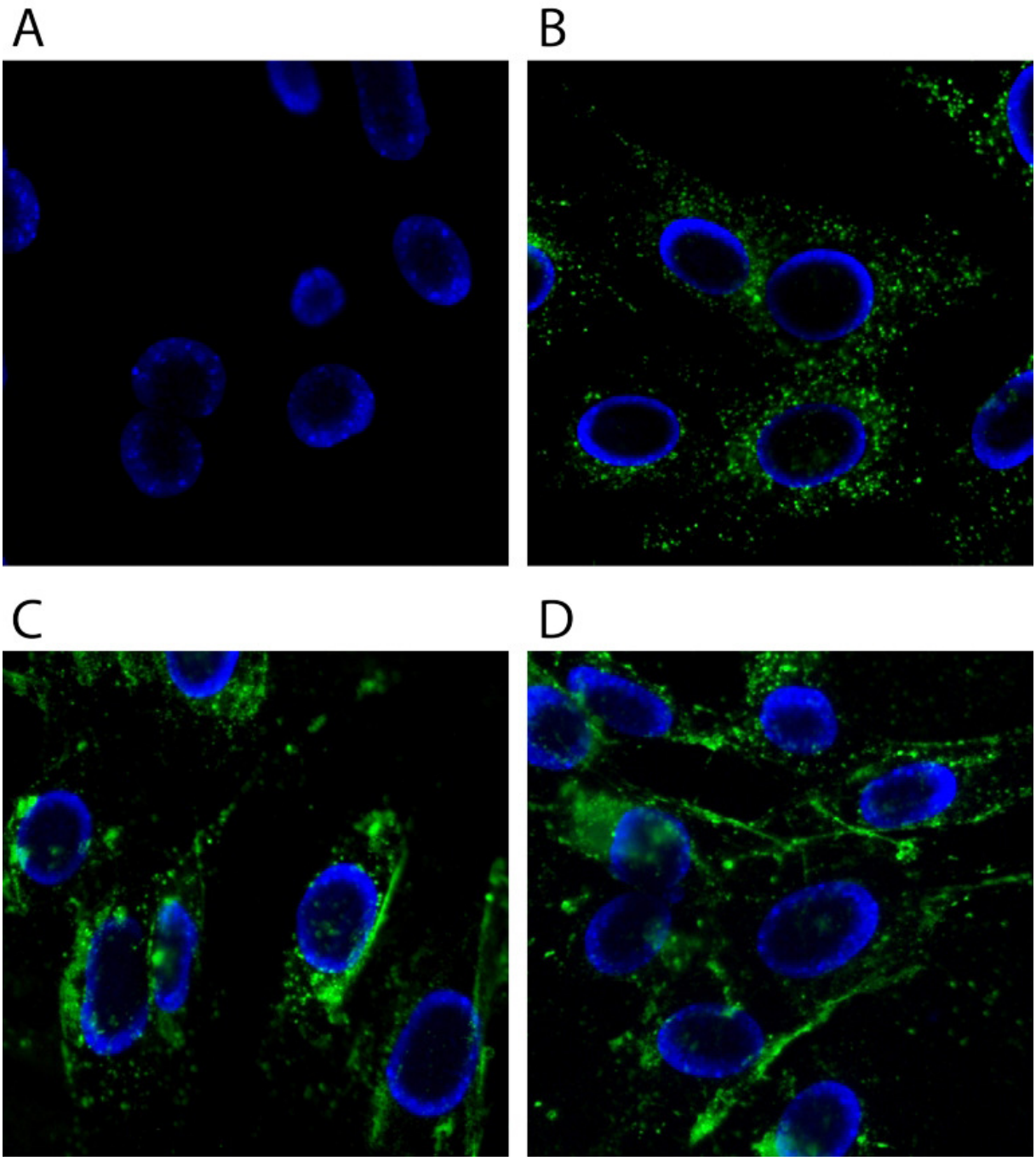

Figure 5.3.17: The effect of PEI and histidine-rich peptide on transfer of FITC conjugated antibody from endosomes to cytolasm, immunofluorescent staining observed with fluorescent microscope

Because we observed an increase in infectivity with MPyV caused by addition of PEI or histidine-rich peptide, we wanted to observe the effects of PEI and $KH_{27}K$ peptide on FITC-AB endocytosis and cellular localisation. FITC-AB was used as a marker of endosomes and it was further stained with goat anti FITC antibody followed by green fluorescent antibody to enhance the signal. The nuclei are stained with DAPI (blue), the antibody is green. **A:** Negative control, untreated cells. **B:** Cells incubated with FITC-conjugated antibody; the vesicles (supposedly endosomes) were stained. **C:** Cells incubated with FITC-AB and PEI. AB signal became diffuse with some vesicles still present. **D:** Cells incubated with FITC-AB and $KH_{27}K$. AB signal was similar to the one with PEI; it was diffused with few vesicles still present.

6. Discussion

6.1. Preparation of universal *VP1* constructs for surface loops modification

Mouse polyomavirus is extensively investigated in the Laboratory of Virology. The focus is on MPyV biology as well as on use of MPyV-derived virus-like particles for various purposes such as vaccine platforms or nanoparticle delivery systems. Many studies focus on development of JCV derived VLPs as DNA delivery systems, for example for treatment of human cancers (Fang et al., 2015; Chao et al., 2015; Chen et al., 2010). The problem with the use of human polyomavirus is higly probable preexisting antibody mediated immunity to virions and VLPs because human polyomaviruses have high prevalence in population (White et al., 2013). Preexisting antibodies can interfere with drug and gene delivery and even cause unwanted side effects. It is believed that preexisting immunity to non-human viruses is not present which makes MPyV derived VLPs more suitable for human medicine.

Development of vaccines or nanoparticle delivery systems form MPyV derived VLPs require surface modification of VLPs that can be achieved by insertion of short epitopes into surface loops of VLPs using methods of gene engineering. Immunogenic epitopes can be exposed on the VLPs surface for vaccine preparation, or receptor binding epitopes can be used for VLPs targeting to different cell types.

To broaden the spectrum of constructs available in the Laboratory of Virology we prepared two *VP1* construct with restriction sites in surface loops. One of the constructs, *VP1_BCmut*, contains three restrictions sites NheI, AgeI and EheI in BC loop. It allows oriented insertion using cohesive ends as well as non oriented blunt end cloning. These restriction sites translate into flexible linkers that should reduce the effect of inserted epitope on VP1 protein structure. BC loop is responsible for receptor binding (Stehle and Harrison, 1997; Stehle et al., 1994), thus the insertion of new epitopes may prevent recognition of the sialic acid.

Previously prepared construct *VP1_7less* (Kojzarová, 2011) with seven deleted amino acids and BamHI restriction site (coding for flexible linkers) in DE loop was combined with *VP1_BCmut* to prepare *VP1_BCmut+DE7less* construct. This construct offers insertion of two different epitopes at the same time or they can be used separately.

Both constructs were cloned in pFastBac1 vector which is a donor vector for baculovirus preparation in Bac-to-Bac® baculovirus expression system. This allows direct use of both modified constructs for bacmid preparation and VLPs production. As insertions of both BC and DE loops were successful in previous works (Kojzarová, 2011; Suchanová, 2012), it is probable that modified VLPs will assemble. However, testing will be required for each new construct.

6.2 Cargo encapsidation

Encapsidation of cargo into a particle, virus-derived or synthetic, is an important step that can help deliver the cargo into the cells, increase its stability in extracellular environment, decrease its toxicity, protect it from sequestration by the immune system and even allow cell targeting. Encapsidation may be the only possible way of use for hydrophobic or toxic cargos. Both diagnostic and therapeutic molecules can be benefit from encapsidation.

Polyomavirus-derived VLPs were previously shown to be suitable tool for delivery into the cells (chapter 2.2.4). Delivery of DNA for gene expression was extensively investigated in various polyomaviruses-derived VLPs including MPyV (Forstová et al., 1995; Krauzewicz et al., 2000).

In this work we decided to use MPyV-derived VLPs for diagnostic small molecule β-cyclodextrin modified by two fluorescein isothiocyanate molecules (FITC), allowing fluorescent microscopy observation of the cargo, and five gadolinium (Gd) complexes. This complex (CD) was prepared as a carrier of Gd which is a contrast agent for magnetic resonance imaging (Kotková et al., 2010). Virus-like particles derived from cowpea chlorotic mottle virus (Allen et al., 2005; Anderson et al., 2006; Liepold et al., 2007), bacteriophage P22 (Qazi et al., 2013; Usselman et al., 2015) and tobacco mosaic virus (Bruckman et al., 2013; Bruckman et al., 2015) were used as carriers for Gd or its complexes and showed enhancement of the diagnostic potential in MRI. The second selected cargo was fluorescently labeled antibody which is small enough to fit the cavity of MPyV derived VLPs.

We decided to encapsidate the cargo in a process of disassembly and reassembly optimized for MPyV VP1-VLPs (Mukherjee et al., 2010; Suchanová, 2012). Such approach was used for encapsidation of propidium iodide into SV40 VLPs (Goldmann et al., 2000). Other small molecules were encapsidated differently, such as by covalent binding of cargo to VP2 protein of MPyV VLPs (Abbing et al., 2004), disulfide bond attachment to cysteins of JCV VP1 (Niikura et al., 2013a) or modification of SV40 VP1 protein N-terminus with His-tag which binds various metals (Li et al., 2009). Proteins were encapsidated into VLPs as fusion proteins with polyomavirus minor proteins (Abbing et al., 2004; Inoue et al., 2008) or by modification of VP1 protein by protein binding domain (Günther et al., 2001) or His-tag (Ohtake et al., 2010) allowing non covalent interaction of cargo and VP1. Thus the encapsidation attempt of both protein and small molecule in simple reassembly and disassembly process is quite innovative.

We prepared MPyV VP1-VLPs with stably associated CD, CD-VLPs and CD+DNA-VLPs. The latter were reassembled with CD in presence of DNA. DNA is a natural cargo for VLPs and CD was shown to interact with DNA (Alves et al., 2015), thus we hypothesized that DNA may help stabilize CD inside the VLPs. However, we did not observe any difference in the cargo association efficiency with VLPs. CD was clearly attached also on the surface of the VLPs as detection of CD in native VLPs was strong. However, the association of CD and VLPs was stable even after

extensive purification process. CD was shown to interact with surface exposed aromatic amino acids that can insert inside the CD molecule cavity (Aachmann et al., 2003; Aachmann et al., 2012). VP1 protein contains aromatic amino acids which makes the interaction with cyclodextrin possible. It was also described that CD binding to proteins can prevent their aggregation (Aachmann et al., 2003) but it did not interfere with VP1-VLPs reassembly.

On the contrary, the attempt to encapsidate fluorescently labeled antibody into MPyV-derived VP1-VLPs in the process of disassembly and reassembly was not successful. The antibody was only weakly associated with VLPs whereas the majority of the antibody remained in the supernatant in the purification steps. In addition the AB-VLPs appeared to be unstable.

In attempt to show that CD can be delivered into cells using MPyV VP1-VLPs, we observed the fate of CD and VP1 in mouse fibroblasts using indirect immunofluorescent staining and fluorescent and confocal microscopy. Even though CD contains two fluorescent moieties (FITC), we also used antibody to detect it because FITC is easily quenched and its fluorescence in acidic environment decreases (Geisow, 1984). We expected extensive colocalisation of CD and VP1. However, CD signal and CD and VP1 colocalisation was detected only in large spots, possibly bigger vesicles containing large amount of VLPs. There was usually only one or two such spots per cell after 6.5 hrs post infection. The reason why we were not able to detect CD in smaller VP1 positive vesicles is unclear. An explanation for this result is that CD was not accessible to antibody in early endosomes, because it was encapsidated or tightly bound to VP1. It only became recognized when the VLPs entered more acidic environment of late endosomes or lysosomes, where the VLPs were partially digested and the cargo released. Nonetheless, we concluded that we managed to deliver CD cargo in MPyV VP1-VLPs into mouse 3T6 cells, thus that MPyV VP1-VLPs are suitable for small molecules encapsidation and cellular delivery, even though further optimization would be required.

When we observed the samples of CD-VLPs and control VLPs using confocal microscopy, we noticed differences in the entry pattern into the cells and nuclear localization of VP1 protein. The control VLPs, which did not undergo reassembly process, were possibly added in excess. They entered in small vesicles, often organized in fiber-like pattern localized closed to cell periphery (figure 5.2.9). In such cells the nuclear VP1 signal was rarely observed. The reassembled VLPs, both carrying CD and empty, were possibly added in smaller amount and were observed to enter in larger vesicles and were more frequently localized inside nuclei after 6.5 hours post infection.

The nuclear entry of MPyV virions and virus-like particles is extensively investigated in the Laboratory of Virology and the VP1-VLPs were observed in nuclei quite rarely (Richterová et al., 2001). The fiber-like organization of VLPs inside cells was observed in previous works and was described to be associated with actin cytoskeleton stress fibers (Krauzewicz et al., 2000;

Richterová et al., 2001). The actin associated pathway does not lead to efficient gene transfer mediated by MPyV VP1-VLPs (Krauzewicz et al., 2000).

An explanation for such a striking difference in entry and nuclear localization between control VLPs and reassembled VLPs can be either due to the reassembly process (e.g. by heterogenous composition of VLPs with various size), but not due to cargo as reassembled VLPs without cargo behaved the same as CD-VLPs, or due to VLPs dose per cell. Such dose-dependent difference in entry pattern may be associated with cellular defense mechanism and remains to be further tested. If the dose-dependent way of entry was confirmed, it would have a big impact on cargo delivery into nucleus by MPyV VP1-VLPs and the research of MPyV infection mechanisms.

6.3 Preparation of MPyV VP1-VLPs with enhanced endosome escape properties

Polyomaviruses-derived VP1-VLPs can deliver foreign DNA into cells leading to gene expression. Whereas JCV-derived VP1-VLPs are efficient in DNA delivery into cells and nuclei thanks to VLPs interaction with importins (Qu et al., 2004), SV40-derived VP1-VLPs were found to be less potent in gene transfer when compared to VLPs containing both VP2 and VP3 minor proteins (Enomoto et al., 2011). MPyV VP1-VLPs were shown to be able to deliver DNA into nuclei leading to gene expression (Forstová et al., 1995; Henke et al., 2000), although the efficiency was never compared to VLPs containing minor proteins. The minor proteins are crucial for MPyV infectivity (Mannová et al., 2002). Also MPyV VLPs containing minor proteins were described to be stronger competitors with MPyV infection than VP1-VLPs (An et al., 1999). Together with the recent research showing that both VP2 and VP3 are interacting with membranes and may function as viroporins, probably in early steps of infection (Burkert et al., 2014; Huerfano et al., 2010), it is reasonable to expect that MPyV VP1-VLPs are less potent in cargo delivery into cytoplasm or nuclei than VLPs containing minor proteins.

With this in mind we decided to increase the delivery potential of VP1-VLPs by modification of VP1 protein DE surface loop. DE surface loop is not directly involved in receptor binding (Stehle and Harrison, 1997; Stehle et al., 1994), thus it should not affect entry of modified VLPs into the cells (Kojzarová, 2011). The critical step of all delivery systems using endocytosis is the endosome escape to prevent lysosomal degradation. Thus we decided to modify VP1 protein by insertion of multiple histidine moieties inside the DE loop. The modification with histidine was chosen based on the research done on synthetic delivery systems. Histidine was found to have pH dependent endosome escape enhancing effect due to its buffering capacity (Kichler et al., 2003) and possible interaction with membranes (Kichler et al., 2006; Tu et al., 2013), thus increasing the delivery potential on DNA (Hwang et al., 2014; Chen et al., 2010; Nam et al., 2015;

Thomas et al., 2012; Wen et al., 2012; Zhao et al., 2014), RNA (Asseline et al., 2008; Langlet-Bertin et al., 2010) and small molecule cargos (Johnson et al., 2014; Li et al., 2015; Zhang et al., 2014).

Using gene engineering methods and Bac-to-Bac® expression system we prepared three recombinant baculovirus inocula producing His-VP1 protein. Modified VP1 with 7 deleted amino acids replaced with glycine-serine flexible linkers was used for insertion as the flexible linkers are supposed to reduce the effect of insert on the VP1 structure (Kojzarová, 2011). Three different baculovirus inocula were obtained, C5 with one six histidine long insertion (His_6), C14 with two His_6 connected through Gly-Ser-Gly sequence and A7 with four His_6 connected through Gly-Ser sequences inserted into DE loop between Gly-Ser flexible linkers. After time consuming optimization process of the isolation method of His-VP1 nanostructures, we analyzed the obtained material. C5 material did not assemble into VLPs or other organized nanostructures. A7 material formed long tubules and small VLPs of approx. 20 nm in diameter, probably with triangulation number T=1. Finally C14 material predominantly assembled in nanostructures which were never seen before in MPyV VP1-VLPs isolations. These were highly regular planar structures with striped pattern which resembled knitted fabric. They were named nano-jumpers. Interestingly nano-jumpers did not appear to be composed of VP1 pentamers, which are basic morphological units of VLPs and tubular structures commonly seen in MPyV VP1-VLPs isolations in baculovirus expression system. A smaller portion of C14 material assembled also into regular T=7 VLPs and tubular structures composed form VP1 pentamers. Structures similar to nano-jumpers were observed in nuclei of Sf9 cells infected with recombinant baculovirus inocula, which means that nano-jumpers are probably assembling already inside the cells, similarly to regular VLPs (Montross et al., 1991), and are not a result of subsequent isolation process.

The literature investigating the *in vitro* assembly of polyomavirus-derived VLPs and polyomavirus capsid structure was helpful in finding a possible explanation for observed unexpected His-VP1 nanostructures. The *in vitro* assembly of polyomavirus-derived VLPs is dependent on pH, ionic strength and calcium ions concentration (Salunke et al., 1989). Changes in the *in vitro* conditions can lead to various VP1 assembly products such as classical 45nm VLPs with triangulation number 7 (T=7), tiny particles of 22 nm in diameter (T=1), intermediate particles, that may consist of 24 pentamers organized in octahedral structure or can be icosahedral with T=3 or T=4, and even irregular or tubular structures (Kanesashi et al., 2003; Salunke et al., 1989). Similar variety of structures forms also when VP1-VLPs are isolated using baculovirus expression system (Montross et al., 1991). Moreover, assemblies of VP1 in the same conditions vary among different polyomaviruses (Catrice and Sainsbury, 2015; Nicol et al., 2013; Norkiene et al., 2015; Sasnauskas et al., 2002) and single amino acid mutations in VP1 protein

can result in irregular VP1 assemblies such as ribbon-like structures and spirals (Schwartz et al., 2000). In addition, the cellular proteins such as chaperones probably play role in VLPs and virions assembly *in vivo* as the particles are more stable than the one assembled *in vitro* (Simon et al., 2014). Finally nucleic acids can act as a scaffold for VLPs assembly, interestingly RNA scaffold leads to T=1 particles and intermediate particles for longer RNA molecules, whereas VP1 pentamers assemble mostly into T=7 45nm VLPs when DNA molecule acts as a scaffold (Kler et al., 2013).

In a study discussing the structure of VP1 protein and capsid of SV40 polyomavirus (Stehle et al., 1996), the authors hypothesized that structures other than icosahedral VLPs of 45 nm in diameter and T=7 are a result of a mistake that occurred during VLPs assembly. Such a mistake in interpentamer binding would prevent the T=7 particle assembly and, depending on the pentamer interaction, would result in T=1 particles, octahedral particles or tubular structures. Such theory can be applied on the observed differences in VP1 assembly in different pH and ionic strength conditions. Given conditions may affect the probability of binding pentamers correctly so T=7 VLPs would assemble in smaller amount or at all. Kanesashi et al. (2003) observed unusually long tubular structures when MPyV VP1 pentamers were assembled in physiological NaCl concentration (150 mM) and low pH (5.0). Strikingly, our His-VP1 nanostructures obtained in A7 isolations (4 times inserted His_6 separated by Gly-Ser) formed very similar structures in addition to small approx. 20nm VLPs. Thus it is possible that insertion of histidine sequences into DE loop of MPyV VP1 protein resulted in a change of probability in T=7 VLPs formation. The explanation can be extended also to C14 isolations (2 times inserted His_6) containing nano-jumpers. It is possible that the specific insertion of two His_6 sequences separated by Gly-Ser-Gly sequence affected the VP1 interactions necessary for pentamers formation and made other VP1 interactions resulting in nano-jumper structures more favorable. Nonetheless the modification did not prevent formation of pentamers completely as VLPs and tubular structures were still present. This can be further supported by the notice that we were able to disassemble the C14 isolation into pentamers (possibly from pentameric structures), but we were not able to reassemble them into neither nano-jumpers nor VLPs or other organized VP1 structures using the MPyV VP1-VLPs disassembly and reassembly protocol.

To test endosome escape properties of His-VP1 nanostructures, we first needed to select suitable assay. The first selected was Dextran assay (chapter 2.3.3.1) using fluorescein isothiocyanate (FITC)-conjugated dextran (Dx) with molecular weight 3 kDa for endosome escape detection. Such dextran is supposed to by endocyted, label the vesicles and upon endosome disruption the fluorescence should diffuse across the cytoplasm (figure 2.4, Salomone et al., 2012; Suikkanen et al., 2003). Dx experiments were usually done in living cells. However, when we tried to observe Dx in living 3T6 cells, the background of FITC was very strong, almost

as it bound nonspecifically to the surface of the cultivation dish. Thus we fixed the cells after washing and used indirect immunofluorescence to detect CD. Even after that we did not observe expected pattern of fluorescent vesicles. We observed usually only one or two green spots per cell localized close to the nuclei with quite weak signal. In addition we did not observe any proximity of VP1-VLPs signal and Dx signal when applied together. Thus we suppose that the FITC-conjugated Dx (Sigma Aldirch) we obtained was probably badly manufactured. Clearly it contained FITC, as the fluorescence was present, but it might not be bound to dextran.

So what may be the fluorescent structure we observed? Free FITC may enter cells in free diffusion and stain some structures, as it was able to stain vacuoles in yeasts (Preston et al., 1987). Moreover, isothiocyanates (ITCs) are known as anti-cancer substances. They induce cell cycle arrest and apoptosis in various cancer cells (Gupta et al., 2014). ITCs are able to bind thiol and amino groups of various substrates including proteins (Mi et al., 2011). It was found that ITC can bind covalently to tubulin subunits (Mi et al., 2008) leading to tubulin degradation by proteasomes (Mi et al., 2009a). Moreover, ITC binding to tubulin induces tubulin aggregation, disruption of microtubules and formation of aggregosome-like structures enriched in proteasomal activity and tubulin degradation. These aggregosome-like structures were formed close to the nuclei in 4 hours post addition (Mi et al., 2009b). If free FITC has the same effect as other ITC, it is possible that the observed green spots may be aggregosome-like structures, although visualization of tubulin would be necessary to prove this theory.

Even though we could not conclude what the observed FITC-positive structures were, it was clear that Dx we obtained was not working properly as other studies using dextran assay observed labeled vesicles (Salomone et al., 2012; Suikkanen et al., 2003). Thus we could not use this assay in our experiments.

When we tested the optimal conditions for CD-VLPs experiments we noticed that FITC-labeled antibody (FITC-AB), normally used as a secondary fluorescent antibody, was endocyted by 3T6 mouse fibroblasts and labeled the endosomes as we expected in dextran assay. Thus we decided to test if it can be used similarly to Dx assay, which was proven (chapter 6.5). FITC-AB labeling was not used in His-VP1 VLPs and nanostructures endosome escape experiments because of time limitations.

Finally, we chose the SNAP-Trap assay which is based on detection of protein interaction (chapter 2.3.3.2). We tested the endosome escape of A7 His-VLPs and tubular structures using this assay. Although we had some difficulties with detection of VP1 protein, possibly due to combination of His modification and SNAP-tag binding that compromised antibody binding, we prove that His-VLPs and nanostructures efficiently entered cytoplasm, thus escaped the endocytic vesicles, whereas VP1-VLPs failed to do so. Thus we confirmed that histidine modification has positive effect on endosome escape of MPyV virus-like particles composed of

VP1 protein, which is in agreement with the effect of histidine modifications of synthetic delivery systems (Hwang et al., 2014; Chang et al., 2010; Nam et al., 2015; Thomas et al., 2012; Wen et al., 2012; Zhao et al., 2014).

6.4 Effect of histidine-rich peptide on MPyV infectivity and its endosome escape properties

We were also interested what the effect of endosome disrupting agents on infectivity of MPyV was. MPyV enters cells in endocytic vesicles (Gilbert et al., 2003; Liebl et al., 2006; Mannová and Forstová, 2003; Richterová et al., 2001) and its trafficking to nucleus is extensively investigated but still unclear. It was found that low pH of endosomes is important for productive infection (Liebl et al., 2006). MPyV virions were then observed in endoplasmic reticulum but never in Golgi apparatus (Gilbert and Benjamin, 2004; Liebl et al., 2006; Mannová and Forstová, 2003; Qian et al., 2009). Endoplasmic reticulum is thought to be important for MPyV infection and the virions probably exit from this compartment into cytoplasm (Bílkova et al., 2014).

When we infected 3T6 cells with MPyV alone or with known pH dependent endosome disrupting agent polyethylenimine (PEI) or histidine-rich peptide $KH_{27}K$, we observed that both PEI and His-rich peptide increased the number of infected cells 3.6 and 7.2 times respectively. We also compared the effect of PEI and $KH_{27}K$ on endosomes using FITC-labeled antibody that we observed to enter endosomes. Both PEI and $KH_{27}K$ led to transition of FITC-AB from distinct spot pattern of labeled vesicles to diffuse pattern. This proves that both PEI and $KH_{27}K$ have similar effect on endosome membrane, probably creating pores big enough for IgG antibodies.

Taken together, these results show that disruption of endosomal membrane increases the infectivity of MPyV. It is also important to note that the effect of histidine-rich peptide was stronger than the one of PEI. Such observation is in agreement with the results obtained in synthetic gene delivery system, where histidine modification of the nanoparticle led to higher gene delivery efficiency than PEI (Thomas et al., 2012).

We also studied the effect of PEI and histidine-rich peptide on VP1-VLPs using SNAP-Trap assay. Surprisingly, we did not observe VP1-VLPs transition from vesicles into cytoplasm upon treatment with PEI or $KH_{27}K$, whereas histidine modified VP1-VLPs and nanostructures (A7 His-VLPs) were found to localize into cytoplasm without endosome disrupting agent addition.

A possible explanation for such observation can be that the pores in endosomal membrane induced by PEI and his-rich peptide are not big enough for VLPs escape. Only particles that contain a potential membrane interacting or disrupting parts were able to escape the endosomes. That is histidine-modified VP1-VLPs and nanostructures, or native virions containing minor proteins, that are able to interact with membranes and possibly work as

viroporins (Burkert et al., 2014; Huerfano et al., 2010; Mannová et al., 2002). Interestingly, if the endosome disrupting agents truly helped to release virions directly from endosomes, there was no need of endoplasmic reticulum for the virus infectivity. In normal conditions, virus productive infection requires low pH of endosomes and endoplasmic reticulum enzymes (Gilbert et al., 2006; Liebl et al., 2006; Walczak and Tsai, 2011). It is possible that both steps induce partial destabilization of the particle leading to exposure of minor proteins which can then function in endoplasmic reticulum. The primary destabilization induced by endosomal low pH may be not sufficient for minor proteins function in normal infection, but addition of endosome disrupting agents may enable minor proteins function without the need of endoplasmic reticulum enzymes.

6.5 Future prospective for histidine modifications and His-VP1 nanostructures

Even though the preparation of His-VLPs of expected morphology (45 nm, T=7) was not successful, nano-jumpers and other His-VP1 nanostructures are still interesting for various nanotechnology purposes that we want to further investigate. Histidine sequences are long known to interact with metal ions, such as nickel (Ni^{2+}) or cobalt (Co^{2+}). This interaction is used with success for histidine-tag modified proteins isolation via immobilized metal-affinity chromatography (Bornhorst and Falke, 2000). Materials coated in nitrilotriacetic acid (NTA) coordinating Ni^{2+} (together called Ni-NTA) are used for the affinity isolation. Ni-NTA can be also bound to various other substrates such as quantum dots (Susumu et al., 2010), silica coated magnetic nanoparticles (Aygar et al., 2015), gold nanopartices (Hainfeld et al., 1999; Hamley et al., 2014; Swartz et al., 2011) or pepides (Matsuura et al., 2016). Thus a variety of possible modifications of His-VP1 nanosructures remains to be tested.

Furthemore, the experiments with histidine-rich peptide and PEI showed for the first time that MPyV infectivity is increased when endosomes are disrupted. This result will be important for further investigation of MPyV transport to nucleus and the role of MPyV minor proteins.

Moreover, His-VP1 VLPs and nanostructures were able to escape endosomes, whereas simple addition of His-rich peptide or PEI had no effect on VP1-VLPs cytoplasmic localization. This suggests that histidine-rich sequence has to be a part of the VLP. As insertion of histidine sequences into VP1 protein surface loop resulted in changed assembly properties of VP1, so VLPs were not predominant structures in the isolations, it suggests that chemical modification of normal VP1-VLPs with histidine-rich peptide may be another suitable option for preparation of VP1-VLPs with enhanced endosome escape and delivery properties.

7. Conclusions

1. We prepared two universal VP1 constructs for various surface loops modification.

- Constructs were prepared in pFastBac™1 donor plasmid for Bac-to-Bac® baculovirus expression system: *VP1-BCmut* with modified BC loop sequence and *VP1-BCmut+DE7less* with modified BC and DE loop sequences. The vectors will be used in the Laboratory of Molecular Virology for subsequent projects.

2. We demonstrated that MPyV VP1-VLPs can be used as a delivery system into mammalian cells.

- MPyV VP1-VLPs were disassembled and reassembled in presence of selected cargo, FITC and gadolinium conjugated cyclodextrin (CD) alone or together with DNA, or fluorescently labeled antibody (AB).
- We prepared VP1-VLPs with stably associated CD (CD-VLPs and CD+DNA-VLPs), whereas encapsidation of AB into VLPs was unsuccessful. CD was attached also on the surface of VLPs but the association of CD and particles was stable.
- Using fluorescent and confocal microscopy, we proved that CD-VLPs and CD+DNA-VLPs entered mammalian cells. We also proved that CD is delivered into cells using VP1-VLPs.

3. We modified MPyV VP1-VLPs by histidine (His) residues and determined that their endosome escape properties were enhanced.

- MPyV *VP1* sequence was modified by His_6 coding oligonucleotides which were inserted into *VP1 DE loop* sequence. Three *His-VP1* constructs were prepared: C5 with one His_6 oligonucleotide, C14 with two His_6 oligonucleotides and A7 with four His_6 oligonucleotides.
- We optimized the protocol for His-VP1 nanostructures isolation.
- We failed to produce His-VLPs from C5. Formation of regular 45nm VLPs with T=7 was compromised by His_6 modification of VP1 protein. His-VP1 material from A7 formed long tubular structures and small particles of approx. 20 nm in diameter and supposedly triangulation nuber T=1. His-VP1 material from C14 resulted in novel nanostructures which we named nano-jumpers.
- We showed that His-VLPs and nanostructures have enhanced endosome escape properties.

4. We performed other important observations:

- We showed that histidine-rich peptide has similar effect on endosome escape as polyethylenimine.
- We showed that endosome disruption has an enhancing effect on MPyV infectivity.

8. References

Aachmann, F. L., Otzen, D. E., Larsen, K. L. and Wimmer, R. (2003). Structural background of cyclodextrin-protein interactions. *Protein engineering* **16**, 905–12.

Aachmann, F. L., Larsen, K. L. and Wimmer, R. (2012). Interactions of cyclodextrins with aromatic amino acids: a basis for protein interactions. *Journal of Inclusion Phenomena and Macrocyclic Chemistry* **73**, 349–57.

Abbing, A., Blaschke, U. K., Grein, S., Kretschmar, M., Stark, C. M. B., Thies, M. J. W., Walter, J., Weigand, M., Woith, D. C., Hess, J., et al. (2004). Efficient intracellular delivery of a protein and a low molecular weight substance via recombinant polyomavirus-like particles. *The Journal of biological chemistry* **279**, 27410–21.

Akinc, A., Thomas, M., Klibanov, A. M. and Langer, R. (2005). Exploring polyethylenimine-mediated DNA transfection and the proton sponge hypothesis. *The journal of gene medicine* **7**, 657–63.

Allen, M., Bulte, J. W. M., Liepold, L., Basu, G., Zywicke, H. A., Frank, J. A., Young, M. and Douglas, T. (2005). Paramagnetic viral nanoparticles as potential high-relaxivity magnetic resonance contrast agents. *Magnetic resonance in medicine* **54**, 807–12.

Alves, P. S., Mesquita, O. N. and Rocha, M. S. (2015). Controlling cooperativity in β-cyclodextrin-DNA binding reactions. *The journal of physical chemistry letters* **6**, 3549–54.

An, K., Gillock, E. T., Sweat, J. A., Reeves, W. M. and Consigli, R. A. (1999). Use of the baculovirus system to assemble polyomavirus capsid-like particles with different polyomavirus structural proteins: analysis of the recombinant assembled capsid-like particles. *The Journal of general virology* **80**, 1009–16.

Anderson, E. A., Isaacman, S., Peabody, D. S., Wang, E. Y., Canary, J. W. and Kirshenbaum, K. (2006). Viral nanoparticles donning a paramagnetic coat: conjugation of MRI contrast agents to the MS2 capsid. *Nano letters* **6**, 1160–4.

Asseline, U., Gonçalves, C., Pichon, C. and Midoux, P. (2008). Improved nuclear delivery of antisense 2'-Ome RNA by conjugation with the histidine-rich peptide H5WYG. *The journal of gene medicine* **16**, 157–65.

Aygar, G., Kaya, M., Özkan, N., Kocabıyık, S. and Volkan, M. (2015). Preparation of silica coated cobalt ferrite magnetic nanoparticles for the purification of histidine-tagged proteins. *Journal of Physics and Chemistry of Solids* **87**, 64–71.

Barouch, D. H. and Harrison, S. C. (1994). Interactions among the major and minor coat proteins of polyomavirus. *Journal of virology* **68**, 3982–9.

Behr, J. (1997). The proton sponge: a trick to enter cells the viruses did not exploit. *CHIMIA International Journal for Chemistry* **51**, 34–6.

Benjaminsen, R. V, Mattebjerg, M. A., Henriksen, J. R., Moghimi, S. M. and Andresen, T. L. (2013). The possible "proton sponge " effect of polyethylenimine (PEI) does not include change in lysosomal pH. *Molecular therapy : the journal of the American Society of Gene Therapy* **21**, 149–57.

Bílkova, E., Forstová, J. and Abrahamyan, L. (2014). Coat as a dagger: the use of capsid proteins to perforate membranes during non-enveloped DNA viruses trafficking. *Viruses* **6**, 2899–937.

Boeckle, S., von Gersdorff, K., van der Piepen, S., Culmsee, C., Wagner, E. and Ogris, M. (2004). Purification of polyethylenimine polyplexes highlights the role of free polycations in gene transfer. *The journal of gene medicine* **6**, 1102–11.

Bolen, J. B., Anders, D. G., Trempy, J. and Consigli, R. A. (1981). Differences in the subpopulations of the structural proteins of polyoma virions and capsids: biological functions of the multiple VP1 species. *Journal of virology* **37**, 80–91.

Bornhorst, J. A. and Falke, J. J. (2000). Purification of proteins using polyhistidine affinity tags. *Methods in enzymology* **326**, 245–54.

Bouřa, E., Liebl, D., Špíšek, R., Frič, J., Marek, M., Štokrová, J., Holáň, V. and Forstová, J. (2005). Polyomavirus EGFP-pseudocapsids: analysis of model particles for introduction of proteins and peptides into mammalian cells. *FEBS letters* **579**, 6549–58.

Brabec, M., Schober, D., Wagner, E., Bayer, N., Murphy, R. F., Blaas, D. and Fuchs, R. (2005). Opening of size-selective pores in endosomes during human rhinovirus serotype 2 in vivo uncoating monitored by single-organelle flow analysis. *Journal of virology* **79**, 1008–16.

Brady, J. N., Winston, V. D. and Consigli, R. a (1977). Dissociation of polyoma virus by the chelation of calcium ions found associated with purified virions. *Journal of virology* **23**, 717–24.

Bruckman, M. A., Hern, S., Jiang, K., Flask, C. A., Yu, X. and Steinmetz, N. F. (2013). Tobacco mosaic virus rods and spheres as supramolecular high-relaxivity MRI contrast agents. *Journal of materials chemistry. B* **1**, 1482–90.

Bruckman, M. A., Randolph, L. N., Gulati, N. M., Stewart, P. L. and Steinmetz, N. F. (2015). Silica-coated Gd(DOTA)-loaded protein nanoparticles enable magnetic resonance imaging of macrophages. *Journal of materials chemistry. B,* **3**, 7503–10.

Burkert, O., Kreßner, S., Sinn, L., Giese, S., Simon, C. and Lilie, H. (2014). Biophysical characterization of polyomavirus minor capsid proteins. *Biological chemistry* **395**, 871–80.

Carbone, M., Ascione, G., Chichiarelli, S., Garcia, M.-I., Eufemi, M. and Amati, P. (2004). Chromosome-protein interactions in polyomavirus virions. *Journal of virology* **78**, 513–9.

Caruso, M., Belloni, L., Sthandier, O., Amati, P. and Garcia, M.-I. (2003). α4β1 integrin acts as a cell receptor for murine polyomavirus at the postattachment level. *Journal of virology* **77**, 3913–21.

Catrice, E. V. B. and Sainsbury, F. (2015). Assembly and purification of polyomavirus-like particles from plants. *Molecular biotechnology* **57**, 904–13.

Chang, D., Haynes, J. I., Brady, J. N. and Consigli, R. A. (1992). The use of additive and subtractive approaches to examine the nuclear localization sequence of the polyomavirus major capsid protein VP1. *Virology* **189**, 821–7.

Chang, D., Cai, X. and Consigli, R. A. (1993). Characterization of the DNA binding properties of polyomavirus capsid protein. *Journal of virology* **67**, 6327–31.

Chang, D., Fung, C. Y., Ou, W. C., Chao, P. C., Li, S. Y., Wang, M., Huang, Y. L., Tzeng, T. Y. and Tsai, R. T. (1997). Self-assembly of the JC virus major capsid protein, VP1, expressed in insect cells. *The Journal of general virology* **78**, 1435–9.

Chang, K. L., Higuchi, Y., Kawakami, S., Yamashita, F. and Hashida, M. (2010). Efficient gene transfection by histidine-modified chitosan through enhancement of endosomal escape. *Bioconjugate Chemistry* **21**, 1087–1095.

Chao, C.-N., Huang, Y.-L., Lin, M.-C., Fang, C.-Y., Shen, C.-H., Chen, P.-L., Wang, M., Chang, D. and Tseng, C.-E. (2015). Inhibition of human diffuse large B-cell lymphoma growth by JC polyomavirus-like particles delivering a suicide gene. *Journal of Translational Medicine* **13**, 1–9.

Chen, P. L., Wang, M., Ou, W. C., Lii, C. K., Chen, L. S. and Chang, D. (2001). Disulfide bonds stabilize JC virus capsid-like structure by protecting calcium ions from chelation. *FEBS letters* **500**, 109–13.

Chen, L.-S., Wang, M., Ou, W.-C., Fung, C.-Y., Chen, P.-L., Chang, C.-F., Huang, W.-S., Wang, J.-Y., Lin, P. Y. and Chang, D. (2010). Efficient gene transfer using the human JC virus-like particle that inhibits human colon adenocarcinoma growth in a nude mouse model. *Gene therapy* **17**, 1033–41.

Chou, M.-I., Hsieh, Y.-F., Wang, M., Chang, J. T., Chang, D., Zouali, M. and Tsay, G. J. (2010). *In vitro* and *in vivo* targeted delivery of IL-10 interfering RNA by JC virus-like particles. *Journal of biomedical science* **17**, 51.

Choudhury, C. K., Kumar, A. and Roy, S. (2013). Characterization of conformation and interaction of gene delivery vector polyethylenimine with phospholipid bilayer at different protonation state. *Biomacromolecules* **14**, 3759–68.

Chuan, Y. P., Fan, Y. Y., Lua, L. H. L. and Middelberg, A. P. J. (2010). Virus assembly occurs following a pH- or Ca^{2+}-triggered switch in the thermodynamic attraction between structural protein capsomeres. *Journal of the Royal Society, Interface* **7**, 409–21.

DeCaprio, J. A., Imperiale, M. J. and Major, E. O. (2013). Polyomaviruses. In *Fields Virology, Sixth edition* (ed. Knipe, D. M. and Howley, P. M.), pp. 1633 – 61. Lippincott Williams &

Wilkins, a Wolters Kluwer Business, Philadelphia.

Dilworth, S. M. and Griffin, B. E. (1982). Monoclonal antibodies against polyoma virus tumor antigens. *Proceedings of the National Academy of Sciences of the United States of America* **79**, 1059–63.

Dower, W. J., Miller, J. F. and Ragsdale, C. W. (1988). High efficiency transformation of E. coli by high voltage electroporation. *Nucleic acids research* **16**, 6127–45.

Enomoto, T., Kukimoto, I., Kawano, M. A., Yamaguchi, Y., Berk, A. J. and Handa, H. (2011). In vitro reconstitution of SV40 particles that are composed of VP1/2/3 capsid proteins and nucleosomal DNA and direct efficient gene transfer. *Virology* **420**, 1–9.

Eriksson, M., Andreasson, K., Weidmann, J., Lundberg, K., Tegerstedt, K., Dalianis, T. and Ramqvist, T. (2011). Murine polyomavirus virus-like particles carrying full-length human PSA protect BALB/c mice from outgrowth of a PSA expressing tumor. *PloS one* **6**, e23828.

Fang, C.-Y., Tsai, Y.-D., Lin, M.-C., Wang, M., Chen, P.-L., Chao, C.-N., Huang, Y.-L., Chang, D. and Shen, C.-H. (2015). Inhibition of human bladder cancer growth by a suicide gene delivered by JC polyomavirus virus-like particles in a mouse model. *The Journal of urology* **193**, 2100–6.

Forstová, J., Krauzewicz, N., Wallace, S., Street, A. J., Dilworth, S. M., Beard, S. and Griffin, B. E. (1993). Cooperation of structural proteins during late events in the life cycle of polyomavirus. *Journal of virology* **67**, 1405–13.

Forstová, J., Krauzewicz, N., Sandig, V., Elliott, J., Palková, Z., Strauss, M. and Griffin, B. E. (1995). Polyoma virus pseudocapsids as efficient carriers of heterologous DNA into mammalian cells. *Human gene therapy* **6**, 297–306.

Funhoff, A. M., van Nostrum, C. F., Koning, G. A., Schuurmans-Nieuwenbroek, N. M. E., Crommelin, D. J. A. and Hennink, W. E. (2004). Endosomal escape of polymeric gene delivery complexes is not always enhanced by polymers buffering at low pH. *Biomacromolecules* **5**, 32–9.

Garcea, R. L., Salunke, D. M. and Caspar, D. L. (1987). Site-directed mutation affecting polyomavirus capsid self- assembly in vitro. *Nature* **329**, 86–87.

Gedvilaite, A., Frömmel, C., Sasnauskas, K., Micheel, B., Ozel, M., Behrsing, O., Staniulis, J., Jandrig, B., Scherneck, S. and Ulrich, R. (2000). Formation of immunogenic virus-like particles by inserting epitopes into surface-exposed regions of hamster polyomavirus major capsid protein. *Virology* **273**, 21–35.

Gedvilaite, A., Kucinskaite-Kodze, I., Lasickiene, R., Timinskas, A., Vaitiekaite, A., Ziogiene, D. and Zvirbliene, A. (2015). Evaluation of trichodysplasia spinulosa-associated polyomavirus capsid protein as a new carrier for construction of chimeric virus-like particles harboring foreign epitopes. *Viruses* **7**, 4204–29.

Geiger, R., Andritschke, D., Friebe, S., Herzog, F., Luisoni, S., Heger, T. and Helenius, A. (2011). BAP31 and BiP are essential for dislocation of SV40 from the endoplasmic reticulum to the cytosol. *Nature cell biology* **13**, 1305–14.

Geiger, R., Luisoni, S., Johnsson, K., Greber, U. F. and Helenius, A. (2013). Investigating endocytic pathways to the endoplasmic reticulum and to the cytosol using SNAP-trap. *Traffic (Copenhagen, Denmark)* **14**, 36–46.

Geisow, M. J. (1984). Fluorescein conjugates as indicators of subcellular pH. A critical evaluation. *Experimental Cell Research* **150**, 29–35.

Gilbert, J. and Benjamin, T. (2004). Uptake pathway of polyomavirus via ganglioside GD1a. *Journal of virology* **78**, 12259–67.

Gilbert, J. M., Goldberg, I. G. and Benjamin, T. L. (2003). Cell penetration and trafficking of polyomavirus. *Journal of virology* **77**, 2615–22.

Gilbert, J., Ou, W., Silver, J. and Benjamin, T. (2006). Downregulation of protein disulfide isomerase inhibits infection by the mouse polyomavirus. *Journal of virology* **80**, 10868–70.

Gillock, E. T., Rottinghaus, S., Chang, D., Cai, X., Smiley, S. A., An, K. and Consigli, R. A. (1997). Polyomavirus major capsid protein VP1 is capable of packaging cellular DNA when expressed in the baculovirus system. *Journal of virology* **71**, 2857–65.

Gillock, E. T., An, K. and Consigli, R. A. (1998). Truncation of the nuclear localization signal of

polyomavirus VP1 results in a loss of DNA packaging when expressed in the baculovirus system. *Virus research* **58**, 149–60.

Goldmann, C., Stolte, N., Nisslein, T., Hunsmann, G., Lüke, W. and Petry, H. (2000). Packaging of small molecules into VP1-virus-like particles of the human polyomavirus JC virus. *Journal of Virological Methods* **90**, 85–90.

Green, M. R. and Sambrook, J. (2012). *Molecular Cloning A Laboratory Manual*. 4th ed. Cold Spring Harbor Laboratory Press, New York.

Gronemeyer, T., Chidley, C., Juillerat, A., Heinis, C. and Johnsson, K. (2006). Directed evolution of O6-alkylguanine-DNA alkyltransferase for applications in protein labeling. *Protein engineering, design & selection : PEDS* **19**, 309–16.

Gross, L. (1953). A filterable agent, recovered from Ak leukemic extracts, causing salivary gland carcinomas in C3H mice. *Proceedings of the Society for Experimental Biology and Medicine* **83**, 414–21.

Günther, C., Schmidt, U., Rudolph, R. and Böhm, G. (2001). Protein and peptide delivery via engineered polyomavirus-like particles. *FASEB journal : official publication of the Federation of American Societies for Experimental Biology* **15**, 1646–8.

Gupta, P., Wright, S. E., Kim, S.-H. and Srivastava, S. K. (2014). Phenethyl isothiocyanate: a comprehensive review of anti-cancer mechanisms. *Biochimica et biophysica acta* **1846**, 405–24.

Hainfeld, J. F., Liu, W., Halsey, C. M., Freimuth, P. and Powell, R. D. (1999). Ni-NTA-gold clusters target His-tagged proteins. *Journal of structural biology* **127**, 185–98.

Hale, A. D., Bartkeviciūte, D., Dargeviciūte, A., Jin, L., Knowles, W., Staniulis, J., Brown, D. W. G. and Sasnauskas, K. (2002). Expression and antigenic characterization of the major capsid proteins of human polyomaviruses BK and JC in Saccharomyces cerevisiae. *Journal of virological methods* **104**, 93–8.

Hamley, I. W., Kirkham, S., Dehsorkhi, A., Castelletto, V., Adamcik, J., Mezzenga, R., Ruokolainen, J., Mazzuca, C., Gatto, E., Venanzi, M., et al. (2014). Self-assembly of a model peptide incorporating a hexa-histidine sequence attached to an oligo-alanine sequence, and binding to gold NTA/nickel nanoparticles. *Biomacromolecules* **15**, 3412–20.

Heinis, C., Schmitt, S., Kindermann, M., Godin, G. and Johnsson, K. (2006). Evolving the substrate specificity of O6-alkylguanine-DNA alkyltransferase through loop insertion for applications in molecular imaging. *ACS chemical biology* **1**, 575–84.

Henke, S., Rohmann, A., Bertling, W. M., Dingermann, T. and Zimmer, A. (2000). Enhanced in vitro oligonucleotide and plasmid DNA transport by VP1 virus-like particles. *Pharmaceutical research* **17**, 1062–70.

Hoffmann, D. B., Böker, K. O., Schneider, S., Eckermann-Felkl, E., Schuder, A., Komrakova, M., Sehmisch, S. and Gruber, J. (2016). *In vivo* siRNA delivery using JC virus-like particles decreases the expression of RANKL in rats. *Molecular Therapy—Nucleic Acids* **5**, e298.

Huerfano, S., Zíla, V., Boura, E., Spanielová, H., Stokrová, J. and Forstová, J. (2010). Minor capsid proteins of mouse polyomavirus are inducers of apoptosis when produced individually but are only moderate contributors to cell death during the late phase of viral infection. *The FEBS journal* **277**, 1270–83.

Hussain, A. F., Kampmeier, F., von Felbert, V., Merk, H.-F., Tur, M. K. and Barth, S. (2011). SNAP-tag technology mediates site specific conjugation of antibody fragments with a photosensitizer and improves target specific phototoxicity in tumor cells. *Bioconjugate chemistry* **22**, 2487–95.

Hussain, A. F., Krüger, H. R., Kampmeier, F., Weissbach, T., Licha, K., Kratz, F., Haag, R., Calderón, M. and Barth, S. (2013). Targeted delivery of dendritic polyglycerol-doxorubicin conjugates by scFv-SNAP fusion protein suppresses $EGFR^+$ cancer cell growth. *Biomacromolecules* **14**, 2510–20.

Hwang, H. S., Hu, J., Na, K. and Bae, Y. H. (2014). Role of polymeric endosomolytic agents in gene transfection: a comparative study of poly(L-lysine) grafted with monomeric L-histidine analogue and poly(L-histidine). *Biomacromolecules* **15**, 3577–86.

Inoue, T., Kawano, M., Takahashi, R., Tsukamoto, H., Enomoto, T., Imai, T., Kataoka, K. and

Handa, H. (2008). Engineering of SV40-based nano-capsules for delivery of heterologous proteins as fusions with the minor capsid proteins VP2/3. *Journal of biotechnology* **134**, 181–92.

Ishizu, K. I., Watanabe, H., Han, S. I., Kanesashi, S. N., Hoque, M., Yajima, H., Kataoka, K. and Handa, H. (2001). Roles of disulfide linkage and calcium ion-mediated interactions in assembly and disassembly of virus-like particles composed of simian virus 40 VP1 capsid protein. *Journal of virology* **75**, 61–72.

Jao, C. C., Weidman, M. K., Perez, A. R. and Gharakhanian, E. (1999). Cys9, Cys104 and Cys207 of simian virus 40 Vp1 are essential for inter-pentamer disulfide-linkage and stabilization in cell-free lysates. *The Journal of general virology* **80**, 2481–9.

Johnson, R. P., Jeong, Y., John, J. V, Chung, C., Choi, S. H., Song, S. Y., Kang, D. H., Suh, H. and Kim, I. (2014). Lipo-poly(L-histidine) hybrid materials with pH-sensitivity, intracellular delivery efficiency, and intrinsic targetability to cancer cells. *Macromolecular rapid communications* **35**, 888–94.

Juillerat, A., Gronemeyer, T., Keppler, A., Gendreizig, S., Pick, H., Vogel, H. and Johnsson, K. (2003). Directed evolution of O6-alkylguanine-DNA alkyltransferase for efficient labeling of fusion proteins with small molecules in vivo. *Chemistry & biology* **10**, 313–7.

Kanesashi, S., Ishizu, K., Kawano, M., Han, S., Tomita, S., Watanabe, H., Kataoka, K. and Handa, H. (2003). Simian virus 40 VP1 capsid protein forms polymorphic assemblies in vitro. *The Journal of general virology* **84**, 1899–905.

Kawano, M., Matsui, M. and Handa, H. (2013). SV40 virus-like particles as an effective delivery system and its application to a vaccine carrier. *Expert review of vaccines* **12**, 199–210.

Kawano, M., Morikawa, K., Suda, T., Ohno, N., Matsushita, S., Akatsuka, T., Handa, H. and Matsui, M. (2014). Chimeric SV40 virus-like particles induce specific cytotoxicity and protective immunity against influenza A virus without the need of adjuvants. *Virology* **448**, 159–67.

Keppler, A., Gendreizig, S., Gronemeyer, T., Pick, H., Vogel, H. and Johnsson, K. (2003). A general method for the covalent labeling of fusion proteins with small molecules in vivo. *Nature biotechnology* **21**, 86–9.

Keppler, A., Kindermann, M., Gendreizig, S., Pick, H., Vogel, H. and Johnsson, K. (2004). Labeling of fusion proteins of O6-alkylguanine-DNA alkyltransferase with small molecules in vivo and in vitro. *Methods* **32**, 437–44.

Kichler, A., Leborgne, C., März, J., Danos, O. and Bechinger, B. (2003). Histidine-rich amphipathic peptide antibiotics promote efficient delivery of DNA into mammalian cells. *Proceedings of the National Academy of Sciences of the United States of America* **100**, 1564–8.

Kichler, A., Mason, A. J. and Bechinger, B. (2006). Cationic amphipathic histidine-rich peptides for gene delivery. *Biochimica et biophysica acta* **1758**, 301–7.

Kimchi-Sarfaty, C., Ben-Nun-Shaul, O., Rund, D., Oppenheim, A. and Gottesman, M. M. (2002). In vitro-packaged SV40 pseudovirions as highly efficient vectors for gene transfer. *Human Gene Therapy* **13**, 299–310.

Kler, S., Wang, J. C.-Y., Dhason, M., Oppenheim, A. and Zlotnick, A. (2013). Scaffold properties are a key determinant of the size and shape of self-assembled virus-derived particles. *ACS chemical biology* **8**, 2753–61.

Kojzarová, M. (2011). Construction of mouse polyomavirus chimeric VLPs bearing melanoma epitopes. *Diploma thesis,* Faculty of Science, Charles Universitiy in Prague, Prague.

Kosukegawa, A., Arisaka, F., Takayama, M., Yajima, H., Kaidow, A. and Handa, H. (1996). Purification and characterization of virus-like particles and pentamers produced by the expression of SV40 capsid proteins in insect cells. *Biochimica et Biophysica Acta - General Subjects* **1290**, 37–45.

Kotková, Z., Kotek, J., Jirák, D., Jendelová, P., Herynek, V., Berková, Z., Hermann, P. and Lukeš, I. (2010). Cyclodextrin-based bimodal fluorescence/MRI contrast agents: an efficient approach to cellular imaging. *Chemistry - A European Journal* **16**, 10094–102.

Krauzewicz, N., Stokrová, J., Jenkins, C., Elliott, M., Higgins, C. F. and Griffin, B. E. (2000).

Virus-like gene transfer into cells mediated by polyoma virus pseudocapsids. *Gene therapy* **7**, 2122–31.

Kwolek, U., Jamróz, D., Janiczek, M., Nowakowska, M., Wydro, P. and Kepczynski, M. (2016). Interactions of polyethylenimines with zwitterionic and anionic lipid membranes. *Langmuir : the ACS journal of surfaces and colloids* **32**, 5004–18.

Langlet-Bertin, B., Leborgne, C., Scherman, D., Bechinger, B., Mason, A. J. and Kichler, A. (2010). Design and evaluation of histidine-rich amphipathic peptides for siRNA delivery. *Pharmaceutical research* **27**, 1426–36.

Leavitt, A. D., Roberts, T. M. and Garcea, R. L. (1985). Polyoma virus major capsid protein, VP1. Purification after high level expression in Escherichia coli. *The Journal of biological chemistry* **260**, 12803–9.

Li, M. and Garcea, R. L. (1994). Identification of the threonine phosphorylation sites on the polyomavirus major capsid protein VP1: relationship to the activity of middle T antigen. *Journal of virology* **68**, 320–7.

Li, T.-C., Takeda, N., Kato, K., Nilsson, J., Xing, L., Haag, L., Cheng, R. H. and Miyamura, T. (2003). Characterization of self-assembled virus-like particles of human polyomavirus BK generated by recombinant baculoviruses. *Virology* **311**, 115–24.

Li, F., Zhang, Z.-P., Peng, J., Cui, Z.-Q., Pang, D.-W., Li, K., Wei, H.-P., Zhou, Y.-F., Wen, J.-K. and Zhang, X.-E. (2009). Imaging viral behavior in Mammalian cells with self-assembled capsid-quantum-dot hybrid particles. *Small* **5**, 718–26.

Li, Z., Qiu, L., Chen, Q., Hao, T., Qiao, M., Zhao, H., Zhang, J., Hu, H., Zhao, X., Chen, D., et al. (2015). pH-sensitive nanoparticles of poly(L-histidine)-poly(lactide-co-glycolide)-tocopheryl polyethylene glycol succinate for anti-tumor drug delivery. *Acta biomaterialia* **11**, 137–50.

Liang, W. and W. Lam, J. K. (2012). Endosomal Escape Pathways for Non-Viral Nucleic Acid Delivery Systems. In *Molecular Regulation of Endocytosis* (ed. Ceresa, B.), pp. 429–456. InTech.

Liddington, R. C., Yan, Y., Moulai, J., Sahli, R., Benjamin, T. L. and Harrison, S. C. (1991). Structure of simian virus 40 at 3.8-A resolution. *Nature* **354**, 278–84.

Liebl, D., Difato, F., Horníková, L., Mannová, P., Stokrová, J. and Forstová, J. (2006). Mouse polyomavirus enters early endosomes, requires their acidic pH for productive infection, and meets transferrin cargo in Rab11-positive endosomes. *Journal of virology* **80**, 4610–22.

Liepold, L., Anderson, S., Willits, D., Oltrogge, L., Frank, J. A., Douglas, T. and Young, M. (2007). Viral capsids as MRI contrast agents. *Magnetic resonance in medicine* **58**, 871–9.

Liew, M. W. O., Rajendran, A. and Middelberg, A. P. J. (2010). Microbial production of virus-like particle vaccine protein at gram-per-litre levels. *Journal of biotechnology* **150**, 224–31.

Lipin, D. I., Yap, P. C., Neibert, M., Yuan, Y. F. and Middelberg, A. (2006). Processing and in vitro assembly of virus like particle nanostructures. In *Proceedings of the 2006 International Conference on Nanoscience and Nanotechnology, ICONN*, pp. 217–19.

Ludlow, J. W. and Consigli, R. A. (1987). Localization of calcium on the polyomavirus VP1 capsid protein. *Journal of virology* **61**, 2934–7.

Macadangdang, B., Zhang, N., Lund, P. E., Marple, A. H., Okabe, M., Gottesman, M. M., Appella, D. H. and Kimchi-Sarfaty, C. (2011). Inhibition of multidrug resistance by SV40 pseudovirion delivery of an antigene peptide nucleic acid (PNA) in cultured cells. *PloS one* **6**, e17981.

Mannová, P. and Forstová, J. (2003). Mouse polyomavirus utilizes recycling endosomes for a traffic pathway independent of COPI vesicle transport. *Journal of virology* **77**, 1672–81.

Mannová, P., Liebl, D., Krauzewicz, N., Fejtová, A., Stokrová, J., Palková, Z., Griffin, B. E. and Forstová, J. (2002). Analysis of mouse polyomavirus mutants with lesions in the minor capsid proteins. *The Journal of general virology* **83**, 2309–19.

Martens, T. F., Remaut, K., Demeester, J., De Smedt, S. C. and Braeckmans, K. (2014). Intracellular delivery of nanomaterials: How to catch endosomal escape in the act. *Nano Today* **9**, 344–64.

Matsuura, K., Nakamura, T., Watanabe, K., Noguchi, T., Minamihata, K., Kamiya, N. and

Kimizuka, N. (2016). Self-assembly of Ni-NTA-modified β-annulus peptides into artificial viral capsids and encapsulation of His-tagged proteins. *Organic & biomolecular chemistry* **2**, e–published ahead of print.

Maurel, D., Comps-Agrar, L., Brock, C., Rives, M.-L., Bourrier, E., Ayoub, M. A., Bazin, H., Tinel, N., Durroux, T., Prézeau, L., et al. (2008). Cell-surface protein-protein interaction analysis with time-resolved FRET and snap-tag technologies: application to GPCR oligomerization. *Nature methods* **5**, 561–7.

Mi, L., Xiao, Z., Hood, B. L., Dakshanamurthy, S., Wang, X., Govind, S., Conrads, T. P., Veenstra, T. D. and Chung, F.-L. (2008). Covalent binding to tubulin by isothiocyanates. A mechanism of cell growth arrest and apoptosis. *The Journal of biological chemistry* **283**, 22136–46.

Mi, L., Gan, N., Cheema, A., Dakshanamurthy, S., Wang, X., Yang, D. C. H. and Chung, F.-L. (2009a). Cancer preventive isothiocyanates induce selective degradation of cellular alpha- and beta-tubulins by proteasomes. *The Journal of biological chemistry* **284**, 17039–51.

Mi, L., Gan, N. and Chung, F.-L. (2009b). Aggresome-like structure induced by isothiocyanates is novel proteasome-dependent degradation machinery. *Biochemical and biophysical research communications* **388**, 456–62.

Mi, L., Hood, B. L., Stewart, N. A., Xiao, Z., Govind, S., Wang, X., Conrads, T. P., Veenstra, T. D. and Chung, F.-L. (2011). Identification of potential protein targets of isothiocyanates by proteomics. *Chemical research in toxicology* **24**, 1735–43.

Middelberg, A. P. J., Rivera-Hernandez, T., Wibowo, N., Lua, L. H. L., Fan, Y., Magor, G., Chang, C., Chuan, Y. P., Good, M. F. and Batzloff, M. R. (2011). A microbial platform for rapid and low-cost virus-like particle and capsomere vaccines. *Vaccine* **29**, 7154–62.

Midoux, P. and Monsigny, M. (1999). Efficient gene transfer by histidylated polylysine/pDNA complexes. *Bioconjugate chemistry* **10**, 406–11.

Montross, L., Watkins, S., Moreland, R. B., Mamon, H., Caspar, D. L. and Garcea, R. L. (1991). Nuclear assembly of polyomavirus capsids in insect cells expressing the major capsid protein VP1. *Journal of virology* **65**, 4991–8.

Morávková, A. (2001), Příprava protilátek proti hlavnímu strukturnímu proteinu myšího polyomaviru. *Diploma thesis,* Faculty of Science, Charles Univerzity in Prague, Prague

Moreland, R. B., Montross, L. and Garcea, R. L. (1991). Characterization of the DNA-binding properties of the polyomavirus capsid protein VP1. *Journal of virology* **65**, 1168–76.

Mukherjee, S., Abd-El-Latif, M., Bronstein, M., Ben-nun-Shaul, O., Kler, S. and Oppenheim, A. (2007). High cooperativity of the SV40 major capsid protein VP1 in virus assembly. *PloS one* **2**, e765.

Mukherjee, S., Kler, S., Oppenheim, A. and Zlotnick, A. (2010). Uncatalyzed assembly of spherical particles from SV40 VP1 pentamers and linear dsDNA incorporates both low and high cooperativity elements. *Virology* **397**, 199–204.

Nakagawa, O., Ming, X., Carver, K. and Juliano, R. (2014). Conjugation with receptor-targeted histidine-rich peptides enhances the pharmacological effectiveness of antisense oligonucleotides. *Bioconjugate chemistry* **25**, 165–70.

Nam, J.-P., Nam, K., Nah, J.-W. and Kim, S. W. (2015). Evaluation of histidylated arginine-grafted bioreducible polymer to enhance transfection efficiency for use as a gene carrier. *Molecular pharmaceutics* **12**, 2352–64.

Ng, J., Koechlin, O., Ramalho, M., Raman, D. and Krauzewicz, N. (2007). Extracellular self-assembly of virus-like particles from secreted recombinant polyoma virus major coat protein. *Protein engineering, design & selection : PEDS* **20**, 591–8.

Nicol, J. T. J., Robinot, R., Carpentier, A., Carandina, G., Mazzoni, E., Tognon, M., Touzé, A. and Coursaget, P. (2013). Age-specific seroprevalences of merkel cell polyomavirus, human polyomaviruses 6, 7, and 9, and trichodysplasia spinulosa-associated polyomavirus. *Clinical and vaccine immunology : CVI* **20**, 363–8.

Niikura, K., Sugimura, N., Musashi, Y., Mikuni, S., Matsuo, Y., Kobayashi, S., Nagakawa, K., Takahara, S., Takeuchi, C., Sawa, H., et al. (2013a). Virus-like particles with removable cyclodextrins enable glutathione-triggered drug release in cells. *Molecular bioSystems* **9**,

501–7.
Niikura, K., Iyo, N., Matsuo, Y., Mitomo, H. and Ijiro, K. (2013b). Sub-100 nm gold nanoparticle vesicles as a drug delivery carrier enabling rapid drug release upon light irradiation. *ACS applied materials & interfaces* **5**, 3900–7.
Norkiene, M., Stonyte, J., Ziogiene, D., Mazeike, E., Sasnauskas, K. and Gedvilaite, A. (2015). Production of recombinant VP1-derived virus-like particles from novel human polyomaviruses in yeast. *BMC Biotechnology* **15**, 68.
Ohtake, N., Niikura, K., Suzuki, T., Nagakawa, K., Mikuni, S., Matsuo, Y., Kinjo, M., Sawa, H. and Ijiro, K. (2010). Low pH-triggered model drug molecule release from virus-like particles. *Chembiochem : a European journal of chemical biology* **11**, 959–62.
Palková, Z., Adamec, T., Liebl, D., Štokrová, J. and Forstová, J. (2000). Production of polyomavirus structural protein VP1 in yeast cells and its interaction with cell structures. *FEBS letters* **478**, 281–9.
Pawlita, M., Müller, M., Oppenländer, M., Zentgraf, H. and Herrmann, M. (1996). DNA encapsidation by viruslike particles assembled in insect cells from the major capsid protein VP1 of B-lymphotropic papovavirus. *Journal of virology* **70**, 7517–26.
Pleckaityte, M., Bremer, C. M., Gedvilaite, A., Kucinskaite-Kodze, I., Glebe, D. and Zvirbliene, A. (2015). Construction of polyomavirus-derived pseudotype virus-like particles displaying a functionally active neutralizing antibody against hepatitis B virus surface antigen. *BMC biotechnology* **15**, 85.
Preston, R. A., Murphy, R. F. and Jones, E. W. (1987). Apparent endocytosis of fluorescein isothiocyanate-conjugated dextran by Saccharomyces cerevisiae reflects uptake of low molecular weight impurities, not dextran. *The Journal of cell biology* **105**, 1981–7.
Qazi, S., Liepold, L. O., Abedin, M. J., Johnson, B., Prevelige, P., Frank, J. A. and Douglas, T. (2013). P22 viral capsids as nanocomposite high-relaxivity MRI contrast agents. *Molecular pharmaceutics* **10**, 11–7.
Qian, M. and Tsai, B. (2010). Lipids and proteins act in opposing manners to regulate polyomavirus infection. *Journal of virology* **84**, 9840–52.
Qian, M., Cai, D., Verhey, K. J. and Tsai, B. (2009). A lipid receptor sorts polyomavirus from the endolysosome to the endoplasmic reticulum to cause infection. *PLoS pathogens* **5**, e1000465.
Qu, Q., Sawa, H., Suzuki, T., Semba, S., Henmi, C., Okada, Y., Tsuda, M., Tanaka, S., Atwood, W. J. and Nagashima, K. (2004). Nuclear entry mechanism of the human polyomavirus JC virus-like particle: role of importins and the nuclear pore complex. *The Journal of biological chemistry* **279**, 27735–42.
Rayment, I., Baker, T. S., Caspar, D. L. and Murakami, W. T. (1982). Polyoma virus capsid structure at 22.5 A resolution. *Nature* **295**, 110–5.
Richterová, Z., Liebl, D., Horák, M., Palková, Z., Stokrová, J., Hozák, P., Korb, J. and Forstová, J. (2001). Caveolae are involved in the trafficking of mouse polyomavirus virions and artificial VP1 pseudocapsids toward cell nuclei. *Journal of virology* **75**, 10880–91.
Salomone, F., Cardarelli, F., Di Luca, M., Boccardi, C., Nifosì, R., Bardi, G., Di Bari, L., Serresi, M. and Beltram, F. (2012). A novel chimeric cell-penetrating peptide with membrane-disruptive properties for efficient endosomal escape. *Journal of controlled release* **163**, 293–303.
Salunke, D. M., Caspar, D. L. D. and Garcea, R. L. (1986). Self-assembly of purified polyomavirus capsid protein VP1. *Cell* **46**, 895–904.
Salunke, D. M., Caspar, D. L. and Garcea, R. L. (1989). Polymorphism in the assembly of polyomavirus capsid protein VP1. *Biophysical journal* **56**, 887–900.
Sandalon, Z. and Oppenheim, a (1997). Self-assembly and protein-protein interactions between the SV40 capsid proteins produced in insect cells. *Virology* **237**, 414–21.
Sasnauskas, K., Buzaite, O., Vogel, F., Jandrig, B., Razanskas, R., Staniulis, J., Scherneck, S., Krüger, D. H. and Ulrich, R. (1999). Yeast cells allow high-level expression and formation of polyomavirus-like particles. *Biological chemistry* **380**, 381–6.
Sasnauskas, K., Bulavaite, A., Hale, A., Jin, L., Knowles, W. A., Gedvilaite, A., Dargeviciūte, A.,

Bartkeviciūte, D., Zvirbliene, A., Staniulis, J., et al. (2002). Generation of recombinant virus-like particles of human and non-human polyomaviruses in yeast Saccharomyces cerevisiae. *Intervirology* **45**, 308–17.

Shishido, Y., Nukuzuma, S., Mukaigawa, J., Morikawa, S., Yasui, K. and Nagashima, K. (1997). Assembly of JC virus-like particles in COS7 cells. *Journal of medical virology* **51**, 265–72.

Schmidt, U., Rudolph, R. and Böhm, G. (2000). Mechanism of assembly of recombinant murine polyomavirus-like particles. *Journal of virology* **74**, 1658–62.

Schwartz, R., Garcea, R. L. and Berger, B. (2000). "Local rules" theory applied to polyomavirus polymorphic capsid assemblies. *Virology* **268**, 461–70.

Simon, C., Klose, T., Herbst, S., Han, B. G., Sinz, A., Glaeser, R. M., Stubbs, M. T. and Lilie, H. (2014). Disulfide linkage and structure of highly stable yeast-derived virus-like particles of murine polyomavirus. *The Journal of biological chemistry* **289**, 10411–18.

Skrastina, D., Bulavaite, A., Sominskaya, I., Kovalevska, L., Ose, V., Priede, D., Pumpens, P. and Sasnauskas, K. (2008). High immunogenicity of a hydrophilic component of the hepatitis B virus preS1 sequence exposed on the surface of three virus-like particle carriers. *Vaccine* **26**, 1972–81.

Sonawane, N. D., Szoka, F. C. and Verkman, A. S. (2003). Chloride accumulation and swelling in endosomes enhances DNA transfer by polyamine-DNA polyplexes. *The Journal of biological chemistry* **278**, 44826–31.

Stehle, T. and Harrison, S. C. (1996). Crystal structures of murine polyomavirus in complex with straight-chain and branched-chain sialyloligosaccharide receptor fragments. *Structure* **4**, 183–94.

Stehle, T. and Harrison, S. C. (1997). High-resolution structure of a polyomavirus VP1-oligosaccharide complex: implications for assembly and receptor binding. *The EMBO journal* **16**, 5139–48.

Stehle, T., Yan, Y., Benjamin, T. L. and Harrison, S. C. (1994). Structure of murine polyomavirus complexed with an oligosaccharide receptor fragment. *Nature* **369**, 160–3.

Stehle, T., Gamblin, S. J., Yan, Y. and Harrison, S. C. (1996). The structure of simian virus 40 refined at 3.1 A resolution. *Structure* **4**, 165–82.

Stewart, S. E., Eddy, B. E. and Borgese, N. (1958). Neoplasms in mice inoculated with a tumor agent carried in tissue culture. *Journal of the National Cancer Institute* **20**, 1223–43.

Suchanová, J. (2012). Targeting of polyomavirus virus-like particles to prostate cancer cells. *Diploma thesis,* Faculty of Science, Charles University in Prague. Prague.

Suikkanen, S., Antila, M., Jaatinen, A., Vihinen-Ranta, M. and Vuento, M. (2003). Release of canine parvovirus from endocytic vesicles. *Virology* **316**, 267–80.

Summers, M. D. and Smith, G. E. (1988). A Manual of Methods for Baculovirus Vectors and Insect Cell Culture Procedures. *Texas Agricultural Experiment Station Bulletin No.1555* 1–57.

Susumu, K., Medintz, I. L., Delehanty, J. B., Boeneman, K. and Mattoussi, H. (2010). Modification of poly(ethylene glycol)-capped quantum dots with nickel nitrilotriacetic acid and self-assembly with histidine-tagged proteins. *The Journal of Physical Chemistry C* **114**, 13526–31.

Swartz, J. D., Gulka, C. P., Haselton, F. R. and Wright, D. W. (2011). Development of a histidine-targeted spectrophotometric sensor using Ni(II)NTA-functionalized Au and Ag nanoparticles. *Langmuir : the ACS journal of surfaces and colloids* **27**, 15330–9.

Španielová, H., Fraiberk, M., Suchanová, J., Soukup, J. and Forstová, J. (2014). The encapsidation of polyomavirus is not defined by a sequence-specific encapsidation signal. *Virology* **450-451**, 122–31.

Tegerstedt, K., Lindencrona, J. A., Curcio, C., Andreasson, K., Tullus, C., Forni, G., Dalianis, T., Kiessling, R. and Ramqvist, T. (2005). A single vaccination with polyomavirus VP1/VP2Her2 virus-like particles prevents outgrowth of HER-2/neu-expressing tumors. *Cancer research* **65**, 5953–7.

Teunissen, E. A., de Raad, M. and Mastrobattista, E. (2013). Production and biomedical

applications of virus-like particles derived from polyomaviruses. *Journal of controlled release* **172**, 305–21.

Thomas, J. J., Rekha, M. R. and Sharma, C. P. (2012). Unraveling the intracellular efficacy of dextran-histidine polycation as an efficient nonviral gene delivery system. *Molecular pharmaceutics* **9**, 121–34.

Touzé, A., Bousarghin, L., Ster, C., Combita, A. L., Roingeard, P. and Coursaget, P. (2001). Gene transfer using human polyomavirus BK virus-like particles expressed in insect cells. *The Journal of general virology* **82**, 3005–9.

Touzé, A., Gaitan, J., Arnold, F., Cazal, R., Fleury, M. J., Combelas, N., Sizaret, P.-Y., Guyetant, S., Maruani, A., Baay, M., et al. (2010). Generation of Merkel cell polyomavirus (MCV)-like particles and their application to detection of MCV antibodies. *Journal of clinical microbiology* **48**, 1767–70.

Tsai, B., Gilbert, J. M., Stehle, T., Lencer, W., Benjamin, T. L. and Rapoport, T. A. (2003). Gangliosides are receptors for murine polyoma virus and SV40. *The EMBO journal* **22**, 4346–55.

Tu, C., Chen, K., Tian, W. and Ma, Y. (2013). Computational investigations of a Peptide-modified dendrimer interacting with lipid membranes. *Macromolecular rapid communications* **34**, 1237–42.

Türler H. and Beard P. (1985): Simian virus 40 and polyoma virus: growth, titration, transformation and purification of viral components. In *Virology: a practical approaches* (ed. Mahy, B. W. J.), pp. 169-192. IRL Press, Oxford.

Usselman, R. J., Qazi, S., Aggarwal, P., Eaton, S. S., Eaton, G. R., Russek, S. and Douglas, T. (2015). Gadolinium-loaded viral capsids as magnetic resonance imaging contrast agents. *Applied Magnetic Resonance* **46**, 349–55.

Vaidyanathan, S., Chen, J., Orr, B. G. and Banaszak Holl, M. M. (2016). Cationic polymer intercalation into the lipid membrane enables intact polyplex DNA escape from endosomes for gene delivery. *Molecular pharmaceutics* **13**, 1967–78.

Voronkova, T., Kazaks, A., Ose, V., Ozel, M., Scherneck, S., Pumpens, P. and Ulrich, R. (2007). Hamster polyomavirus-derived virus-like particles are able to transfer in vitro encapsidated plasmid DNA to mammalian cells. *Virus genes* **34**, 303–14.

Walczak, C. P. and Tsai, B. (2011). A PDI family network acts distinctly and coordinately with ERp29 to facilitate polyomavirus infection. *Journal of virology* **85**, 2386–96.

Wen, Y., Guo, Z., Du, Z., Fang, R., Wu, H., Zeng, X., Wang, C., Feng, M. and Pan, S. (2012). Serum tolerance and endosomal escape capacity of histidine-modified pDNA-loaded complexes based on polyamidoamine dendrimer derivatives. *Biomaterials* **33**, 8111–21.

White, M. K., Gordon, J. and Khalili, K. (2013). The rapidly expanding family of human polyomaviruses: recent developments in understanding their life cycle and role in human pathology. *PLoS pathogens* **9**, e1003206.

Yue, Y., Jin, F., Deng, R., Cai, J., Chen, Y., Lin, M. C. M., Kung, H. F. and Wu, C. (2011). Revisit complexation between DNA and polyethylenimine - Effect of uncomplexed chains free in the solution mixture on gene transfection. *Journal of Controlled Release* **155**, 67–76.

Zhang, X., Chen, D., Ba, S., Zhu, J., Zhang, J., Hong, W., Zhao, X., Hu, H. and Qiao, M. (2014). Poly(l-histidine) based triblock copolymers: pH induced reassembly of copolymer micelles and mechanism underlying endolysosomal escape for intracellular delivery. *Biomacromolecules* **15**, 4032–45.

Zhao, G. X., Tanaka, H., Kim, C. W., Li, K., Funamoto, D., Nobori, T., Nakamura, Y., Niidome, T., Kishimura, A., Mori, T., et al. (2014). Histidinylated poly-L-lysine-based vectors for cancer-specific gene expression via enhancing the endosomal escape. *Journal of biomaterials science. Polymer edition* **25**, 519–34.